

N64-27277

code 1 cat. -27  
NASA 6056890

OTS PRICE

XEROX	\$	11.50 ph
MICROFILM	\$	

## FOREWORD

An analytical research program to assess the feasibility and desirability of improving launch vehicle performance by means of air-augmented rocket propulsion systems has been conducted by the Aero-Space Division of The Boeing Company for the National Aeronautics and Space Administration under Contract NAS 8-11017. The contract was initiated on June 29, 1963 and completed on June 15, 1964.

This program was sponsored by the George C. Marshall Space Flight Center, Huntsville, Alabama, with technical direction from Mr. D. D. Thompson of the Propulsion and Vehicle Engineering Laboratory. Panel members having cognizance of this program were Messers R. V. Hensley and J. A. Suddreth (Program Managers) NASA Headquarters; L. K. Donehoo, MSFC; G. R. Woodcock, MSFC; P. K. Pierpont, NASA Langley; M. A. Beheim, NASA Lewis; W. E. Supp, USAF, WPAFB.

The Boeing Company Propulsion personnel who cooperated in the research and preparation of this report were: Mr. R. W. Carkeek, Mr. R. E. Fitch, and Dr. D. L. Emmons. Personnel from other groups in Flight Technology; Structures and Materials; Applied Mathematics; and Product Development who assisted in the study included Messrs. D. Faltens, G. Woodhead, J. R. Bender, R. J. Sartell, F. M. Knox, L. E. Savage, E. G. Cate, L. B. Trabert, J. Lauderdale, and Mrs. M. Manro.

This report consists of two volumes. Volume I, D2-23217, is Unclassified and contains the material on the analytical models, engine concepts, component operating characteristics, and powerplant performance. Volume II, D2-23217-1, is classified Confidential and contains the material on powerplant

integration, vehicle performance, and the correlation of the analytical models with experimental data.

# ABSTRACT

27277

The document reports the results of a study performed by The Boeing Company under Contract NAS 8-11017 with Marshall Space Flight Center, National Aeronautics and Space Administration. The purpose of the study was to analytically assess the feasibility of improving launch vehicle performance by means of an air augmented rocket propulsion system.

The course of action taken was as follows:

1. Develop an analytical model, with which to evaluate the significance and sensitivity of primary system variables on system performance.
2. Produce conceptual designs of interest for propulsion systems on launch vehicles.
3. Investigate methods of integrating the vehicle and augmented engine systems.
4. Determine effects of augmentation on system performance.
5. Delineate problem areas requiring further investigation.

To this end, three computer programs were developed or modified and extensively used during the course of the investigation. A one-dimensional augmented engine cycle analysis program was written in order to investigate performance trends and to outline those areas not warranting further analysis. An existing perfect gas, frozen composition, method of characteristics nozzle plume program was revised to describe the inviscid interaction between a supersonic plume and an isentropic one-dimensional stream confined by a wall. A finite difference mixing program was developed which accounts for axial pressure gradient, equilibrium chemistry, and confinement of the secondary stream by a duct wall.

AUTHOR

The major portion of the study was spent in the development of the analytical models and in determining the effects of the inlet and mixing section

interactions. These interactions present over-all performance limitations due to component matching requirements which are not evident from a conventional one-dimensional analysis. The lower limit of combustor operation is found to be adequately defined by the inviscid plume analysis, confirmed by available experimental data (Volume II, Confidential). When the mixing section entrance conditions are known, the mixing program predicts with good accuracy the operating characteristics of the section. This is also confirmed by experimental data.

Based upon the one-dimensional analysis, augmentation factors of 1.5 and 2.0 are predicted for flight conditions and inlet-combustor geometries for which there are no compatible conditions of matching operation, as determined from the more realistic plume and mixing programs. The required matching of hardware imposes practical limitations in flight path selection and, in general, reduction in augmentation factor.

The S-IC stage of the Saturn V Vehicle was selected as the launch system upon which to study the effects of air augmentation. The propulsion system was changed from a five-engine base cluster to a 36 engine annular arrangement surrounded by a shroud 94 feet long with a diameter of 60 to 70 feet. Augmentation factors of 1.1 to 1.25 in the Mach 2 to 5 range were calculated for this configuration. The net payload change as a function of stage inert weight increase is shown in Volume II (Confidential).

## TABLE OF CONTENTS

	Page
VOLUME I - Unclassified	
INTRODUCTION	1
STUDY DESCRIPTION	3
A. Analytical Approach Philosophy	3
B. Analytical Models	9
1. One-Dimensional Cycle Analysis	9
2. Inviscid Combustor Analysis (Quasi 2-D)	19
3. Two-Dimensional Mixing Analysis	28
C. Discussion	51
1. Configurations	51
a. Engine Concepts	51
b. Vehicle Concepts	56
c. Inlet	61
2. Combustor Mixing Section Analysis	63
RESULTS	67
A. Component Operating Characteristics	67
1. Inlet	67
2. Mixing Section	72
3. Inlet - Combustor Matching	85
B. Powerplant Performance	90
1. One-Dimensional Cycle Analysis	93
a. Base Line Performance	93
b. Parametric Performance	96

TABLE OF CONTENTS (Cont'd)

	Page
2. Engine Performance with Inlet Combustor Matching	107
a. S-2A Engine Performance with Matching	108
b. Engine Performance from Two-Dimensional Mixing Analysis	110
CONCLUSIONS AND RECOMMENDATIONS	126
REFERENCES	128
APPENDIX - Distribution List	130
VOLUME II - Confidential	
SUMMARY	1
POWERPLANT DESIGN, INTEGRATION, AND PERFORMANCE	3
A. Design and Integration	3
B. Weights	8
C. Performance	12
CORRELATION OF THEORETICAL WITH EXPERIMENTAL DATA	26
A. Two-Dimensional Mixing Correlation	26
B. Inviscid Plume Correlation	31
CONCLUSIONS AND RECOMMENDATIONS	37
REFERENCES	39

## LIST OF FIGURES

<u>Figure</u>		<u>Page</u>
1	Air Augmented Rocket Flow Diagram	4
2	Analysis Flow Diagram	8
3	Air Augmented Rocket - Analytical Model	10
4	One-Dimensional Combustor Solutions	16
5	Flow Models, Quasi Two-Dimensional Inviscid Analysis	20
6	Inviscid Interface Matching Technique	29
7	Two-Dimensional Mixing Flow Model	29
8	Finite Difference Grid Network	34
9	Experimental and Theoretical $\sigma$ Values for Free Jets	39
10	Theoretical Effect of Velocity Ratio on the Similarity Parameter Ratio	41
11	Effect of Reaction Mechanism and Rate Constants on Theoretical Static Temperature Distribution	46
12	Comparison of Theoretical Temperature Profiles for Non-Equilibrium and Equilibrium Flow	46
13	Simple Air Augmented Rocket Engine Concept	52
14	Multiple Nozzle Augmented Engine Concept	52
15	Primary Nozzle Shapes to Promote Mixing	53
16	Air Augmented Plug Cluster Concept	55
17	Air Augmented Aerodynamic Nozzle Concept	55
18	Horizontal Take-Off Rocket Plane	57
19	S-1A Configuration	58
20	S-2A Configuration	60
21	Typical Inlet Performance	62
22	Air Augmented Rocket Schematic	66
23	Annular Inlet Configurations	68
24	Inlet Operating Characteristics	69

LIST OF FIGURES (Cont'd)

<u>Figure</u>		<u>Page</u>
25	Adiabatic Impulse Function	71
26	Combustor Configurations	74
27	Combustor Inviscid Operation Characteristics	75
28	Combustor Inviscid Operation Characteristics	76
29	Combustor Inviscid Operation Characteristics	77
30	Mixing Section Study Configuration	80
31	Mach Number Profiles	82
32	Comparison of Theoretical Combustor Inviscid and Viscous Operating Characteristics	83
33	Inlet-Combustor Match Point Operation	86
34	Inlet-Combustor Matching Effects on Trajectory	88
35	Theoretical Rocket Specific Impulse	92
36	S-1A Baseline Performance	94
37	S-2A Baseline Performance	95
38	Effects of Primary Area Ratio on Augmentation	97
39	Effects of Primary O/F on Augmentation	97
40	Effects of Normal Shock Recovery on S-1A Performance	97
41	Effects of Variable Inlet Recovery on S-2A Performance	99
42	Effects of Secondary Flow Rate on Augmentation	101
43	Effects of Secondary Flow Rate on Augmentation	102
44	Effect of Secondary Mach Number on Augmentation Ratio	104
45	Component Thrust Contribution	105
46	Effect of Combustor Area Ratio on S-2A Augmentation	106

LIST OF FIGURES (Cont'd)

<u>Figure</u>		<u>Page</u>
47	Effects of Secondary Fuel Injection on Augmentation	106
48	S-2A Performance with Matching	109
49	Configurations Employed in Engine Performance Studies	111
50	Mach Number Profiles	114
51	Case 1 Mixing Section Pressure Distribution	114
52	Mach Number Profiles	116
53	Mach Number Profiles	118
54	Mach Number Profiles	118
55	Static Temperature Profiles	120
56	Mach Number Profile	120
57	Mixing Region Boundaries	122
58	Theoretical Augmentation Rate with Change in Dynamic Pressure	123
59	Theoretical Augmentation Rate with Change in Area Ratio	123

# NOMENCLATURE

A	Area - ft. <sup>2</sup>
C <sub>K</sub>	Concentration of K <sup>th</sup> Species - lb./lb. <sub>mixture</sub>
C <sub>P</sub>	Specific Heat at Constant Pressure - BTU/lb. <sub>m</sub> °-R
D	Diameter - ft.
$\mathcal{L}$	Impulse function - lb <sub>f</sub> /ft. <sup>2</sup>
F	Augmentation Factor
g <sub>o</sub>	Proportionality Constant - $\frac{32.2 \text{ lb}_m - \text{ft.}}{\text{lb}_f - \text{sec.}^2}$
H°	Total enthalpy - BTU/lb <sub>m</sub>
H <sub>EQUIL</sub>	Static enthalpy from equilibrium routine
H <sub>VEL</sub>	Static enthalpy from energy equation
h <sub>K</sub>	Enthalpy of the K <sup>th</sup> species - BTU/lb <sub>m</sub>
I <sub>s</sub>	Specific Impulse - $\frac{\text{lb}_f - \text{sec.}}{\text{lb}_m}$
I <sub>sR</sub>	Reference Specific Impulse - $\frac{\text{lb}_f - \text{sec.}}{\text{lb}_m}$
L	Length - ft.
Le <sub>t</sub>	Turbulent Lewis Number
$\dot{m}$	Mass flow rate lb <sub>m</sub> /sec.
M	Mach number
P	Pressure - lb <sub>f</sub> /ft. <sup>2</sup>
P <sub>o</sub>	Secondary stagnation pressure at which primary plume completely fills the mixing section
Pr <sub>T</sub>	Turbulent Prandtl Number
q	Incompressible dynamic pressure ( $\frac{1}{2} \rho v^2$ ) - lb <sub>f</sub> /ft. <sup>2</sup>
r	Radial distance - ft.
T	Temperature - °R
T	Thrust - lb <sub>f</sub>
u,v,V	Velocity - ft./sec.

$w_K$	Net rate of production of species K - $\text{lb}_m/\text{ft.}^3 - \text{sec.}$
X	Axial distance - ft.
$\gamma$	Ratio of Specific Heats
$\delta$	1   Axially Symmetric Flow 0   Two-Dimensional Flow
$\epsilon_0$	Reichardt's Coefficient - $\text{ft.}^2/\text{sec.}$
$\epsilon_v$	Eddy Viscosity - $\text{lb}_m/\text{ft.-sec.}$
$\eta_{KE}$	Kinetic Energy Efficiency
$\theta$	Angle of flow with axis of symmetry - degrees
$\rho$	Density - $\text{lb}_m/\text{ft.}^3$
$\sigma$	Similarity parameter
$\psi$	Stream function - $\text{lb}_m/\text{sec.}$

#### Subscripts

1	Primary rocket exit plane
2	Aft end of mixing and combustion section
$\infty$	Free stream (flight) conditions
c	Combustion chamber
D	Mixing-combustor duct
e	Exit
i	Inlet; $i^{\text{th}}$ point
p	Primary
s	Secondary
sl	Slip line
SF	Secondary fuel

#### Superscripts

o	Stagnation conditions
*	Critical conditions

## INTRODUCTION

A fundamental measure of the efficiency of a propulsive device is the thrust per unit mass rate of fuel consumption, referred to as specific impulse. The range of values available vary from approximately 400 for high energy liquid rockets to 10,000 for hydrogen turbofans with the ramjet maximum occurring in between. Unfortunately, the thrust-to-weight ratios of these engines vary inversely as specific impulse with the rockets having values as high as one hundred, the turbofans around eight and ramjets zero at static conditions.

Widespread efforts have been conducted with the aim of increasing the fuel efficiency of the rocket while maintaining the advantage of high thrust to weight ratio. A great deal of time and effort is currently being devoted to specific impulse improvement by increasing the chemical energy of propellants. In the case of stable liquid or hybrid systems, it appears that 456 seconds specific impulse, at standard conditions, is the theoretical maximum. In the case of solids one might optimistically expect improvements on the order of twenty percent at most in the next decade, and then only after the expenditure of considerable effort.

The specific impulse improvements obtained by increasing the chemical energy of the propellant, important as they may be, are not startling when compared to the possible specific impulse increases accruing from inclusion of air-breathing features with the basic rocket propulsion mode.

Early investigations into such composite air-rocket propulsion systems were concentrated mainly in providing ramjets with static thrust capability by the addition of fuel rich rockets (References 1 through 5). These resulted in

systems which had static thrust capability at relatively low thrust-to-weight ratio in addition to the high specific impulse essential for cruise application. These engines, the ducted or ram rockets, were characterized by air to rocket mass flow ratios of approximately twenty to forty. Due to the low thrust to weight ratio, they are primarily competitive with turbojets.

The design of the composite engine for launch vehicle applications presents a different emphasis upon the relative importance of specific impulse and thrust to weight ratio. In this case, high thrust to weight ratio must be maintained at the expense of potential specific impulse gains. In keeping with the high thrust-to-weight requirement, the basic concept to accomplish this is to utilize a single composite air-rocket engine cycle in which the air, provided by a conventional inlet, and the moderately fuel rich rocket exhaust gases enter a common duct, mix and combust, and then exhaust. The basic rocket engine is modified only to the extent of changing mixture ratio or expansion ratio to enhance the mixing process. Such a cycle is referred to as the Air-Augmented Rocket, and is characterized by low air to rocket mass flow ratios up to four, an order of magnitude less than the ducted rocket or ram rocket. It is not new in concept and has been studied both analytically and experimentally by many individuals and agencies (e.g., Reference 6). There have resulted from these investigations some experimental data but no adequate analytical methods.

It was the purpose of this study to develop adequate analytical models and methods with respect to the basic mixing and combustion processes, using experimental data; and establish trades between the air inlet, rocket mixing section, and expansion components to serve as a means of evaluating the performance potential of selected air-augmented rocket engine designs.

## STUDY DESCRIPTION

### A. Analytical Approach Philosophy

The evaluation of any thermodynamic cycle requires a thorough understanding of the separate component operations and processes, as well as their interactions. The air augmented rocket cycle, is shown in block diagram form in Figure 1. The basic rocket engine cycle includes the chamber process, which is the mixing and combustion of the primary (rocket) propellants, and the expansion of the combustion products through a supersonic nozzle. The air inlet conducts the secondary (air) to the mixing and combustion section wherein the chemical reaction between the air and fuel rich primary exhaust products occurs. The expansion section allows the mixed stream to expand to the system exhaust conditions.

From both the analytical and experimental standpoints, the inlet, rocket and expansion processes have previously been sufficiently well defined for the purposes of this study. However, a satisfactory analysis of the mixing and combustion process has not been available, and experimental data directly applicable to this concept are meager. In addition to the requirement for a mixing and combustion analysis, it was essential to have a means of linking the component processes together in order to generate over-all cycle performance data. To these ends, the following three computer programs have been developed and are described in the following pages.

1. One dimensional cycle analysis
2. Inviscid combustor analysis

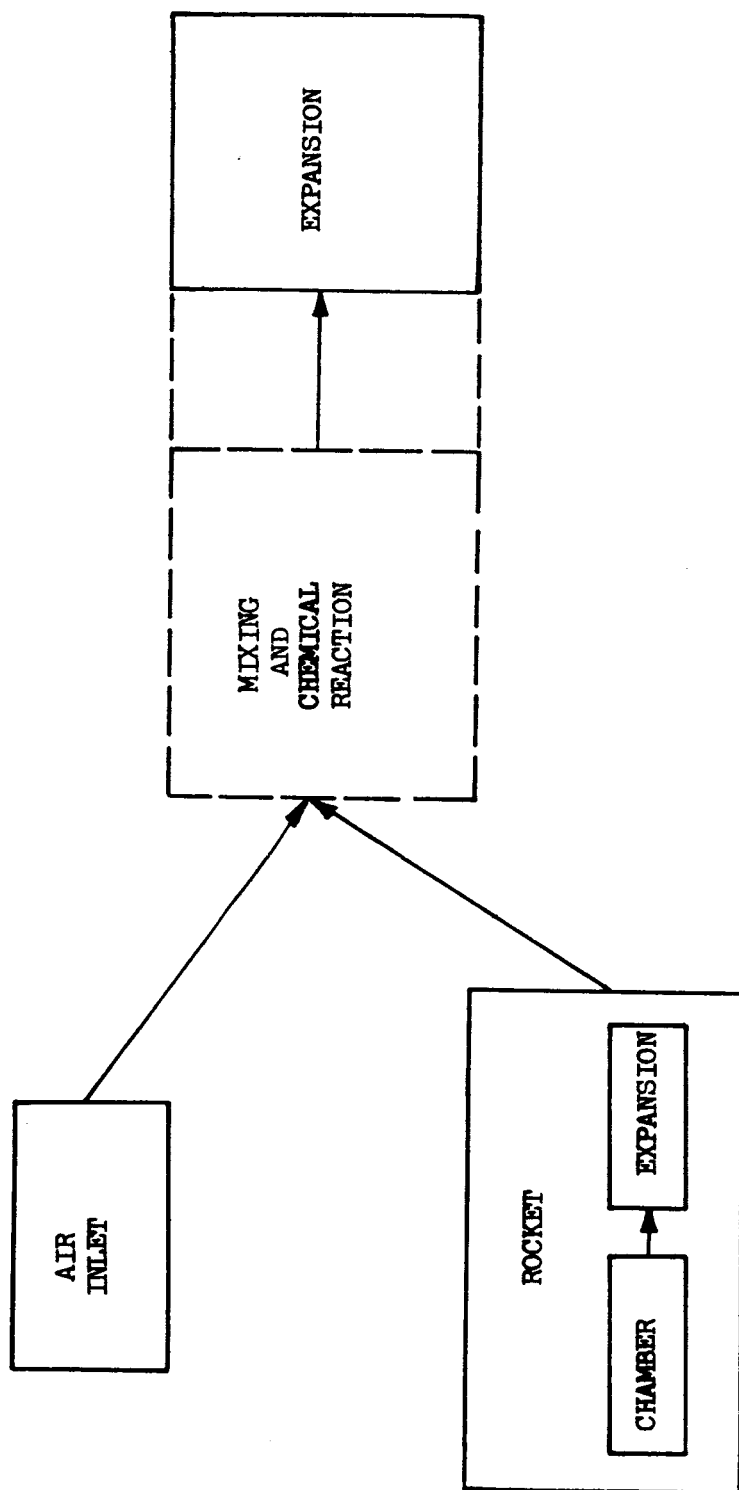


Figure 1 - Air-Augmented Rocket Flow Diagram

### 3. Two dimensional mixing analysis

#### One-Dimensional Cycle Analysis

This program was written to generate overall cycle performance data on a parametric basis along the lines of the classical one-dimensional treatment. It is the simplest of the three programs with respect to the mixing flow field analysis and was used to produce large sets of cycle data in order to outline those areas of flight conditions, flow rate ratios, area ratios, etc., which warranted more sophisticated analysis; and to exclude from further consideration those areas which obviously did not offer promise. The analysis of the mixing section is based upon the assumption that mixing of the secondary and primary streams is complete and that the mixture is in chemical equilibrium. The program calculates net engine thrust, specific impulse and the flow properties at the mixing and expansion stations. In view of the fact that complete mixing and combustion rarely occur in a physical situation, cycle performance as calculated by this program was assumed to be the maximum that could be achieved.

The assumption of complete mixing and combustion at some unspecified distance downstream from the initial mixing plane permits one to ignore, in the analysis, the detailed interactions between the primary and secondary streams in the mixing section, and hence the "pumping" effect of the process on each of the entering streams. As will be shown later, this "pumping" action results in a fixed relationship between the operation of the mixing section and the operation of the inlet. The failure of the program to adjust to this matching requirement is a gross limitation of analyses of this type and often leads to large errors in cycle performance calculations. If, however, the matching requirements established

from the other analyses are satisfied, the program calculates cycle performance with acceptable accuracy.

#### Inviscid (Quasi-Two-Dimensional) Combustor Analysis

The inviscid analysis of the mixing section assumes that the primary and secondary streams interact in the absence of viscosity and mixing. The secondary stream is confined between the mixing duct wall and the primary plume boundary, which is likewise confined by the secondary stream. In other words, the two streams make their separate but mutually dependent ways through the duct, the primary based upon two-dimensional or axisymmetric characteristic-type flow, the secondary upon one-dimensional flow. The program calculates the flow properties of both streams in the duct for a given duct shape and stream condition at the entrance to the section and is also used to determine the entrance secondary stream condition resulting in choked secondary flow somewhere in the duct. It will be shown that this method of analysis adequately describes the operation of the combustor when the opportunity for mixing of the two streams is restricted by a short combustor length and the inviscid interaction is dominant.

#### Two Dimensional Mixing Analysis

The two-dimensional mixing program is the most sophisticated of the three and was developed in order to analyze and examine, in detail, the mixing and reaction resulting from the turbulent exchange processes. When the pluming action of the jet is strong and the opportunity for mixing is limited, the mixing produces a relatively minor perturbation on the combustor operation. However, when the pluming effect is negligible, i.e. when the nozzle is over-expanded in the duct, the mixing becomes dominant

in establishing combustor operating characteristics. The program computes a complete flow field map throughout the mixing zone including the axial and transverse gradients in flow properties, the location of the duct wall as a function of a prescribed pressure gradient and the thrust upon the duct. This program represents the most significant contribution to the state-of-the-art to evolve from this study and is a powerful tool in the analysis of shear type flows.

As previously stated, the operating conditions of the inlet and combustor must be matched in order for the calculated cycle performance to be valid. The general flow of information and the relationships between programs in the overall analysis are as shown in Figure 2.

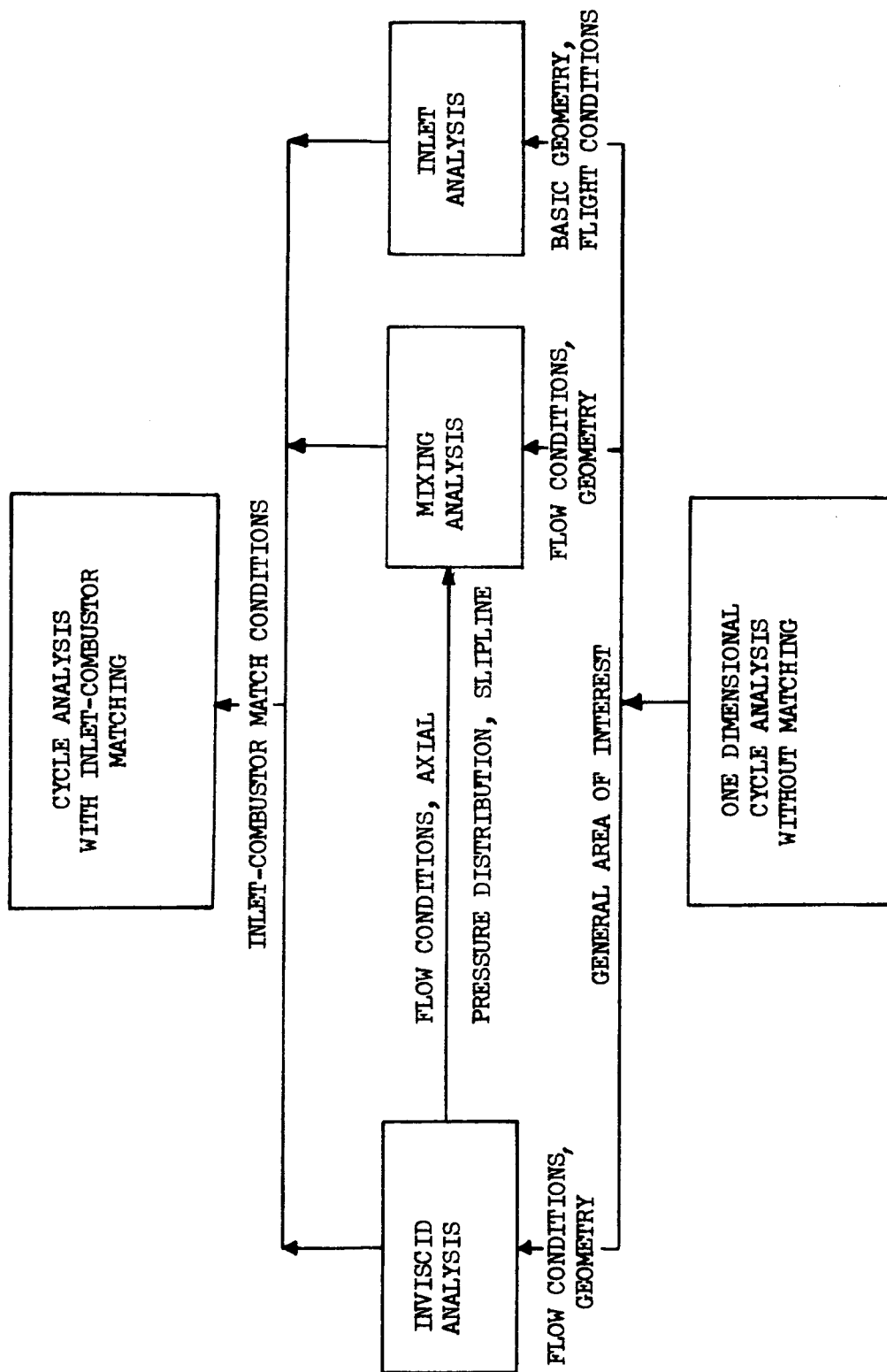


Figure 2 - Analysis Flow Diagram

## B. Analytical Models

### 1. One-Dimensional Cycle Analysis

The idealized one-dimensional analysis was developed and programmed for the IBM 709<sup>4</sup> to provide a fast, economical means of generating large quantities of data in order to determine the influences of various operating parameters on engine performance and to outline those areas not warranting further investigation. A complete description of the program and the details of operation are provided in Reference 7.

Flow Model: The flow model is as shown in Figure 3. The primary jet is provided by a conventional chemical rocket for which the exit conditions are fully known. The secondary stream is introduced into the inlet at a specified flow rate and total pressure recovery. The streams mix and combustion takes place between Stations 1 and 2 followed by expansion in the nozzle between Station 2 and Station e. The most serious limitation of this analysis is the failure of the program to adjust the secondary inlet conditions so as to be compatible with the operation of the mixing and combustion section. In a physical situation, the pumping action of the mixing process is of prime importance in influencing the secondary flow conditions.

Assumptions: The following assumptions were made in translating the physical system into a workable mathematical model:

- a. All streams are homogeneous and uniform
- b. The secondary stream is a perfect gas with a constant ratio of specific heats ( $\gamma = 1.4$ ).

8

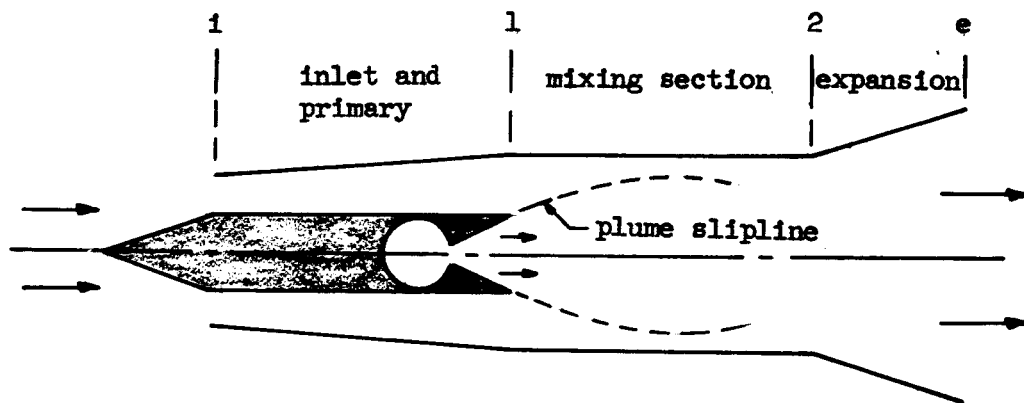


Figure 3 - Air-Augmented Rocket - Analytical Model

- c. Complete mixing and chemical equilibrium are achieved at Station 2 -- an unspecified distance downstream of the jet exit plane.
- d. The expansion between Stations 2 and e is isentropic.
- e. The pressure-area integral on the combustor wall is determined by use of the average pressure,

$$\int_1^2 PdA = \frac{P_2 + P_{1s}}{2} (A_2 - A_1)$$

- f. Friction and heat transfer between the streams and the walls are absent throughout the combustor and nozzles.

Program Options: The primary jet is described at its exit (pressure, area, velocity, total enthalpy and weight flow). The secondary stream is described through use of the various options as shown in Table 1.

The operation of the combustor section is described by specifying either its area ratio or pressure ratio. When the area ratio is specified, both a subsonic and supersonic solution are possible. The expansion from Station 2 to Station e may be specified by expansion to a pressure, an area, or an area ratio. The equilibrium sub-routine of the program allows the use of a large number of rocket propellants and has the capability of handling several hundred chemical species. The program requires estimates of the species concentrations at Station 2. Correctness of the estimates is not critical when there are no condensed phases; however, when condensed phases exist the estimates must be reasonably accurate in order that the equilibrium calculations converge.

TABLE 1  
SECONDARY FLOW INPUT OPTIONS

$P_{\infty}$	$T_{\infty}$	$A_{\infty}$	$V_{\infty}$	$M_{\infty}$	$T_{ls}^{\circ}$	$P_{ls}^{\circ}$	$H_{ls}^{\circ}$	$P_{ls}$	$A_{ls}$	$\dot{m}_s$	$M_{ls}$
x	x	x	x or x		x	x	x	x			
x	x	x	x or x		x	x	x		x		
x	x	x	x or x		x	x	x				x
x	x		x or x		x	x	x	x	x		
x	x		x or x		x	x	x	x		x	
x	x		x or x		x	x	x		x	x	
x	x		x or x		x	x	x		x		x
x	x		x or x		x	x	x			x	x

Calculation Technique: Several sample cases with the equations used are presented in detail in Reference 7. For the purposes of illustration, the equations and the technique of calculation will be presented here for an example with the following given conditions:

Primary Rocket

$$P_{1p}, A_{1p}, H_p^*, V_p, \dot{m}_p$$

Secondary

Same as Line 1, Table 1

Combustor

$$A_2 = a (A_{1s} + A_{1p}) = a (A_1), \text{ Trial } V_2 \text{ and } R_2$$

(Fixed combustor area ratio)

Expansion

$$A_e \text{ (Expansion to specified area)}$$

#### Inlet

The standard one-dimensional perfect gas isentropic flow and state equations are used for the calculation of the secondary flow conditions as follows:

$$\rho_\infty = \frac{P_\infty}{R T_\infty} \quad (1)$$

$$V_\infty = M_\infty (\gamma g R T_\infty)^{\frac{1}{2}} \quad (2)$$

$$\dot{m}_s = \dot{m} = \rho_\infty A_\infty V_\infty \quad (3)$$

$$M_{1s} = \left[ \frac{(P_{1s}^*)^{\frac{\gamma-1}{\gamma}} - (P_{1s})^{\frac{\gamma-1}{\gamma}}}{\frac{\gamma-1}{2} (P_{1s})^{\frac{\gamma-1}{\gamma}}} \right]^{\frac{1}{2}} \quad (4)$$

$$A_{1s} = \dot{m}_s \left[ \frac{P_{1s}^* \left( \frac{\gamma}{RT_{1s}^*} \right)^{\frac{1}{2}}}{\left( 1 + \frac{\gamma-1}{2} M_{1s}^2 \right)^{\frac{\gamma+1}{2(\gamma-1)}}} \right]^{-1} \quad (5)$$

$$T_{1s} = T_s^* \left( 1 + \frac{\gamma-1}{2} M_{1s}^2 \right)^{-1} \quad (6)$$

$$V_{1s} = M_{1s} (\gamma g R T_{1s})^{\frac{1}{2}} \quad (7)$$

The calculations proceed in the following steps:

1. Calculate  $\dot{m}_s$  from Equations (1), (2), and (3).
2. Calculate  $A_{1s}$  from Equations (4) and (5).
3. Calculate  $V_{1s}$  from Equations (6) and (7).

All necessary secondary stream conditions are now defined.

#### Combustor

The combustor solution is obtained by iteration from the conservation equations and the equations of state:

Conservation of Mass:

$$\dot{m}_2 = \rho_2 A_2 V_2 = \dot{m}_s + \dot{m}_p \quad (8)$$

Conservation of Momentum:

$$P_{1s} A_{1s} + \frac{\dot{m}_s V_{1s}}{g} + P_{1p} A_{1p} + \frac{\dot{m}_p V_{1p}}{g} + \int_1^2 P dA = P_2 A_2 + \frac{\dot{m}_s + \dot{m}_p}{g} V_2 \quad (9)$$

Conservation of Energy:

$$H_2^* = \frac{\dot{m}_s H_s^* + \dot{m}_p H_p^*}{\dot{m}_s + \dot{m}_p} \quad (10)$$

$$H_{2VEL} = H_2^* - \frac{V_2^2}{2gJ}$$

Equations of State:

$$T_2 = \frac{P_2}{\rho_2 R_2} \quad (11)$$

$$H_{2\text{EQUIL}} = f(P_2, T_2) \quad (12)$$

The steps of the calculation are as follows:

1. Select a trial  $V_2$
2. Calculate  $\rho_2$  from Equation (8)
3. Calculate  $P_2$  from Equation (9)
4. Select a trial  $R_2$
5. Calculate  $T_2$  from Equation (11)
6. Calculate  $R_2$  and  $H_{2\text{EQUIL}}$  as a function of  $P_2$  and  $T_2$ .  
This is accomplished in the equilibrium chemistry routine which is similar in technique to that described in Reference 8.
7. Repeat Steps 5 and 6 using new  $R_2$  until a constant value of  $R_2$  is reached.
8. Calculate  $H_{2\text{VEL}}$  from Equation (10)
9. Compare  $H_{2\text{VEL}}$  and  $H_{2\text{EQUIL}}$ .
10. Repeat Steps 1 through 9 until  $H_{2\text{VEL}} = H_{2\text{EQUIL}}$

Figure 4 shows a representative plot of  $H_{2\text{VEL}}$  and  $H_{2\text{EQUIL}}$  versus  $V_2$  for various combustor area ratios,  $a$ . Secondary flow conditions may be selected which, for a given area ratio, may produce no real solution, as represented by the lower  $a = 1.0$  curve. If  $a$  is increased sufficiently, two real solutions may then be found, one subsonic and one supersonic. At a unique value of  $a$ , the two real solutions are coincident at the sonic condition. The no-solution case, then, corresponds to the situation in which the combination of mixing and heat release "overchokes" the stream. This means that manipulation of

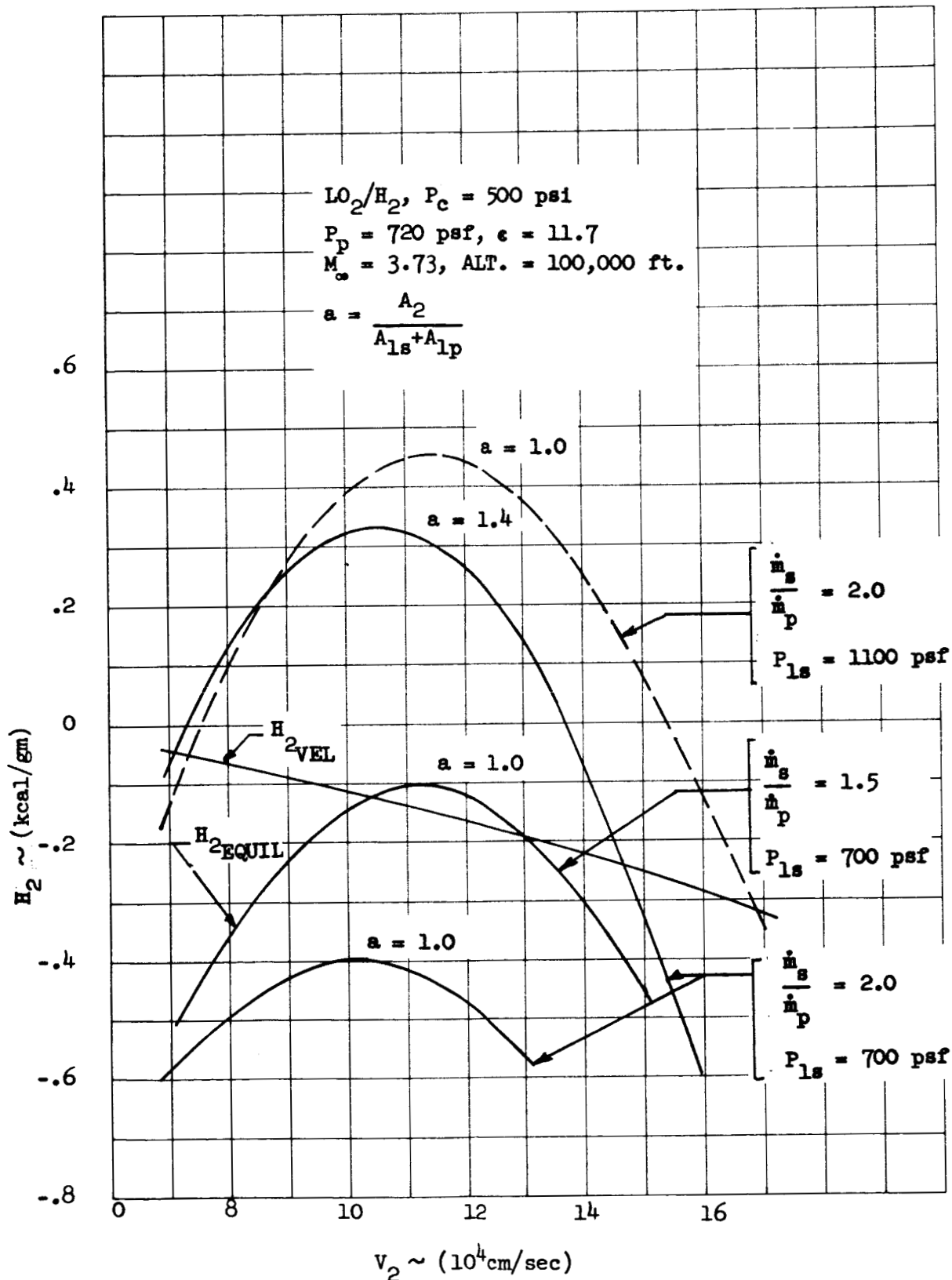


Figure 4 - One Dimensional Combustor Solutions

the secondary stream conditions is necessary before a proper solution can be obtained.

The program calculates either the subsonic or supersonic solution, if available, at the option of the user. If desired, a profile may be calculated in which  $V_2$  is varied in fixed steps between desired limits so as to produce a map as shown in the figure.

### Expansion

The expansion calculation to a fixed area is a standard one and involves iteration around the equations of state and conservation of mass and energy, maintaining entropy constant.

$$\dot{m}_e = \rho_e A_e V_e \quad (13)$$

$$V_e^2 = 2gJ(H_2^\circ - H_e) \quad (14)$$

$$S_e = S_2 = f(P_e, T_e) \quad (\text{Equilibrium Routine}) \quad (15)$$

$$H_e = f(P_e, T_e) \quad (\text{Equilibrium Routine}) \quad (16)$$

The steps of the calculation are as follows:

1. Select trial  $P_e$  and  $T_e$
2. Enter equilibrium routine and calculate  $S_e$ ,  $H_e$
3. Compare  $S_e$  with  $S_2$
4. Change  $T_e$
5. Repeat Steps 2, 3, and 4 until  $S_e = S_2$
6. Calculate  $V_e$  from Equation (14)
7. Calculate  $P_e$  from Equation of State. (1)
8. Calculate  $A_e$  from Equation (13)
9. Compare  $A_e$  with input  $A_e$
10. Repeat Steps 1 through 9 until the correct value of  $A_e$

is obtained and the stream properties are calculated.

Now that the exit conditions are determined, the engine performance is calculated from:

$$\text{THRUST} = (\dot{m}_s + \dot{m}_p)V_e - \dot{m}_s V_\infty + A_e(P_e - P_\infty) \quad (17)$$

$$I_{sp\text{AUG}} = \frac{\text{THRUST}}{\dot{m}_p} \quad (18)$$

No external drags such as spillage, cowl or skin friction are included in the calculations of net engine thrust.

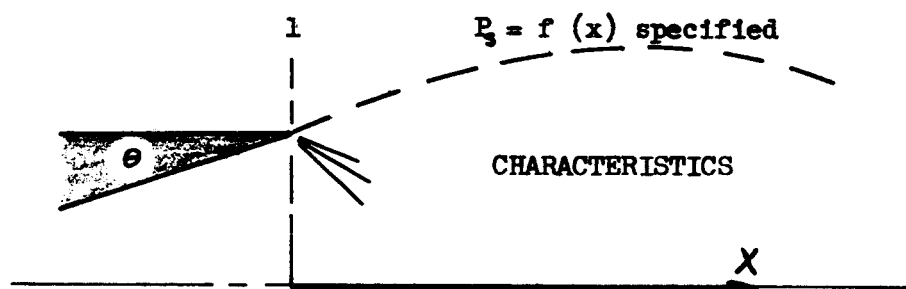
## 2. Inviscid Combustor Analysis (Quasi 2-D)

This program is a modification of a method of characteristics analysis previously developed by The Boeing Company, programmed for the IBM 709<sup>4</sup>, for the calculation of two-dimensional and axisymmetric perfect gas nozzle plumes in still air (SPURT A) and with supersonic external flow (SPURT X).

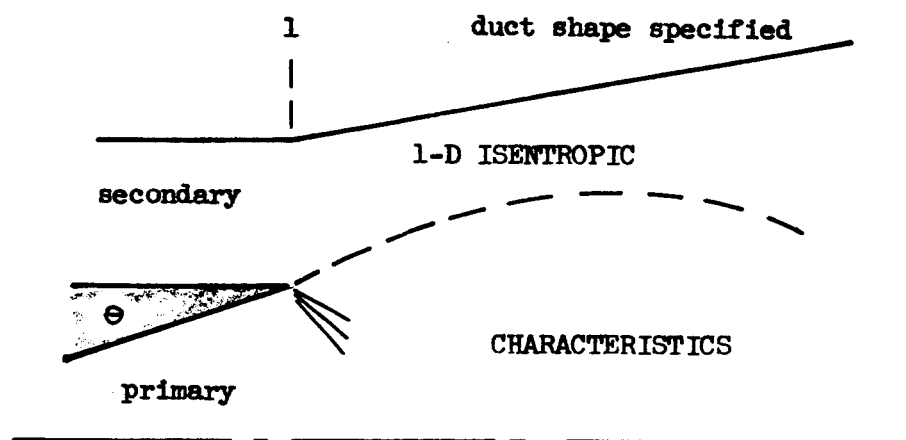
Flow Models: As a part of this study, SPURT A was modified so as to provide the two flow models shown in Figure 5. In the first, Ambient Pressure Input, the plume is calculated based upon a specified streamwise pressure distribution at the plume external streamline. In the second, Duct Shape Input, the plume shape is determined from inviscid interaction with the confined secondary stream. The secondary stream may be specified to be initially either subsonic or supersonic. The primary jet pressure must always be greater than the secondary pressure. A complete description of the program is given in Reference 9.

Assumptions: The assumptions used in this analysis are as follows:

1. The expansion of the plume is isentropic except that the program will handle one inward running shock wave.
2. The plume flow is a perfect gas of frozen composition, with a constant ratio of specific heats.
3. The secondary stream is a perfect gas with a constant ratio of specific heats.
4. The secondary stream is one dimensional and isentropic. This renders the secondary supersonic flow option invalid, in general, when the conditions are such as to produce shock and



Ambient pressure input



Duct shape input

Figure 5 - Flow Models, Quasi Two-Dimensional Analysis

expansion waves.

5. No mixing occurs between the two streams, nor is there friction or heat transfer in the system.

Inputs: The conditions of the jet are specified at the exit plane in terms of flow direction, temperature, pressure,  $\gamma$ , gas constant, and Mach number. The secondary conditions of weight flow, total temperature, and total pressure are defined. Both the axial pressure distribution in the case of Ambient Pressure Input and the duct shape in the case of Duct Shape Input may be specified in either polynomial or tabular form.

General Features: When the ambient axial pressure distribution is specified as the boundary condition for the characteristics network, the plume flow field is calculated based upon that streamline pressure distribution. When the duct shape input is used, the plume is calculated by an inviscid matching with the confined secondary stream such that the pressure of the external streamline and the one-dimensional secondary stream are equal and compatible with the secondary stream tube area formed between the duct wall and the plume. A similar technique has been reported by Addy (Reference 10). In general, it is desirable that the duct be either constant area or diverging in order that there be no forward facing surfaces which would produce a pressure drag on the duct itself. With the constant area or diverging duct, the plume tends to billow outward and then turn inward. If the secondary stream is subsonic initially, it will remain subsonic unless the plume causes sufficient constriction of the secondary stream tube to choke the flow. If this choking is not present, the ambient pressure, which during supersonic flight is less than the exit pressure of

the duct, will feed back upstream through the subsonic secondary flow and force a readjustment of the secondary conditions at the primary exit plane. This change will cause the plume shape to change so that the choking condition will occur.

Calculation Technique: The steps in the analysis of the Duct Shape Input problem are described based upon the following inputs:

#### Duct Shape

Coordinates in tabular or polynomial form.

#### Primary Jet

$$\left. \begin{array}{l} r_{lp}, R_{lp} \\ M_{lp}, P_{lp} \\ T_{lp}, \gamma_{lp} \end{array} \right\} \quad \text{Constant across jet exit}$$

$\theta$  May be varied across jet exit

#### Secondary

$$P_{1s}^*, T_s^*, \dot{m}_s, \gamma_s, R_s$$

The equations used in the calculation of the secondary stream are as follows:

$$A_s^* = \frac{0.1762 \dot{m}_s}{P_{1s}^* \left[ \frac{\gamma}{R_s T_s^*} \left( \frac{2}{\gamma+1} \right)^{\gamma+1/\gamma-1} \right]^{\frac{1}{2}}} \quad (19)$$

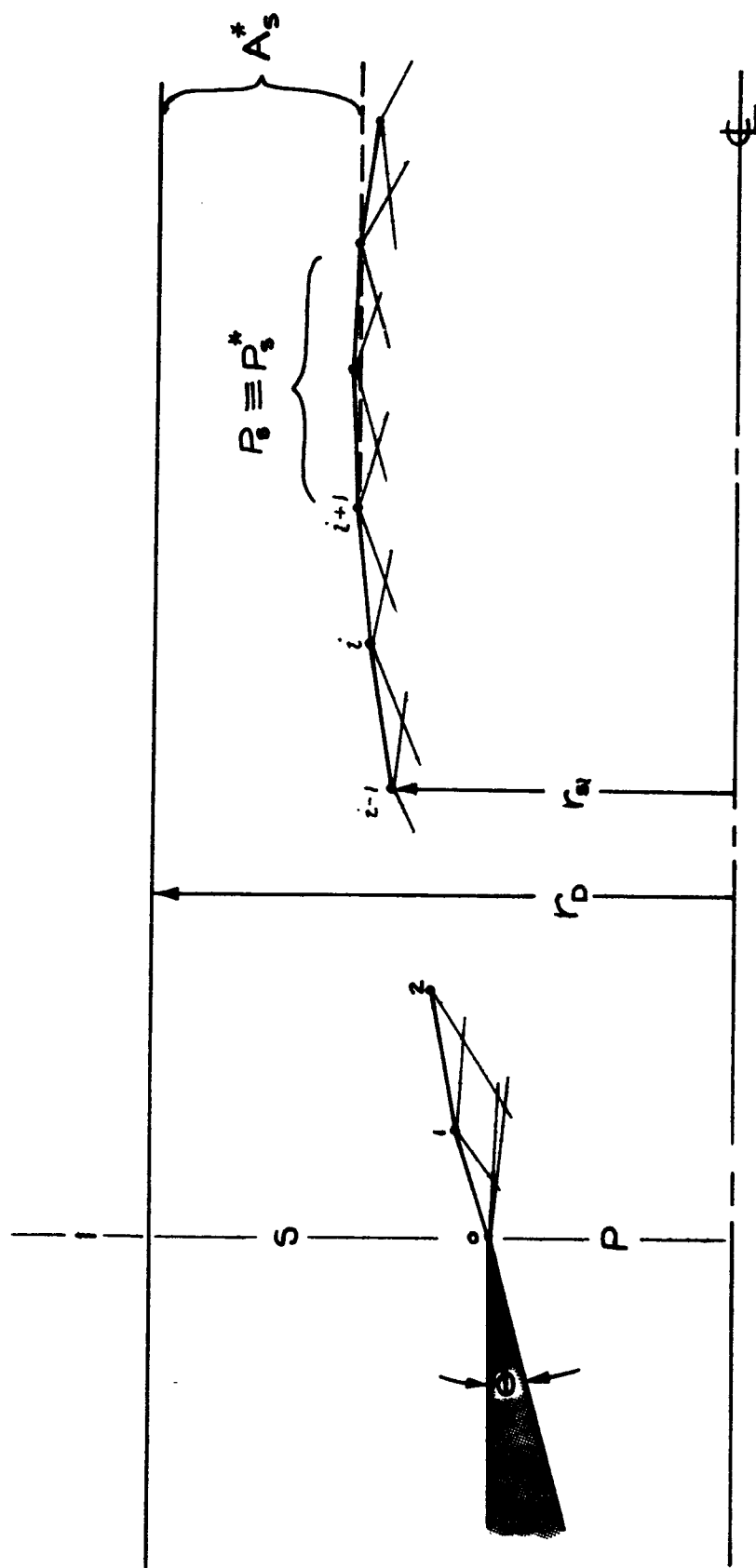
$$A_s = \pi (r_D^2 - r_{sL}^2) \quad (20)$$

$$\left( \frac{P_s}{P_s^*} \right)^{2/\gamma} - \left( \frac{P_s}{P_s^*} \right)^{\frac{1+\gamma}{\gamma}} = \left( \frac{A_s^*}{A_s} \right)^2 \left( \frac{\gamma-1}{2} \right) \left( \frac{\gamma+1}{2} \right)^{\frac{1+\gamma}{1-\gamma}} \quad (21)$$

The calculations performed for the primary jet are handled entirely in SPURT A which is a standard method-of-characteristics program and is fully described in Reference 9.

The calculation procedure is as follows: (See Figure 6)

1. Calculate  $A_g^*$  from Equation (19)
2. Calculate  $A_{1s}$  from Equation (20)
3. Calculate  $P_{1s}$  from Equation (21) (This equation has two real roots, one subsonic and one supersonic. Either is available at the option of the user).
4. Enter SPURT A and calculate the initial slope of the plume slipline, based upon a Prandtl-Meyer expansion from the jet pressure ( $P_{lp}$ ) to  $P_{1s}$ .
5. Commence calculation of characteristics net in SPURT A.
6. At the intersection of each left running characteristic with the slipline, points 1, 2, ....1,.... calculate  $A_{s1}$  from Equation (20) (the slipline extension is based upon a linear extrapolation in SPURT A from the last two points).
7. Calculate  $P_{s1}$  from Equation (21). Since Equation (21) has two real roots, a selection must be made as to which to choose as the solution, as with  $P_{1s}$ . If  $P_{1s} < P_g^*$ , i.e.,  $M_{1s} > 1$  (input option) then the supersonic solution to  $P_{s1}$  is always used. However, if  $P_{1s} > P_g^*$  ( $M_{1s} < 1$ ), the mode of solution is based upon a linear extrapolation of  $P_{s1}$  from the previous two points. If the extrapolated pressure is greater than  $P_g^*$ , then the subsonic solution is determined for that point. If the extrapolated



pressure is less than  $P_g^*$ , the supersonic solution is determined for that and all succeeding points.

8. Enter SPURT A and calculate a value of  $P_{s1_i}$  in the characteristics net based upon the location of point i on the slipline.
9. Compare  $P_{s_i}$  with  $P_{s1_i}$ .
10. Change  $r_{s1_i}$ .
11. Repeat Steps 6 through 9 until  $P_{s_i} = P_{s1_i}$ .
12. Calculate all secondary properties using standard isentropic perfect gas relations.

As will be discussed later, it is believed that the best operation of the engine cycle, from a performance standpoint, results from a configuration such that the secondary Mach number at the entrance to the combustor is in the low subsonic region ( $M_{1s} = 0.1 - 0.3$ ). An essential function of the combustor then is to restrict or choke the secondary flow in order to produce the high back pressure on the inlet necessary to sustain this low secondary Mach number condition. With respect to this condition, there are three possible situations which can exist analytically in the combustor. The first occurs when the initial pressure differential between primary and secondary is low, and the corner expansion of the jet at the jet exit lip is low. In this case, the plume width is somewhat restricted and reaches its maximum diameter without ever having choked the secondary. The secondary stream, having entered with a low Mach number, is accelerated to the point of maximum constriction and then decelerated, remaining all the while

subsonic. This is not a physically possible solution because of the feedback of ambient pressure discussed previously in this section.

The opposite situation results from a large pressure differential at the primary jet exit, with a large flow turn at the corner of the nozzle lip. This produces an over constriction of the secondary stream tube by the plume such that this stream tube area is less than the secondary critical area for sonic flow. This situation would force readjustment of the secondary flow conditions.

The third case, and the one which is sought in the use of this program, occurs when the inlet conditions and the duct geometry are such that the initial plume expansion and subsequent recompression are just sufficient to exactly choke the secondary stream at the point of maximum constriction by the plume. Analytically and physically this involves the transition of the stream from subsonic to supersonic flow.

In the analysis, this transition was initially handled as outlined in Step (7) above. Whenever the extrapolated pressure was equal to or less than  $P_g^*$  the supersonic solution was obtained. Another control was that whenever  $A_{s_1}$  was less than  $A_g^*$ , the program stopped because of the impossibility of the solution. Unfortunately, out of several hundred cases run, this transition was never achieved in the analysis because whenever the transition point was reached, and  $P_{s_1} < P_g^*$ , then always  $A_{s_1} < A_g^*$ . Consequently, the control on  $A_{s_1}$  was relaxed so that

when  $0.9 A_g^* < A_{g_1} < A_g^*$ , the program continued with  $P_{g_1}$  identically equal to  $P_g^*$ . At the point where the plume converged sufficiently so that the secondary stream tube area as defined by the duct wall and plume slipline was greater than the critical choking area, the calculation proceeded as before, but using the supersonic solution to Equation (20), rather than the subsonic one.

Of these three flow situations which can analytically exist in the combustor, only the choked case (transition from subsonic to supersonic flow) has any real significance in the physical situations of interest in this study. The reason for this situation is fully discussed in Section C.2. The program is used to determine the initial secondary conditions for a given primary-combustor combination which produces the choked secondary. Using this sonic criteria, it is possible to determine the operating characteristics of the combustor insofar as the inviscid interaction of the plume and secondary stream is concerned. The inviscid interaction tends to dominate over the mixing process when either the duct is very short and the opportunity for mixing is limited, or when the secondary stream area is very large in comparison with the primary plume.

The operation of the combustor is more completely described in the Combustor Analysis Section (C.2) of this report.

### 3. Two-Dimensional Mixing Analysis

#### a. General Discussion

The development of the mixing analysis described herein parallels that of other investigators except that consideration is given to the following factors: (1) confinement of the secondary air stream by a duct, which necessitates the consideration of axial pressure gradients, and (2) chemical reactions between the species comprising the rocket exhaust and the air stream. Libby (Reference 11 ) and Vasiliu (Reference 12 ), for example, have analyzed the unconfined mixed flow field assuming equilibrium and non-equilibrium chemistry, respectively. Mikhail (Reference 13 ), on the other hand, has treated the mixing of coaxial incompressible streams in a duct but has assumed no chemical reactions. The present analysis provides a method for calculating the chemically reactive mixed flow field within a duct of arbitrary geometry.

The flow model employed in the development of the analysis is presented in Figure 7 . It is assumed that at the exit plane of the rocket nozzle the air stream flows in a direction parallel to the axis of symmetry. At the periphery of the nozzle exit, where the two streams first come into contact, the mixing region begins and widens along both sides of the plume slipline as the flow moves downstream. As the mixing region widens the inner boundary moves inward toward the jet centerline and the outer boundary outward toward the duct wall, until at a certain axial distance the mixing region may be considered to occupy the entire duct. As the flow proceeds in the downstream direction the non-uniformities in the flow change so that the

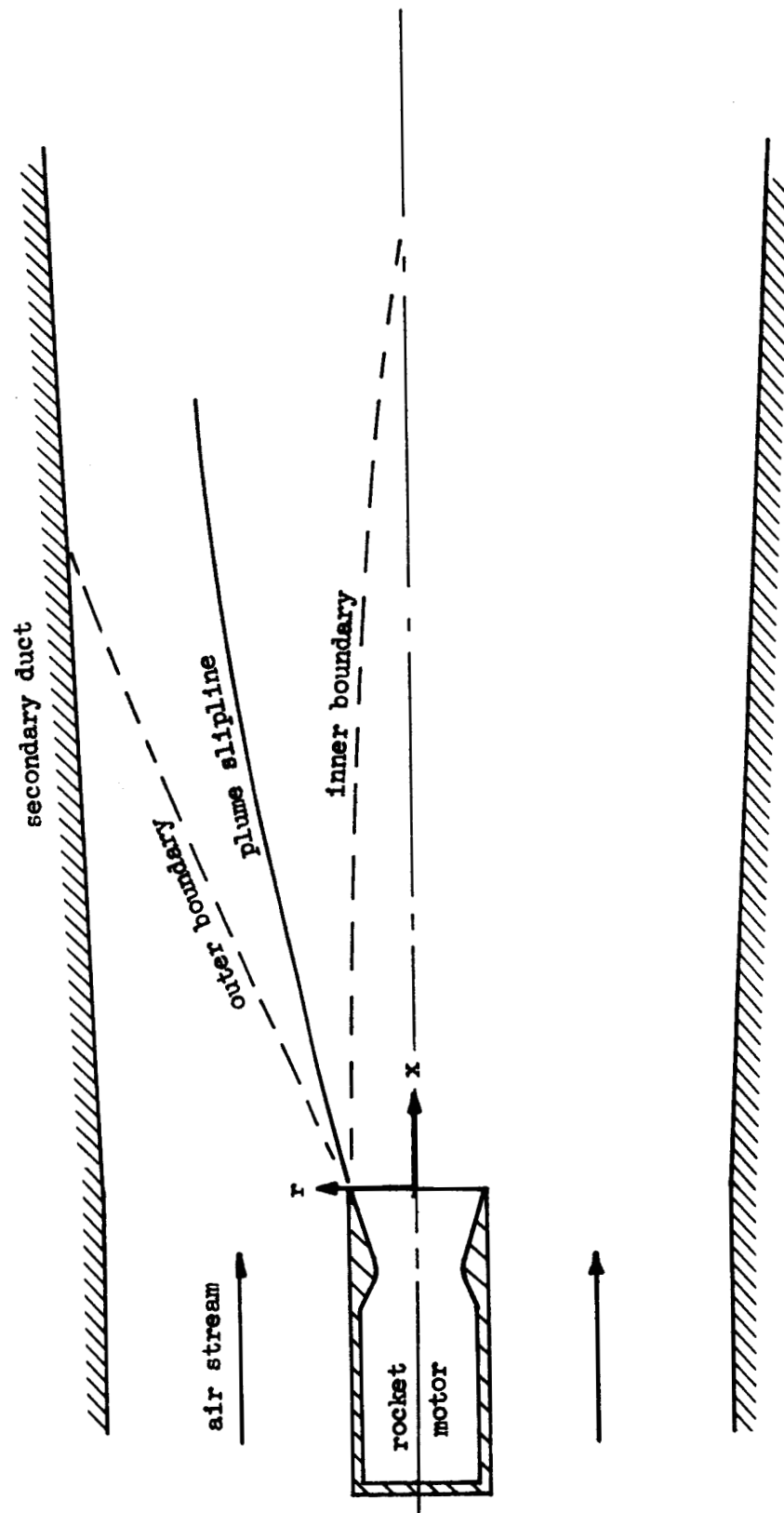


Figure 7 - Two Dimensional Mixing Flow Model

radial gradients of velocity, temperature, and composition approach zero, corresponding to a completely mixed flow. In the areas outside the mixing region, the flow is considered to be inviscid with uniform velocity, temperature, and composition in the radial direction. Within the mixing region turbulent transport processes are assumed to prevail with all molecular transfer considered negligible. This assumption is justified for the problem under consideration since the flow is generally turbulent, and the turbulent transport coefficients are usually several orders of magnitude greater than their molecular counterparts.

The major assumptions employed in the development of analysis are as follows:

- a. Axisymmetric or two-dimensional flow model.
- b. The entire flow field is turbulent.
- c. Prandtl's boundary layer equations are applicable.
- d. The perfect gas law is valid.
- e. Negligible radial pressure gradient across the mixing zone.
- f. Mass transfer due to thermal and pressure gradients are negligible.
- g. The turbulent Prandtl and Lewis numbers are constant but may have values other than unity.
- h. The boundary layer which develops between the internal mixed flow and the combustor wall is neglected. The boundary layers in the primary rocket nozzle and the air stream at the initial point of contact, however, may be considered.

## b. Fundamental Equations

The fundamental equations which describe the flow field in the mixing region are taken to be the turbulent boundary layer equations with the properties therein being the time-averaged values. Thus:

Global Continuity:

$$\frac{\partial(\epsilon u r^\delta)}{\partial x} + \frac{\partial(\epsilon v r^\delta)}{\partial r} = 0 \quad (22)$$

Species Continuity:

$$\epsilon u \frac{\partial C_k}{\partial x} + \epsilon v \frac{\partial C_k}{\partial r} = \frac{1}{r^\delta} \frac{\partial}{\partial r} \left[ \frac{r^\delta \epsilon_v Le_t}{Pr_t} \frac{\partial C_k}{\partial r} \right] + \dot{\omega}_k \quad (23)$$

Momentum Equation:

$$\epsilon u \frac{\partial u}{\partial x} + \epsilon v \frac{\partial u}{\partial r} = - \frac{\partial P}{\partial x} + \frac{1}{r^\delta} \frac{\partial}{\partial r} \left( \epsilon_v r^\delta \frac{\partial u}{\partial r} \right) \quad (24)$$

Energy Equation:

$$C_p \left( \epsilon u \frac{\partial T}{\partial x} + \epsilon v \frac{\partial T}{\partial r} \right) = u \frac{\partial P}{\partial x} + \epsilon_v \left( \frac{\partial u}{\partial r} \right)^2 + \frac{1}{r^\delta} \frac{\partial}{\partial r} \left[ C_p r^\delta \frac{\epsilon_v}{Pr_t} \frac{\partial T}{\partial r} \right] + \epsilon_v \frac{Le_t}{Pr_t} \sum_k C_{p_k} \frac{\partial T}{\partial r} \frac{\partial C_k}{\partial r} - \sum_k \dot{\omega}_k h_k \quad (25)$$

(For notation see Nomenclature). The exponent  $\delta$ , for the terms  $r^\delta$  makes the equations applicable for either two-dimensional or axisymmetric flow.

In solving the above equations using the finite difference technique, it is convenient to transform the equations utilizing the Von Mises transformation. Thus, introduction of the stream function  $\psi$ , defined from the equations

$$\left( \frac{\partial \psi}{\partial r} \right)_x = \epsilon u r^\delta \quad (26)$$

$$\left( \frac{\partial \psi}{\partial x} \right)_r = - \epsilon v r^\delta \quad (27)$$

is seen to satisfy equation (22) identically. The transformation of the remaining equations is accomplished by noting that

$$\left(\frac{\partial f}{\partial r}\right)_x = \left(\frac{\partial \psi}{\partial r}\right)_x \left(\frac{\partial f}{\partial \psi}\right)_x = \rho u r^\delta \left(\frac{\partial f}{\partial \psi}\right)_x$$

and

$$\begin{aligned} \left(\frac{\partial f}{\partial x}\right)_r &= \left(\frac{\partial \psi}{\partial x}\right)_r \left(\frac{\partial f}{\partial \psi}\right)_x + \left(\frac{\partial f}{\partial x}\right)_\psi \\ &= -\rho v r^\delta \left(\frac{\partial f}{\partial \psi}\right)_x + \left(\frac{\partial f}{\partial x}\right)_\psi \end{aligned}$$

where  $f$  represents any of the dependent variables. Hence, the transformed conservation equations become

Species Continuity:

$$\frac{\partial C_k}{\partial x} = \frac{\partial}{\partial \psi} \left[ \frac{\epsilon_v k \epsilon_c}{\rho r_\tau} \rho u r^{2\delta} \frac{\partial C_k}{\partial \psi} \right] + \frac{\dot{w}_k}{\rho u} \quad (28)$$

Momentum Equation:

$$\frac{\partial u}{\partial x} = -\frac{1}{\rho u} \frac{dP}{dx} + \frac{\partial}{\partial \psi} \left[ \epsilon_v \rho u r^{2\delta} \frac{\partial u}{\partial \psi} \right] \quad (29)$$

Energy Equation:

$$\begin{aligned} \frac{\partial T}{\partial x} &= -\frac{1}{\rho C_p} \frac{dP}{dx} + \frac{\epsilon_v \rho u r^{2\delta}}{C_p} \left(\frac{\partial u}{\partial \psi}\right)^2 + \frac{1}{C_p} \frac{\partial}{\partial \psi} \left[ C_p \frac{\epsilon_v \rho u r^{2\delta}}{\rho r_\tau} \frac{\partial T}{\partial \psi} \right] + \\ &\quad \frac{\rho u r^{2\delta}}{C_p} \frac{\epsilon_v k \epsilon_c}{\rho r_\tau} \sum_{i=1}^K C_{p,i} \frac{\partial T}{\partial \psi} \frac{\partial C_i}{\partial \psi} - \frac{1}{\rho u C_p} \sum_{i=1}^K \dot{w}_i h_i \end{aligned} \quad (30)$$

Thus, a system of  $K + 4$  equations (including the equation of state) are available for determining the unknown parameters  $u$ ,  $t$ ,  $C_k$ ,  $\dot{w}_k$ ,  $\epsilon_v$ , and  $\rho$ .  $K$  is the total number of species comprising the gas streams. A solution may be obtained, therefore, if appropriate expressions for the parameters  $\dot{w}_k$  and  $\epsilon_v$  are available in terms of the remaining unknown parameters. Such expressions will be developed later in this section. However, for the present, these parameters will be retained in this present form with the

assumption that suitable expressions are available.

c. Development of the Finite Difference Equations

The finite difference technique utilized in solving the above equations consists of replacing the partial derivatives by finite difference ratios, which is equivalent to replacing the continuous flow system by a network of finite elements, hereafter referred to as the grid network. For example, consider the system illustrated in Figure 8, wherein is shown a grid network with a radial grid size of  $\Delta\psi$  and an axial grid size of  $\Delta x$ . Assume that the values of the flow parameters are known at the grid points designated as  $m, n$ ;  $m, n-1$ ; and  $m, n+1$  along the line denoted as  $x = m$ , hereafter referred to as front  $m$ . It is desired to find values of the flow properties at the grid point  $m+1, n$  located on the  $m+1$  front.

Following Wu (Reference 14), the  $x$ -derivative at the midpoint between  $m, n$  and  $m+1, n$  may be expressed as

$$\frac{\partial f}{\partial x} = \frac{f_{m+1,n} - f_{m,n}}{\Delta x} \quad (31)$$

where  $f$  represents any of the dependent variables. The  $\psi$ -derivative is expressed as an average difference approximation, thus

$$\frac{\partial f}{\partial \psi} = \frac{f_{m,n+1} - f_{m,n-1}}{2 \Delta \psi} \quad (32)$$

The second derivative with respect to  $\psi$  is given by the finite difference approximation

$$\frac{\partial^2 f}{\partial \psi^2} = \frac{f_{m,n+1} - 2f_{m,n} + f_{m,n-1}}{\Delta \psi^2} \quad (33)$$

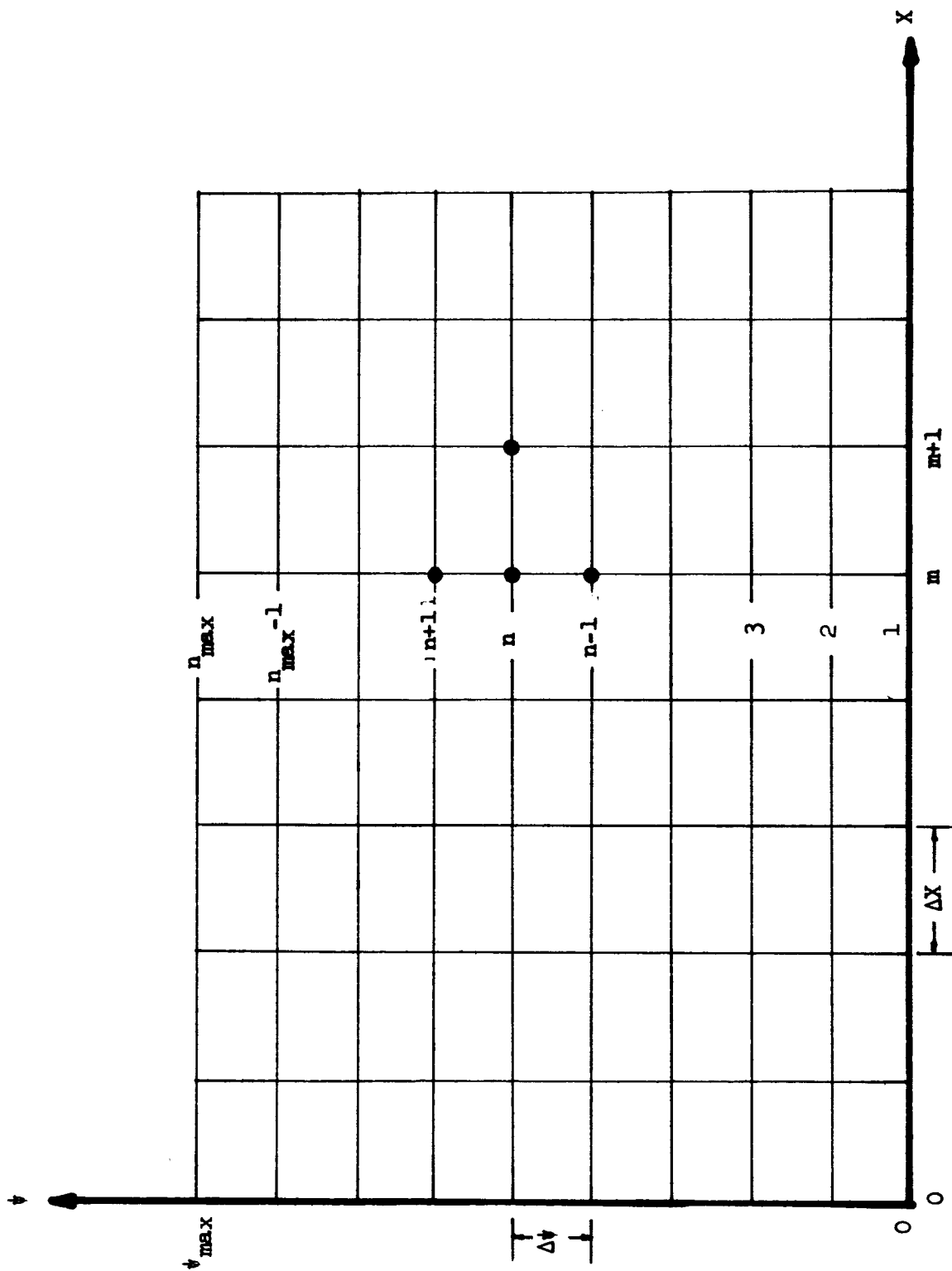


Figure 8 - Finite Difference Grid Network

The product terms are approximated by

$$\frac{\partial f}{\partial \psi} \cdot \frac{\partial g}{\partial \psi} = \frac{(f_{m,n+1} - f_{m,n-1}) \cdot (g_{m,n+1} - g_{m,n-1})}{4 \Delta \psi^2} \quad (34)$$

Substituting the above approximations for the derivatives in equations (28) through (30) and rearranging terms, yields

$$\begin{aligned} C_{k,m+1,n} = & C_{k,m,n} + \frac{\Delta x}{\Delta \psi^2} \left( eur^{2\delta} \epsilon_v \frac{Le_t}{Pr_t} \right)_{m,n} \cdot (C_{k,m,n+1} - 2C_{k,m,n} + C_{k,m,n-1}) + \\ & \frac{\Delta x}{4\Delta \psi^2} \left[ \left( \frac{\epsilon_v Le_t}{Pr_t} \right)_{m,n+1} \cdot \{ (eur^{2\delta})_{m,n+1} - (eur^{2\delta})_{m,n-1} \} \cdot (C_{k,m,n+1} - C_{k,m,n-1}) + \right. \\ & \left. \left\{ \left( \frac{\epsilon_v Le_t}{Pr_t} \right)_{m,n+1} - \left( \frac{\epsilon_v Le_t}{Pr_t} \right)_{m,n-1} \right\} (C_{k,m,n+1} - C_{k,m,n-1}) (eur^{2\delta})_{m,n} \right] + \left( \frac{\dot{w}_k \Delta x}{\rho u} \right)_{m,n} \quad (35) \end{aligned}$$

$$\begin{aligned} u_{m+1,n} = & u_{m,n} - \left( \frac{\Delta x g}{\rho u} \right)_{m,n} \left( \frac{dP}{dX} \right)_m + \frac{\Delta x}{\Delta \psi^2} \left( eur^{2\delta} \epsilon_v \right)_{m,n} \cdot \\ & (u_{m,n+1} - 2u_{m,n} + u_{m,n-1}) + \frac{\Delta x}{4\Delta \psi^2} \left[ \epsilon_{v,m,n} \{ (eur^{2\delta})_{m,n+1} - (eur^{2\delta})_{m,n-1} \} \right. \\ & \left. (u_{m,n+1} - u_{m,n-1}) + (eur^{2\delta})_{m,n} (\epsilon_{v,m,n+1} - \epsilon_{v,m,n-1}) (u_{m,n+1} - u_{m,n-1}) \right] \quad (36) \end{aligned}$$

$$\begin{aligned} T_{m+1,n} = & T_{m,n} + \left( \frac{\Delta x}{J \rho c_p g} \right)_{m,n} \left( \frac{dP}{dX} \right)_m + \\ & \frac{\Delta x}{4\Delta \psi^2} \left( eur^{2\delta} \right)_{m,n} \left[ \frac{(u_{m,n+1} - u_{m,n-1})^2}{(c_p g J)_{m,n}} + \right. \\ & 4\epsilon_{v,m,n} (T_{m,n+1} - 2T_{m,n} + T_{m,n-1}) + \left\{ \left( \frac{\epsilon_v}{Pr_t} \right)_{m,n+1} - \right. \\ & \left. \left( \frac{\epsilon_v}{Pr_t} \right)_{m,n-1} + \left( \frac{\epsilon_v}{eur^{2\delta} c_p Pr_t} \right)_{m,n} \cdot \{ (eur^{2\delta} c_p)_{m,n+1} - \right. \\ & \left. \left. (eur^{2\delta} c_p)_{m,n-1} \} \} \cdot (T_{m,n+1} - T_{m,n-1}) + \right. \\ & \left. \left( \frac{\epsilon_v Le_t}{c_p Pr_t} \right)_{m,n} \cdot c_{p,i,m,n} (T_{m,n+1} - T_{m,n-1}) \cdot (c_{i,m,n+1} - \right. \\ & \left. c_{i,m,n-1}) \right] - \left( \frac{\Delta x}{\rho c_p} \right)_{m,n} \dot{w}_i h_{i,m,n} \quad (37) \end{aligned}$$

Thus, since all the parameters involved in the right-hand side of the above equations are known, it is possible to determine the velocity, temperature, and concentrations of the species at the  $m + 1$  front. Since it is assumed that the axial pressures are given, the density may also be obtained from the equation of state. The solutions in the physical plane  $(x, r)$  are obtained by considering the definition of the stream function. Thus, for a fixed  $x$ , the radial coordinate to any  $\psi$ -line is given by:

$$r = \left[ r_0^{\delta+1} + (\delta + 1) \int_0^{\psi} \frac{d\psi}{\rho U} \right]^{1/\delta+1} \quad (38)$$

where  $r_0$  is the radius corresponding to the reference streamline ( $\psi = 0$ ). The reference streamline may be specified as either being coincident with the centerline of the flow system, or coincident with the plume slipline as determined from the inviscid method of characteristics program described previously.

The technique employed in solving for the flow properties throughout the grid network is as follows. At the first front ( $x = 0$ ) it is assumed that all the flow properties are given -- these properties are termed the initial conditions. In addition, at the second front, it is assumed that the properties are known on the reference  $\psi$ -line ( $\psi = 0$ ) and the maximum  $\psi$ -line ( $\psi_{\max}$ ) --- these properties are termed the boundary conditions. Employing Equations (35) through (37), the flow properties at the second front are then calculated beginning with the grid point  $m = 2$ ,  $n = 2$ , and ending with the grid point  $m = 2$ ,  $n = n_{\max} - 1$ . The boundary conditions at the second front are obtained by assuming

that the flow outside the mixing region is inviscid. For those fronts where the mixing region, as defined by concentration profiles, extends to either the duct wall or the jet centerline, the corresponding boundary condition is obtained by specifying that the radial gradients of all flow properties are zero. Application of the above technique for each successive front gives the flow properties throughout the entire grid network.

d. Eddy Viscosity

Before the above finite difference equations can be solved, it is necessary that an expression for the eddy viscosity  $\epsilon_v$ , be established in terms of parameters which are known or readily available. Such expressions have been developed utilizing Prandtl's mixing length theory with the assumption that the eddy kinematic viscosity  $\epsilon_v/\rho$ , is constant across the mixing region. According to Prandtl the eddy viscosity may be expressed as

$$\epsilon_v = k b \rho (u_{max} - u_{min}) \quad (39)$$

where  $k$  is a proportionality factor,  $b$  is the width of the mixing zone, and  $u_{max} - u_{min}$  is the difference between the maximum and minimum velocities in the mixing region. Setting  $b = cx$  equation (39) becomes

$$\begin{aligned} \epsilon_v &= k c x \rho (u_{max} - u_{min}) \\ &= K x \rho (u_{max} - u_{min}) \end{aligned} \quad (40)$$

where the product of the two proportionality factors  $kc$ , is replaced by another proportionality factor  $K$ . Following Schlichting (Reference 15), the constant  $K$  may be expressed in terms of the similarity parameter  $\sigma$ . Thus

$$K = \frac{U_{max} + U_{min}}{4\sigma^2(U_{max} - U_{min})}, \quad (41)$$

which when substituted into equation (40) yields

$$\epsilon_v = \frac{ex(U_{max} - U_{min})}{4\sigma^2} \quad (42)$$

According to Reichardt's theory (Reference 16) a similar expression for  $\epsilon_v$  may be obtained, thus

$$\epsilon_v = \epsilon_0 e^{(C + x/L)^n}, \quad (43)$$

where  $\epsilon_0$  is a constant referred to as Reichardt's coefficient, C is a constant which accounts for a virtual origin of the mixing region, L is a reference length, and n is a number having a value between 0 and 1 depending upon the degree of mixing. The constant C may be assumed to account for the boundary layers that build-up in the two streams prior to the point of initial contact ( $x = 0$ ) which produce, in effect, a mixing region of finite width at  $x = 0$ . For the case where  $C = 0$  and  $n = 1$ , as generally is assumed, equation 43 becomes

$$\epsilon_v = \epsilon_0 e^{x/L} \quad (44)$$

Equating equations (42) and (44) and solving for  $\epsilon_0$  gives

$$\epsilon_0 = \frac{L(U_{max} - U_{min})}{4\sigma^2} \quad (45)$$

Experimentally determined values of  $\sigma$  for free jets exhausting into a quiescent atmosphere have been obtained for various jet Mach numbers ranging up to approximately 3.0 (Reference 17).

Figure 9 illustrates the variation of  $\sigma$  with jet Mach number for a jet exhausting into still air. The solid line faired through the experimental data was originally presented in Reference 17. The dashed line illustrates the estimated variation of  $\sigma$  with Mach number as given by Korst (Reference 18). The

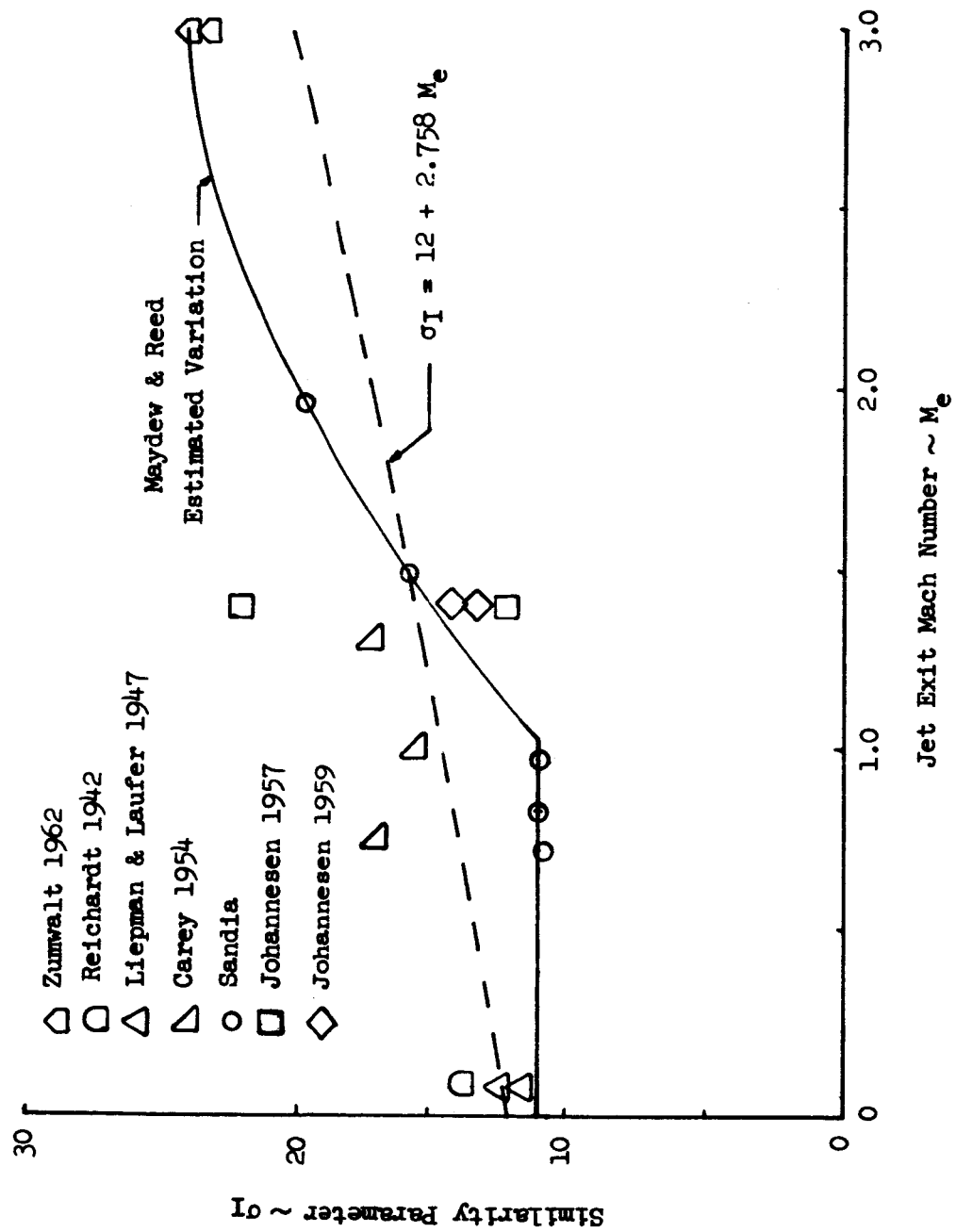


Figure 9 - Experimental and Theoretical  $\sigma$  Values for Free Jets

majority of the experimental data were obtained with air jets having temperatures approximately equal to that of the ambient air. For Mach numbers less than unity the value of  $\sigma$  has been relatively well established as being  $\sigma = 12.0$ . For Mach numbers greater than unity, the data illustrate that  $\sigma$  increases considerably. The scatter in the data indicate that insufficient experimental data are available to accurately predict  $\sigma$  values for free jets in the high Mach number range.

For the turbulent mixing between two compressible coaxial streams, analytical attempts (Reference 19) have resulted in relating the two-stream  $\sigma$  value to an "equivalent" single stream  $\sigma$  value and the velocity ratio between the two streams. The equivalent single stream value is obtained from Korst's empirical relationship

$$\sigma_T = 12 + 2.758 M_{T_a} \quad (46)$$

where  $M_{T_a}$  is an equivalent single stream Mach number related to the jet stream Crocco number as shown in Figure 10. Also shown in Figure 10 is the ratio of the aforementioned two  $\sigma$  values as a function of the velocity ratio between the two streams; indicating that the two stream  $\sigma$  value increases with increasing velocity ratio. This trend has also been established from experimental data. However, it should be noted that insufficient data are available for adequate correlation with the above theory, and therefore, the theoretical values should be used with reservation.

Since experimental data for predicting two stream  $\sigma$  values are

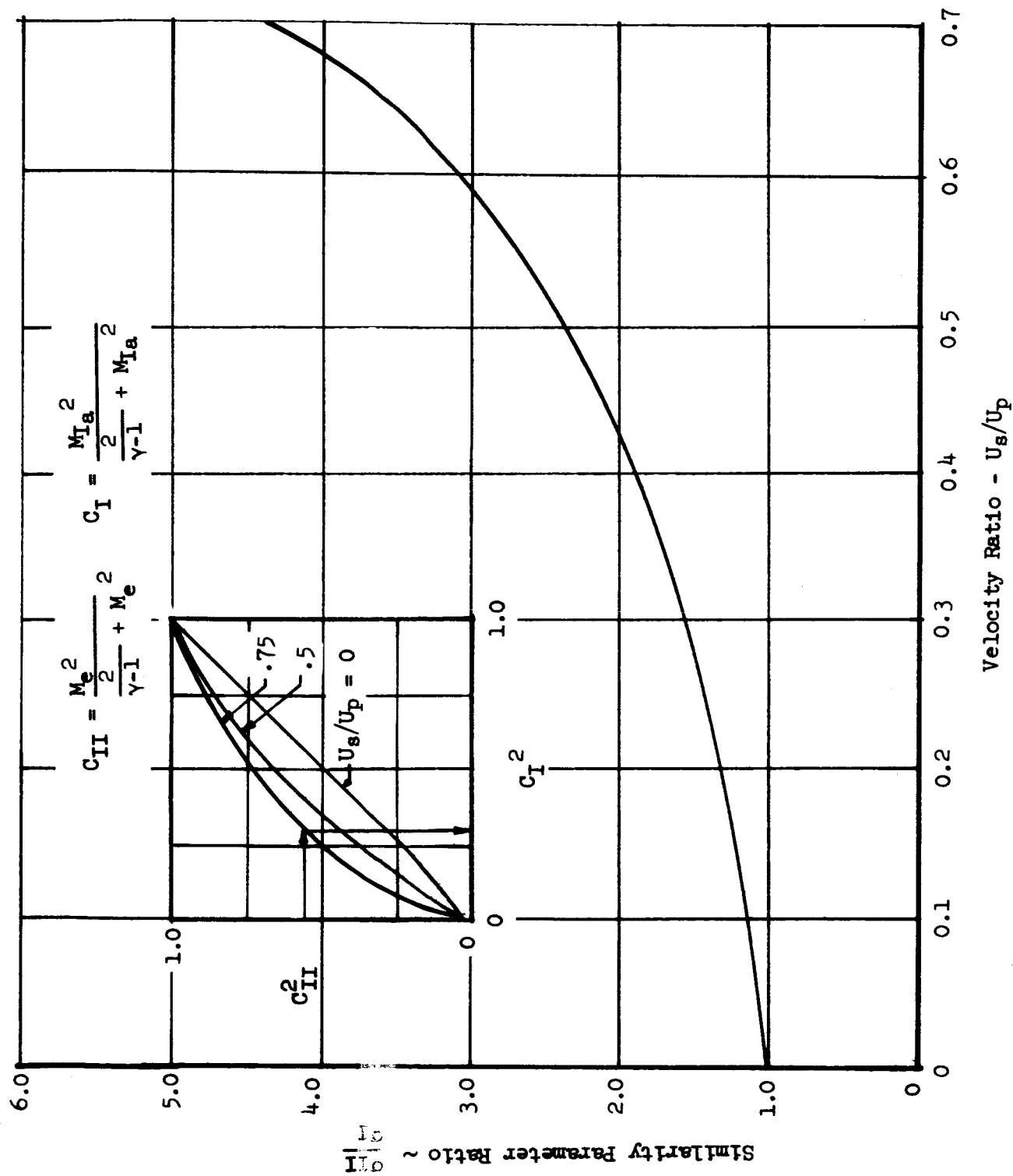


Figure 10 - Theoretical Effect of Velocity Ratio on Similarity Parameter Ratio

not available the above technique for evaluating  $\sigma$  has been adopted herein with the exception that the equivalent single stream  $\sigma_I$  value is obtained from Figure 9 corresponding to the equivalent single stream Mach number.

e. Chemical Model

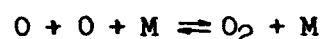
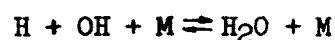
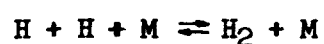
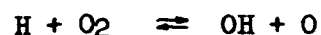
General

In considering the chemical aspects of the problem two choices of chemical behavior are available; namely, equilibrium or nonequilibrium chemistry. Herein, both chemical models are independently treated with the assumption that the external stream is air and the rocket exhaust contains only the species  $H_2O$ ,  $H_2$ ,  $O_2$ ,  $CO$ , and  $CO_2$ . Since high velocities are encountered in rocket exhaust jets it appears that nonequilibrium chemistry would prevail throughout most of the flow field. The most accurate analysis should, therefore, be based upon nonequilibrium flow including the complicated chain reaction equations describing the chemical reaction mechanism. However, in view of the complexity of such an analysis and the resulting lengthy calculations, it is advantageous to use equilibrium chemistry whenever that choice leads to accurate results. In the discussion that follows the equations for both equilibrium and nonequilibrium flow are developed and the results compared.

Nonequilibrium Chemistry

For nonequilibrium chemistry the net rate of production of the species  $w_k$ , is determined using the methods of theoretical reaction kinetics. For example, consider the chemical reaction

between hydrogen and oxygen forming water vapor. It is well known that the reaction mechanism between these molecules actually consists of several chain-type reactions such as the following:



where M is a third body usually taken to represent all the molecules in the mixture.

In order to determine the net rates of production of the various species entering the above reactions it is necessary to apply the reaction kinetics equations to each of the reactions. In order to simplify the present analysis, however, it is assumed that the above complex chain reactions for the  $\text{H}_2 - \text{O}_2$  system may be replaced by the following one-step reaction equation



In addition, it is also assumed that the reaction mechanism for the  $\text{CO} - \text{O}_2$  system may be described by the one-step reaction.



where  $k_f^1$  and  $k_f^2$  are "overall" reaction rate constants.

Following Penner (Reference 20) it can be shown that the net rate of production of  $\text{H}_2\text{O}$ , in accordance with reaction (47), may

be expressed as

$$\dot{\omega}_1 = 2 W_1 k_f' e^3 \frac{C_3}{W_3} \left( \frac{C_2}{W_2} \right)^2 \left[ 1 - \frac{W_3}{K_p' R T e C_3} \left( \frac{C_1 W_4}{W_1 C_2} \right)^2 \right] \quad (49)$$

where  $k_f'$  is the forward reaction rate constant,  $K_p'$  is the equilibrium constant, and  $W$  is the molecular weight.

Similarly, the net rate of production of  $\text{CO}_2$  is given by

$$\dot{\omega}_4 = 2 W_4 k_f' e^3 \frac{C_3}{W_3} \left( \frac{C_2}{W_2} \right)^2 \left[ 1 - \frac{W_3}{K_p' R T e C_3} \left( \frac{C_1 W_5}{W_4 C_2} \right)^2 \right] \quad (50)$$

(The subscripts 1, 2, 3, 4, 5, 6 correspond to the species  $\text{H}_2\text{O}$ ,  $\text{H}_2$ ,  $\text{O}_2$ ,  $\text{CO}_2$ ,  $\text{CO}$ , and  $\text{N}_2$ , respectively).

From further application of the reaction rate equations it may be shown that the net rates of production of  $\text{H}_2$  and  $\text{CO}$  are related to those of  $\text{H}_2\text{O}$  and  $\text{CO}_2$ . Thus

$$\dot{\omega}_2 = -\dot{\omega}_1 \frac{W_2}{W_1} \quad (51)$$

$$\dot{\omega}_5 = -\dot{\omega}_4 \frac{W_5}{W_4} \quad (52)$$

Since  $\text{N}_2$  is considered inert, its net rate of production is

$$\dot{\omega}_6 = 0$$

From conservation of mass the net rate of production of  $\text{O}_2$  becomes

$$\dot{\omega}_3 = -[\dot{\omega}_1 + \dot{\omega}_2 + \dot{\omega}_4 + \dot{\omega}_5] \quad (53)$$

The expressions for the reaction rate constants  $k_f'$  and  $k_f''$  are assumed to be of the form

$$k_f = B T^\gamma \exp \left( -\frac{E}{RT} \right) \quad (54)$$

where  $B$  is the frequency factor,  $E$  is the activation energy, and  $\gamma$  is a constant.

Equations (49) through (53) may be employed in solving the finite difference energy and species conservation equations provided the empirical constants in equation (54) may be established. The primary difficulty in all nonequilibrium problems is that of establishing the reaction mechanism and associated expressions for the reaction rate constants. For the  $H_2 - O_2$  system the complex chain reaction equations and rate constants are relatively well established. It is possible therefore, to establish an expression for an "overall" reaction rate constant in the following manner. Utilizing the chain reactions and the associated reaction rate constants, the temperature distribution throughout a stream tube may be calculated for a range of initial conditions of the flow parameters employing the one-dimensional analysis of Reference 21 . Then, using the same analytical technique and the one-step chemical reaction a value of the overall reaction rate constant may be determined which best reproduces the previously determined temperature distribution.

The above technique was employed for a range of initial conditions corresponding to those anticipated for the problem being considered herein. Typical results are shown in Figure 11 wherein are presented the calculated temperature distributions resulting from the use of the chain reactions (the solid line) and the one-step reaction using various expressions for the overall reaction rate constant (the broken lines). The reaction equations employed in calculating the solid line were those presented on page 43 of the present report.

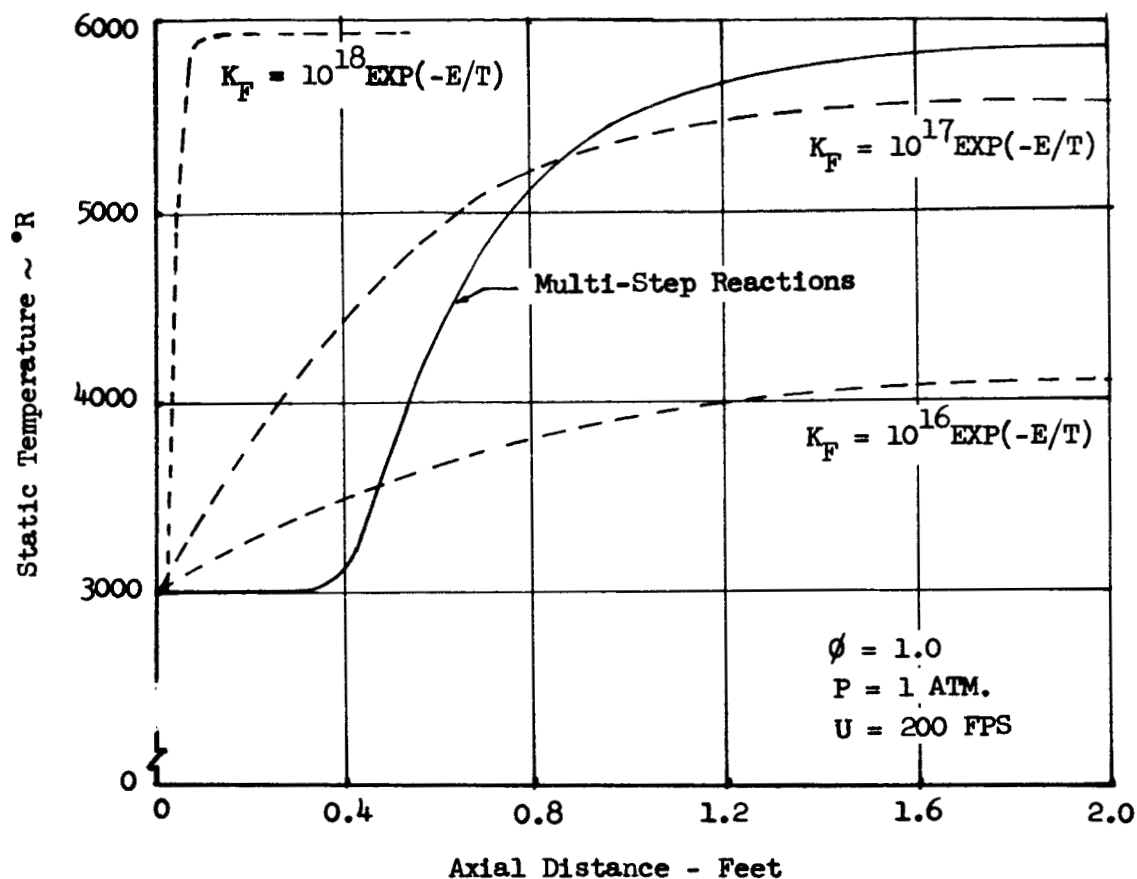


Figure 11 - Effect of Reaction Mechanism and Rate Constants on Theoretical Static Temperature Distribution

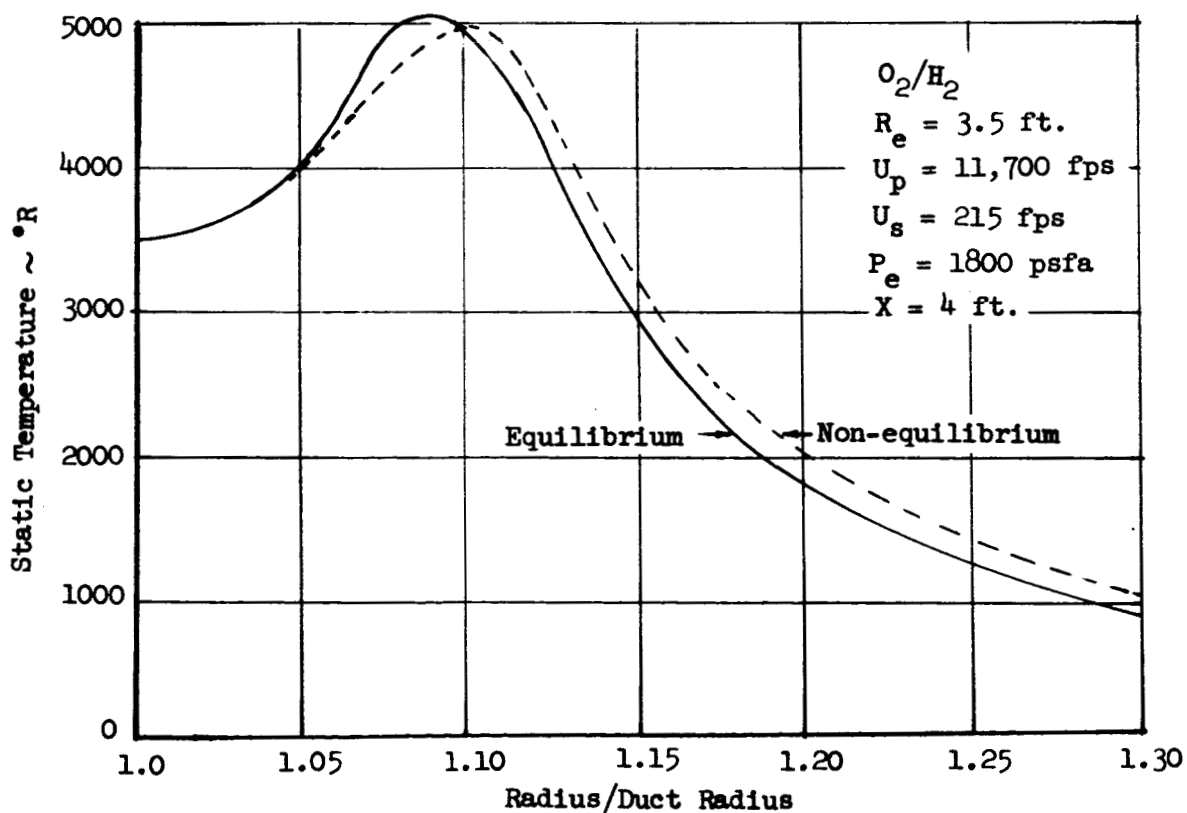


Figure 12 - Comparison of Theoretical Temperature Profiles for Non-Equilibrium and Equilibrium Flow

The value of the overall reaction rate constant was varied by altering the frequency factor; the activation energy was assumed constant at  $1.6 \times 10^4$  cal/gm-mole. The average value of the frequency factor which best correlated the results obtained from the complex reactions was  $B = 10^{16}$ . Thus, the expression employed for the overall reaction rate constant for the  $H_2 - O_2$  reaction was determined to be

$$k_f' = 10^{16} T^{0.5} \exp \left( -\frac{1.45 \times 10^4}{T} \right) \quad (55)$$

In a similar manner the overall reaction rate constant for the  $CO - O_2$  system may be determined. Unfortunately, however, the reaction mechanism for this chemical reaction has not been established and thus, an overall reaction rate constant cannot be determined. In view of the lack of data the value given by Vasiliu may be employed. Thus

$$k_f'' = 5.7 \times 10^7 T^{0.5} \exp \left( -\frac{2.25 \times 10^4}{T} \right) \quad (56)$$

#### Equilibrium Chemistry

For equilibrium chemistry the net rate of production of each species is calculated from the equation

$$\dot{w}_k = \frac{e_k (C_k - \bar{C}_k)}{\Delta X} \quad (57)$$

where  $\bar{C}_K$  and  $C_K$  are the concentrations of species K immediately before and after the chemical reaction, respectively. The problem, therefore, reduces to that of calculating the equilibrium composition  $C_K$ , for initial concentrations  $\bar{C}_K$  at a given temperature and pressure.

From an atom balance the following relations may be obtained which are valid for both reactants and products:

$$\tilde{C}_2 = \bar{C}_2 + \bar{C}_1 \frac{W_2}{W_1} \quad (58)$$

$$\tilde{C}_3 = \bar{C}_3 + \bar{C}_1 \frac{W_3}{2W_1} + \bar{C}_4 \frac{W_3}{W_4} + \bar{C}_5 \frac{W_3}{2W_5} \quad (59)$$

$$\tilde{C}_4 + \tilde{C}_5 \frac{W_4}{W_5} = \bar{C}_4 + \bar{C}_5 \frac{W_4}{W_5} \quad (60)$$

$$\tilde{C}_6 = \bar{C}_6 \quad (61)$$

where  $\tilde{C}_K$  is a pseudo-mass fraction defined by the above equations. For the reaction equations (47) and (48) the equilibrium constants, expressed in mass fractions, are

$$K_P^1 = \frac{W_3}{C_3 P W_M} \left( \frac{C_1 W_2}{W_1 C_2} \right)^2 \quad (62)$$

$$K_P^2 = \frac{W_3}{C_3 P W_M} \left( \frac{C_4 W_5}{W_4 C_5} \right)^2 \quad (63)$$

where  $W_M$  is the average molecular weight of the gas mixture. Values of  $K_P^1$  and  $K_P^2$  are obtained from tables giving the equilibrium constants at various temperatures. Thus, a system of six equations are available for determining the six unknown concentrations  $C_K$ . The solution comprises an iteration technique for calculating the concentrations of the products. The net rates of production of the species are then calculated utilizing equation (57).

#### Comparison of Equilibrium and Nonequilibrium Chemistry

In order to illustrate the differences between equilibrium and nonequilibrium chemistry, solutions were obtained for a typical

problem employing both chemical models. Shown in Figure 12 is the temperature profile throughout the mixed flow field at an axial distance of four feet downstream from the exhaust nozzle of a  $\text{LO}_2/\text{LH}_2$  rocket motor. The conditions of the rocket exhaust and secondary air stream at the exit plane of the nozzle are noted in the Figure. As can be seen the difference between the two cases is not great, thus demonstrating that the selection of equilibrium chemistry provides sufficiently accurate results for the given conditions. As a point of interest it is worthwhile to note that the machine computation times for equilibrium and nonequilibrium flow were approximately 2 and 110 minutes, respectively. In view of the long computation times required for nonequilibrium flow and since equilibrium flow gave accurate results, the latter chemical model was assumed for the problem under study herein.

f. Computer Program

In summary, the solution of the differential equations is obtained by first transforming the equations using the Von Mises transformation, expressing the transformed equations in finite difference form, and then solving the resulting finite difference equations utilizing a computer program developed for the IBM 7094. Details of the program are presented in Reference 9. Consideration is given to the stability and convergence of the solution utilizing the criteria established by Wu (Reference 14). The parameters which must be input to the program are (1) the initial conditions of velocity, temperature, pressure, and concentrations of the species comprising the two streams, (2) the

turbulent Lewis and Prandtl number, (3) axial step-size, (4) axial pressure gradient, and (5) supplemental data as noted in Reference 9 .

In order to calculate the mixed flow field for a problem involving an air-augmented rocket engine the steps outlined below are followed in utilizing the mixing program. Assume that the rocket exhaust conditions as well as the secondary stream flow rate, total temperature, and total pressure are known; and that the mixing section geometry is specified. With these given conditions the following steps are taken for cases where  $P_{1s} < P_{1p}$ .

1. The slipline coordinates and the secondary stream static pressure, static temperature, and velocity at the nozzle exit plane are obtained from the inviscid plume program.
2. The above values are input to the mixing program along with a selected axial pressure gradient for the mixing section.
3. Iterate with the mixing program using various axial pressure gradients until the specified duct geometry is obtained.

For the cases where  $P_{1s} > P_{1p}$ , step one is omitted and only the mixing program is employed.

## C. Discussion

### 1. Configurations

Early in the study, it was necessary to establish some ground rules and constraints upon the engine concepts and vehicle applications toward which the air-augmented rocket cycle analysis was to be oriented. A requirement of the contract work statement was that maximum use was to be made of existing systems and that no new vehicle designs were to be generated, except as necessary to incorporate the augmentation feature.

#### a. Engine Concepts

A wide variety of augmented engine configurations may be conceived having varying degrees of refinement and analytical difficulty. The concepts which were considered in the selection of the basic engine designs are as follows:

Single Primary - Single Secondary. The simplest augmented engine concept, and the most tractable from an analytical point of view, consists of a single rocket engine surrounded by a symmetrical shroud as shown in Figure 13. This concept is suited to liquid or solid strap-on applications.

Multiple Primary. It is advantageous from both the inviscid interaction and mixing standpoints to divide the primary flow into several streams in order to maximize the contact area of the primary and secondary. This may be accomplished with either a multiple engine arrangement (Figure 14), or a multiple throat and nozzle. Another way to increase mixing surface area is to utilize a convoluted, star-shaped, or slotted nozzle exit shape (Figure 15).

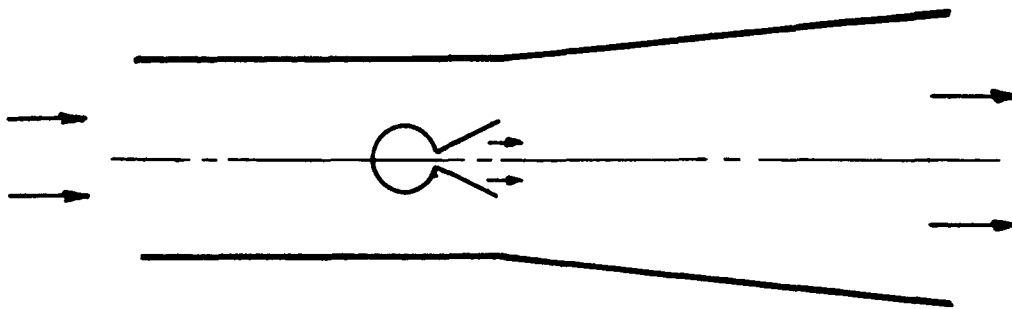


Figure 13 - Simple air augmented rocket engine concept

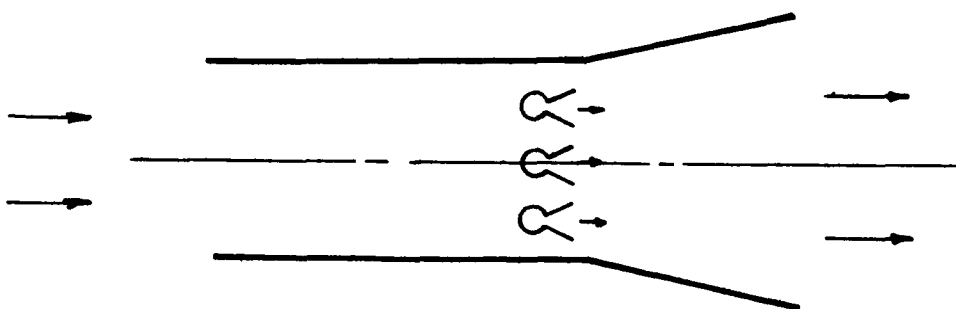


Figure 14 - Multiple nozzle augmented engine concept

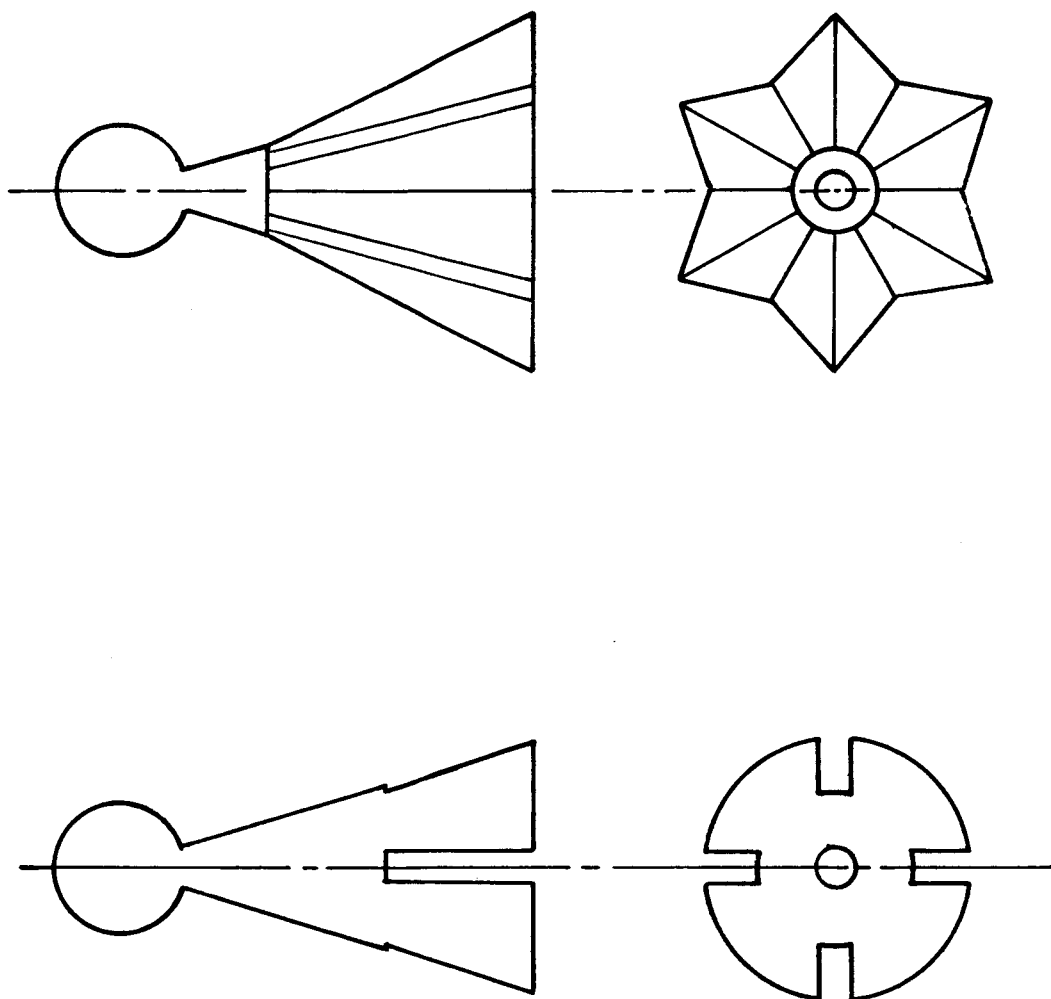


Figure 15 - Primary nozzle shapes to promote mixing

Multiple Secondary. Similar results may be obtained by dividing the secondary stream into a number of streams by a multiple aperture arrangement.

Altitude Compensation - Variable Geometry. A problem common to the concepts discussed so far arises from the fact that the duct is made to diverge so as to provide a surface upon which the mixed stream may act to produce thrust at flight Mach numbers above one, approximately. However, at launch the internal pressures are less than ambient by virtue of the secondary flow, and this form of over-expansion produces a significant drag contribution. A duct with a variable area ratio would prevent this. In the absence of variable geometry it is possible that the problem may be avoided by the use of doors in the duct located near the primary jet exit. The doors would open to the atmosphere to admit additional secondary air into the combustor to promote separation and raise the internal pressure to approach ambient pressure.

An alternative scheme is to utilize the altitude compensating features of the plug cluster (Figure 16) or the aerodynamic nozzle (Figure 17). A limitation of these two, however, when applied to air augmentation, is the lack of confinement of the secondary and primary streams during the inviscid interaction and mixing process except by the gas dynamical means resulting from inward tilt of the primary streams. The lack of confinement by surfaces, oriented to produce thrust, virtually eliminates the beneficial effects which would otherwise accrue from mixing and combustion of

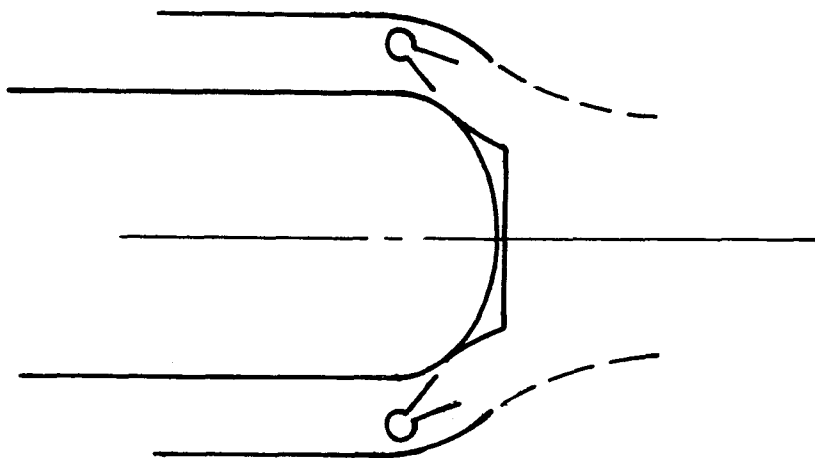


Figure 16 - Air augmented plug cluster concept.

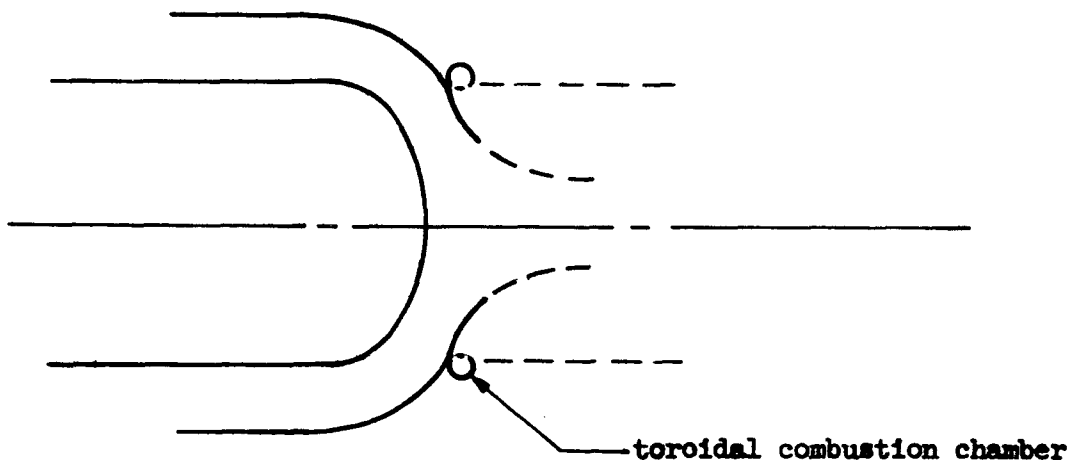


Figure 17 - Air augmented aerodynamic nozzle concept.

the two streams. It might be feasible to fit a variable shroud around the aft end of the engine system similar to the fixed geometry shroud associated with the first concept discussed.

The lack of confinement and asymmetry of the primary stream preclude a realistic solution of the inviscid interaction of the streams with the present analytical tools (Plume Program.) This program requires orientation of the characteristics network with respect to a centerline (in the case of two-dimensional flow a plane wall will suffice). However, it could be modified to accept variable boundary conditions.

b. Vehicle Concepts

The vehicle concepts considered for demonstration of the air augmentation application were limited to current existing designs. Those initially selected were a hydrogen fueled, horizontal take-off rocket plane (Figure 18) and the Saturn V. During the course of the study, the program was re-directed in order to increase emphasis upon the investigation of component and engine performance characteristics. The design and integration studies were then limited to the Saturn V. The initial augmented configuration involved the least modifications to the basic stage and is shown in Figure 19. This modified stage is referred to in this report as the S-1A. It consists of a single duct placed around the Saturn V with its original propellant system and F-1 engines. The engines operate with  $LO_2/RP-1$  at a nominal chamber pressure of 1000 psia. As will be shown later, based upon the one-dimensional analysis, the optimum mixture ratio and nozzle expansion ratio in the augmented version appeared to be 2.3 and 10 to 12

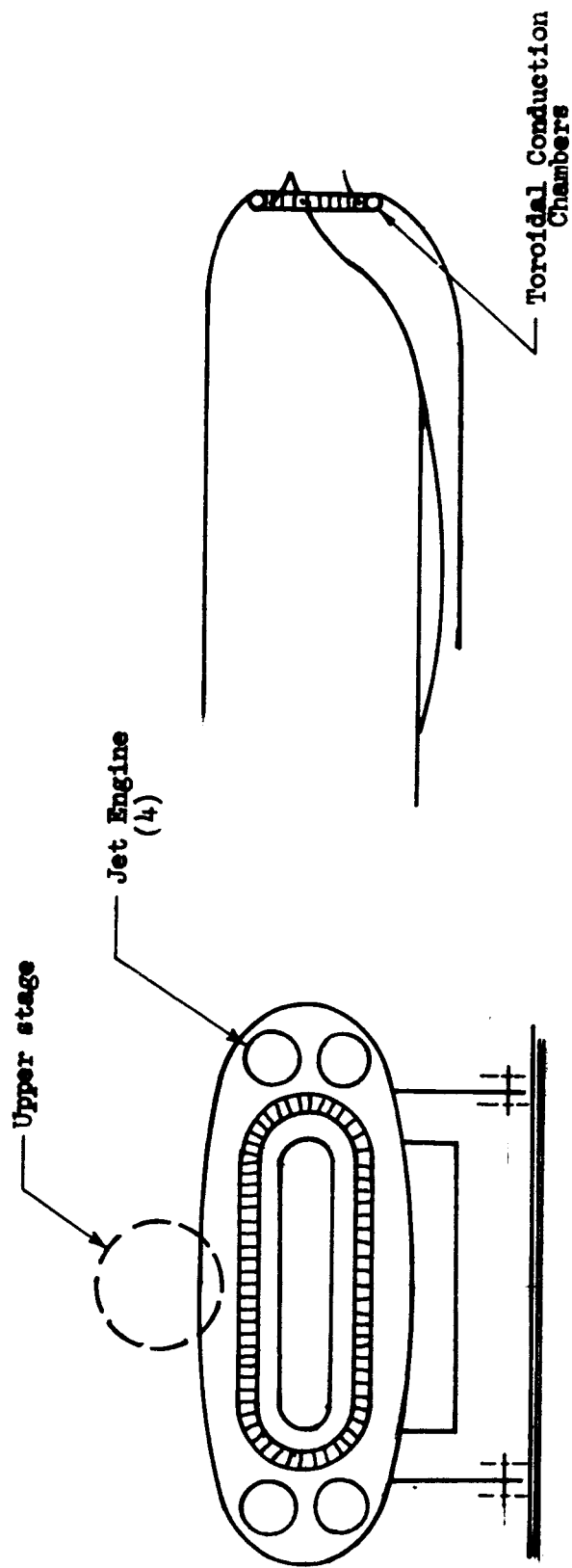


Figure 18 - Horizontal take-off rocket plane

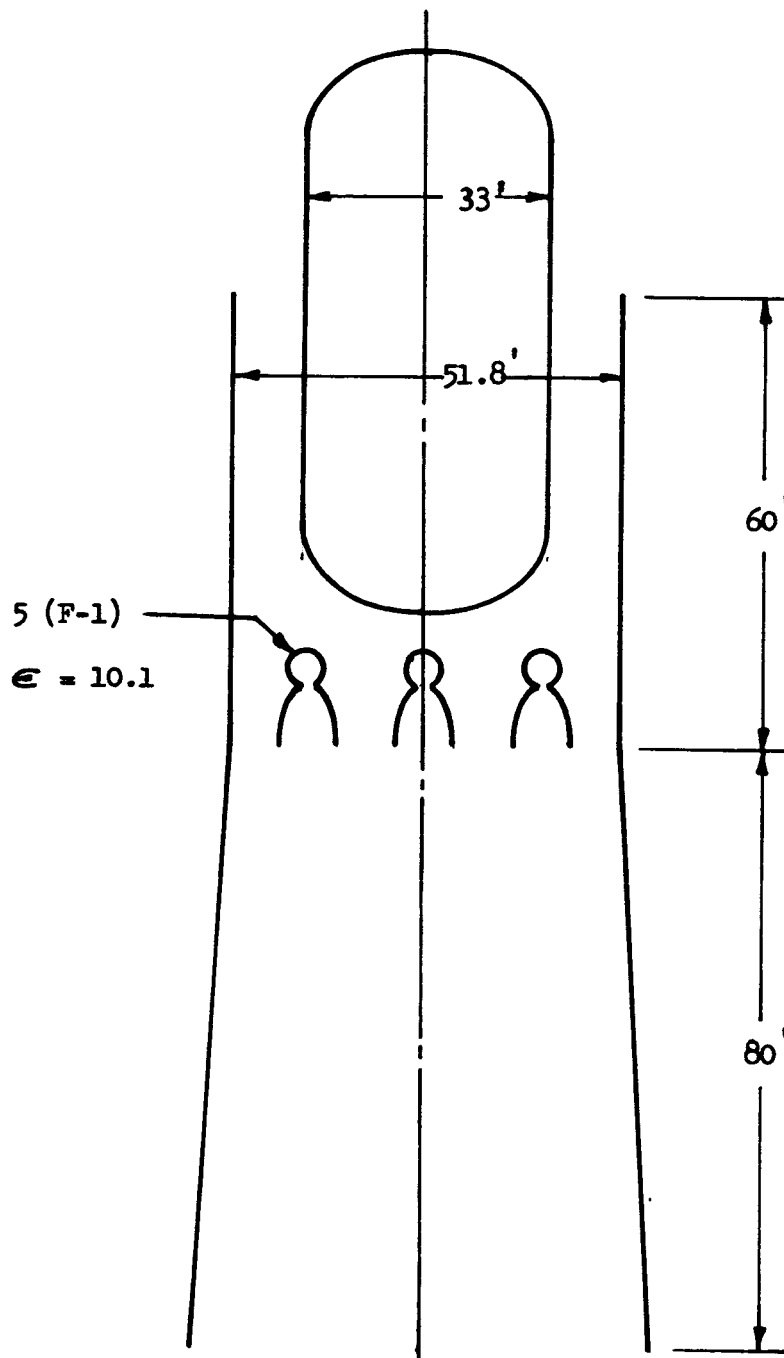


Figure 19 - S-1A configuration.

respectively, and these values were used throughout the analysis. The duct diameter was sized somewhat arbitrarily; it appeared to be as large as was practical for the vehicle, and an inlet which was compatible with the duct size provided representative secondary to primary mass flow ratios of from .25 to 2.5, depending upon flight conditions. The inlet geometry was unspecified but it was assumed to operate with a kinetic energy efficiency of 92% for this initial performance analysis. The mixing duct length was established at 80 feet from considerations postulating a duct length to primary nozzle diameter ratio of 8 to 10 required to achieve moderate mixing of the two streams. This configuration has several undesirable aspects. The length and weight of the duct required to contain the mixing region are large. The location of the mixing duct aft of the vehicle is a serious limitation because of vehicle support and hold-down considerations and the requirement for freedom of lateral movement of the vehicle base at lift-off. Also any thrust vectoring loads would have to be taken by the duct, requiring high strength of the duct and attachment fittings.

S-2A. In order to avoid the principal disadvantages of the S-1A, the S-2A configuration (Figure 20) was designed to integrate the propulsion system and vehicle into a shorter length system with no extension beyond the vehicle base. The use of 36 smaller engines (H-1 type) permits a shorter length for the combustor. This duct arrangement allows the use of conventional hold down and support mechanisms and provides for thrust vectoring loads to be taken directly into the vehicle base. It does require additional thermal protection for the propellant tank wall which is now exposed to

36 Engines  
215,000 lb thrust  
each

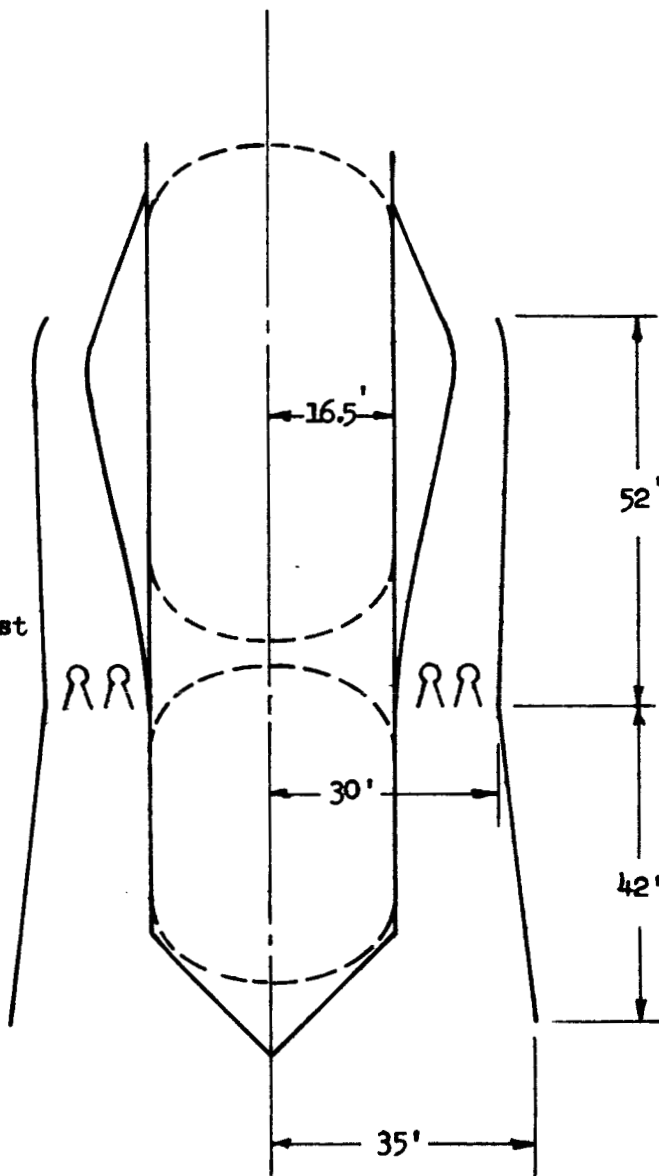


Figure 20 - S-2A Configuration

severe heating by radiation and convection from the mixed stream.

The rocket engine chamber pressure, mixture ratio, and expansion ratio were the same as the S-1A; 1000 psia, 2.3, and 10:1, respectively. As will be discussed later, increasing secondary mass flow rate, in general, has a beneficial effect on system specific impulse. Consequently, the size of the duct and inlet capture area were increased, again somewhat arbitrarily, to what was considered to be the practical limit with respect to basic Saturn V structure.

c. Inlet

The selection of the inlet required consideration of inlet performance, complexity, and necessary range of operation. Figure 21 shows the total pressure recovery of a variety of inlet types as a function of flight Mach number. The upper curve represents the upper limit of performance of a variety of inlets, both fixed and variable geometry, operating on design, and measured experimentally over the past several years. Since it was not the purpose of this investigation to determine optimum system performance, use of a variable geometry inlet on an integrated vehicle-propulsion system of this size was considered unwarranted. The two shock (one oblique, one normal) fixed geometry annular inlet was selected as being a reasonable compromise between inlet performance, complexity, and weight. It was designed to provide optimum performance at a flight Mach number of 3, the approximate midpoint of the supersonic portion of the flight range over which significant augmentation was expected. For the purposes of this study, the inlet analysis was confined to consideration of shocks

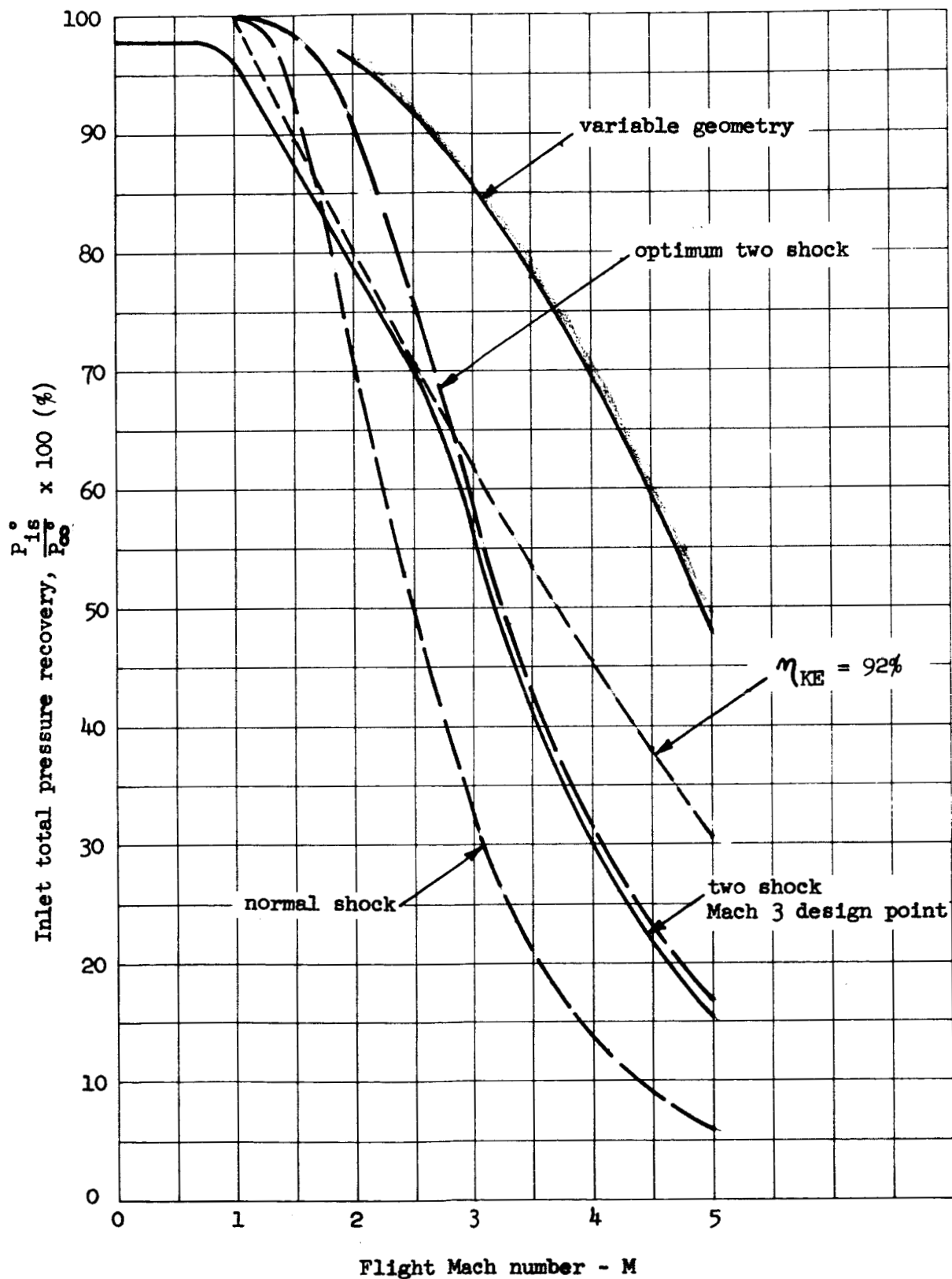


Figure 21 - Typical inlet performance.

and area variations only. Effects of friction, leading edge bluntness, flow variations across the stream, boundary layer, etc. were ignored.

## 2. Combustor-Mixing Section Analysis

Now that the means have been developed by which the flow fields in the mixing section can be determined for given initial flow conditions, the question must be answered as to what flow patterns in the combustor are physically realistic, and how initial secondary stream conditions are determined which produce this realistic situation.

Figure 22 illustrates an axisymmetric engine consisting of an inlet, a rocket engine, and a mixing-combustion duct, hereafter referred to as the mixing section or combustor. Consider first, the flow through the mixing section. Assume that the ambient pressure, as well as the flow conditions of the rocket, are constant, the only variables being the secondary air stream flow conditions at the exit plane of the primary nozzle (Station 1). For values of the air stream static pressure,  $P_{1s}$ , less than the rocket exhaust static pressure  $P_{1p}$ , the exhaust plume forms a restriction to the secondary flow as shown in the figure. Assume, for the present, that the secondary flow is subsonic at Station 1 and remains subsonic throughout the mixing section (this condition is physically possible only when  $P_e = P_\infty$ ). As  $P_{1s}$  is decreased, the plume diverges outward and further restricts the inviscid secondary flow, until at a specific value of  $P_{1s}$  the secondary flow attains sonic conditions at some point along the mixing section. Once this "choking" condition is established, decreasing the pressure downstream of this point will have no effect on the secondary flow conditions.

Now, consider again the case where subsonic secondary flow exists throughout the mixing section. Since the flow is subsonic, pressure disturbances will be propagated upstream, affecting  $P_{1s}$  in such a manner that either  $P_e$  will equal  $P_{\infty}$ , or the flow will become choked. The effects of mixing are superimposed on the inviscid flow field and the secondary flow conditions. It should be noted that the foregoing discussion has been limited to include only those cases where  $P_{1s} < P_{1p}$ .

For most cases of interest here, the secondary flow is forced into the mixing section due to the vehicle being propelled through the atmosphere by the air-augmented rocket powerplant and consequently  $P_{1s}$  may be greater than  $P_{1p}$  at certain points along the trajectory. In such cases the plume does not form a restriction to the secondary flow as previously described, hence, the choking condition can only be achieved as a result of mixing and/or heat release within the mixing section. At other points along the trajectory, however,  $P_{1s}$  will be slightly less than  $P_{1p}$  and the choking condition will be attained as a result of the combination of plume "blockage", mixing and heat release between the two streams. It is noted that for stable operation of the engine, the flow at some point in the mixing section must be choked.

The problem of analyzing the flow system, therefore, reduces to that of determining the secondary flow conditions which result in choked flow for a given duct geometry and primary rocket conditions.

No efforts were made to determine the effects of plume and/or mixing zone impingement resulting from a multiple nozzle arrangement such as the S-2A. It was assumed that the multiple nozzle configuration operation was equal to that of a single nozzle surrounded by a single duct of

such diameter that the ratios between secondary and primary stream at station 1 were the same for both. The purpose for considering the S-2A configuration was to develop approximate propulsion weights, as described in Volume II.

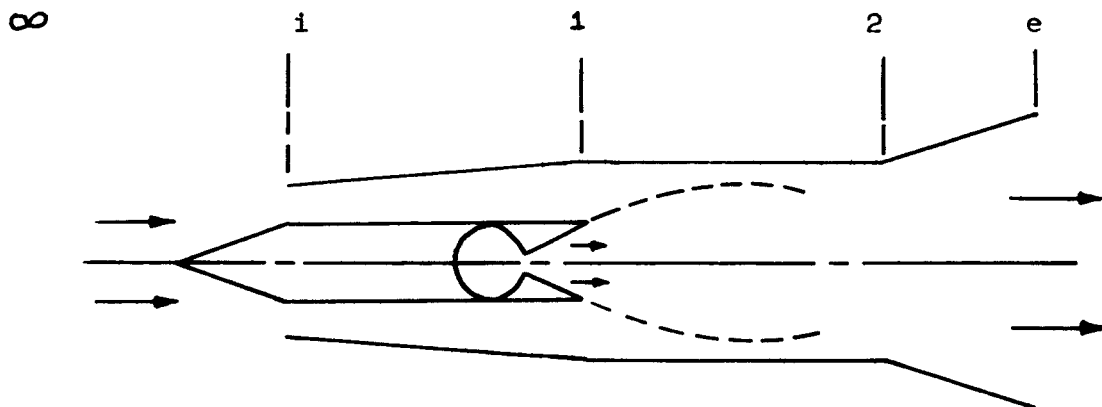


Figure 22 - Air-Augmented Rocket Schematic

## RESULTS

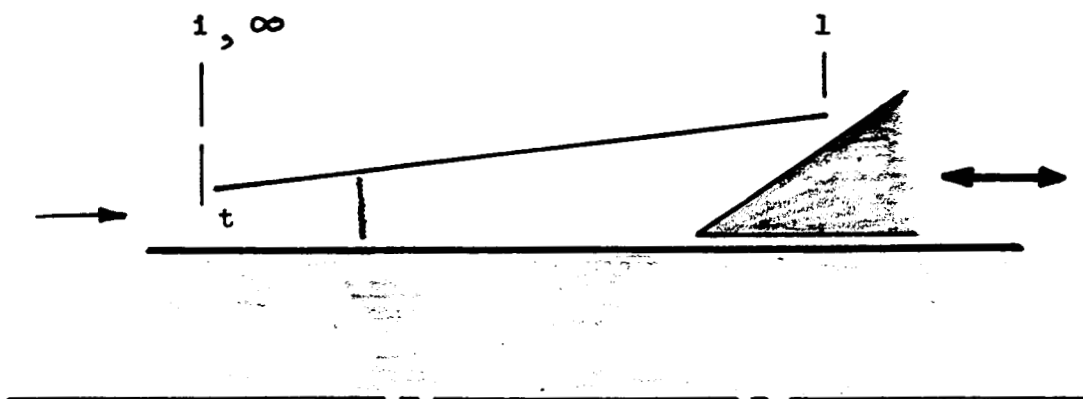
### A. Component Operating Characteristics

#### 1. Inlet

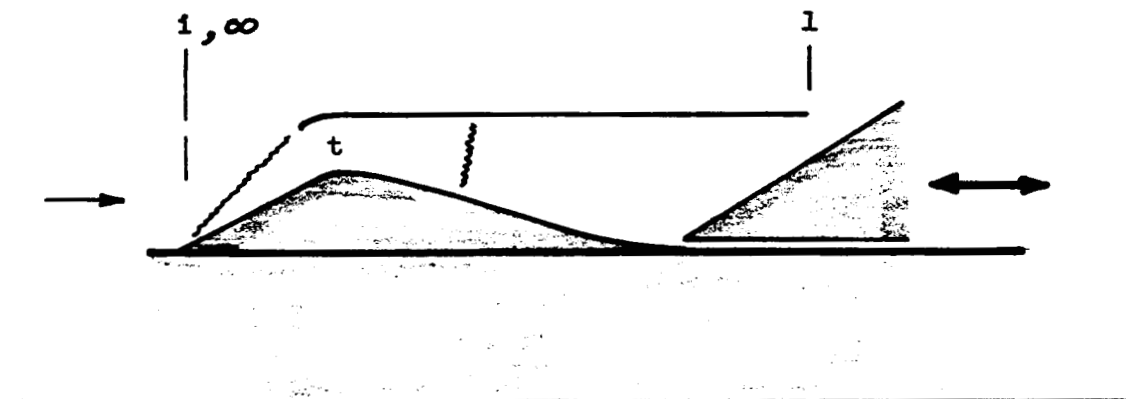
The purpose of a subsonic combustion airbreathing inlet, in general, is essentially two fold: to provide the proper flow rate of air at the conditions required by the combustor section, and to provide surfaces upon which the diffusion process can act to produce thrust. Before the integration of the inlet and combustor can be accomplished with an appropriate degree of realism, and the effects of one upon the other can be established, it is necessary to understand the general operating features of the inlet.

In order to illustrate the inlet operation, two simple annular inlets as shown in Figure 23 have been selected as examples. In the normal shock inlet the flow is assumed to be one-dimensional. In the two-shock inlet the flow is two-dimensional up to the throat, and one-dimensional thereafter. The inlet plugs are shown to illustrate the variable constriction of the inlet outflow by means of thermal choking, geometric throat, etc, which are normally encountered. This constriction serves to regulate inlet back pressure, fix the position of the normal shock, and hence establish total pressure recovery and exit Mach number. The performance of the inlets was calculated using perfect gas ( $\gamma = 1.4$ ) shock and isentropic flow relations.

The performance of the two inlets in terms of static and total pressures delivered for flight Mach numbers of 2.37 and 4.59 at various altitudes is shown in Figure 24a. The data are shown in this way in order to facilitate comparison with the combustor operating



Normal shock



Two shock.

Figure 23 - Annular inlet configurations.

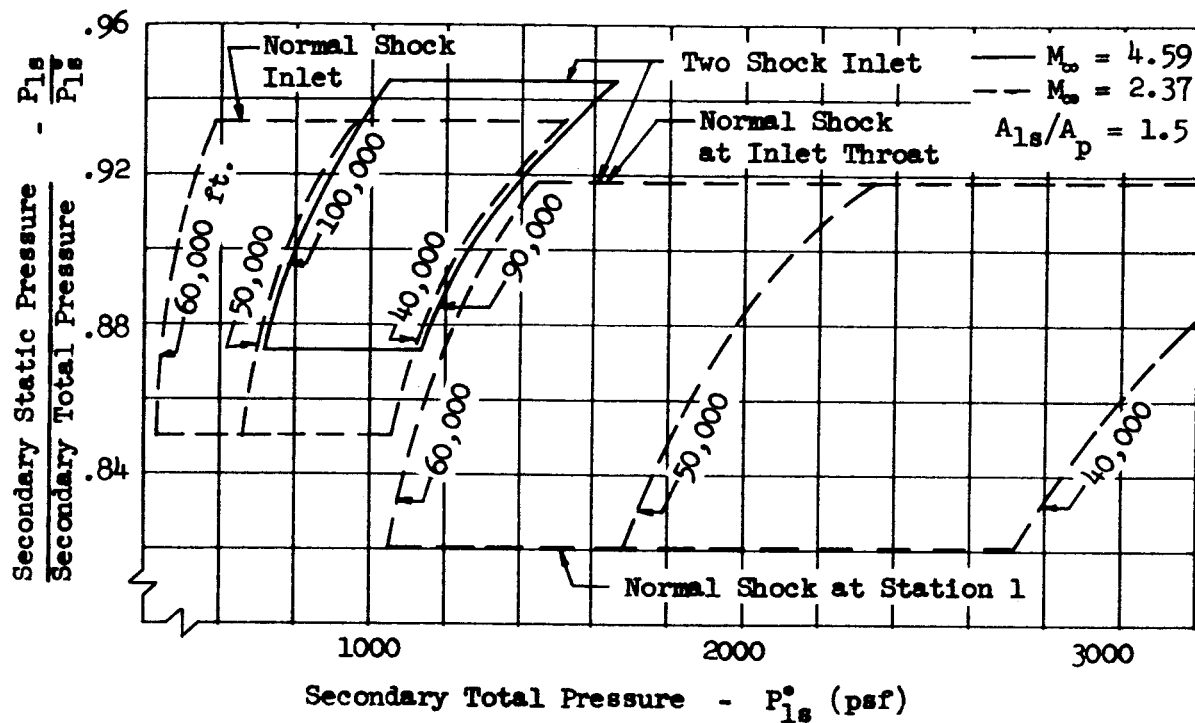


FIGURE 24a - Supersonic Operation

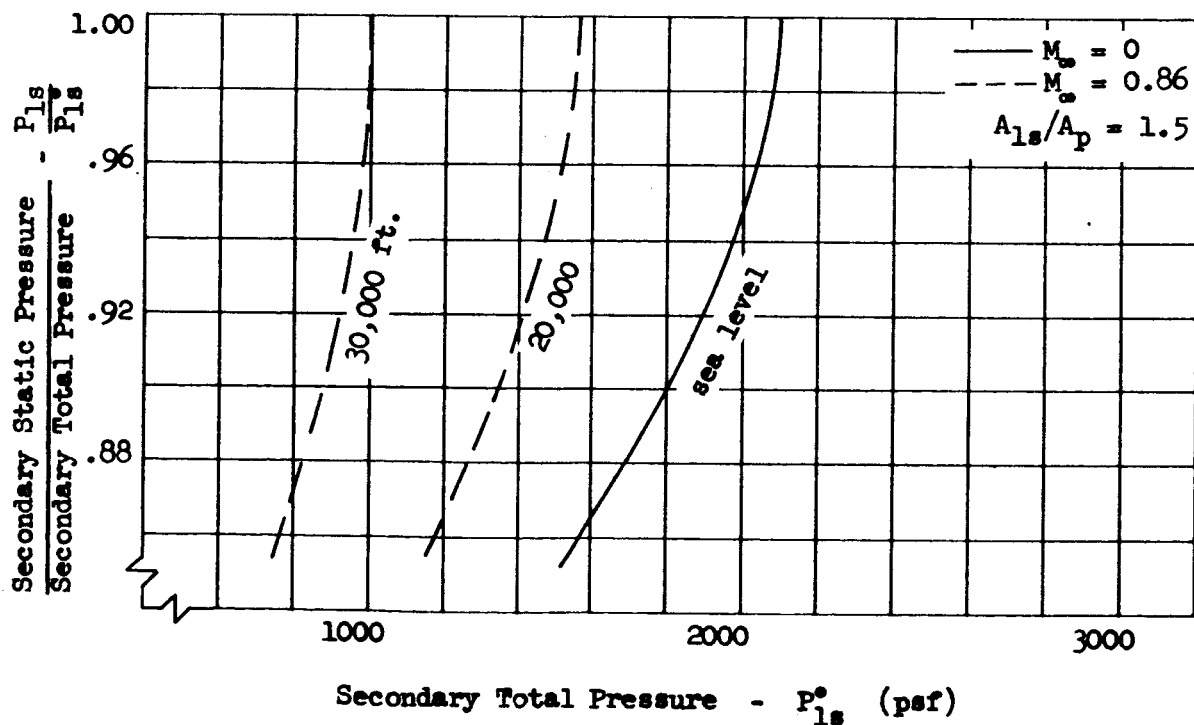


FIGURE 24b - Subsonic Operation

FIGURE 24 - INLET OPERATING CHARACTERISTICS

conditions which will be described later. The upper and lower horizontal lines of each set represent the diffuser exit pressure ratios obtained with the normal shock at the inlet throat and diffuser exit plane. The internal thrust produced by the inlet may be described in terms of the impulse function:

$$\mathcal{F} = PA + \dot{m}V = PA (1 + \gamma M^2)$$

where the thrust is equal to the difference between diffuser exit and free stream impulse functions:

$$T_{\text{inlet}} = \int_{\infty}^{1s} P dA = \mathcal{F}_{1s} - \mathcal{F}_{\infty}$$

Since  $\mathcal{F}_{\infty}$  is constant for given weight flow and flight condition, inlet thrust will maximize when  $\mathcal{F}_{1s}$  is a maximum. Figure 25 shows a plot of  $\mathcal{F}/\mathcal{F}^*$  as a function of Mach number.  $\mathcal{F}^*$  is a function only of weight flow rate, total temperature, gas constant, and gamma, hence is constant for this adiabatic flow situation. From this curve one can conclude that the inlet will produce the most thrust when the exit Mach number is very low, a lesser amount when it is high, and the least when  $M_{1s} = 1.0$ . It is then desirable to operate the inlet along the upper limit line, if possible. This condition corresponds to maximum total pressure (recovery) which is generally regarded as being axiomatically required for best airbreathing performance. Henceforth, the word "quality" will be used to describe, on a comparative basis, the condition of the secondary air as it leaves the inlet. High quality means low Mach number and high total pressure, and vice versa. High quality air is produced by operation along the upper limit line, and low quality by operation along the lower limit line.

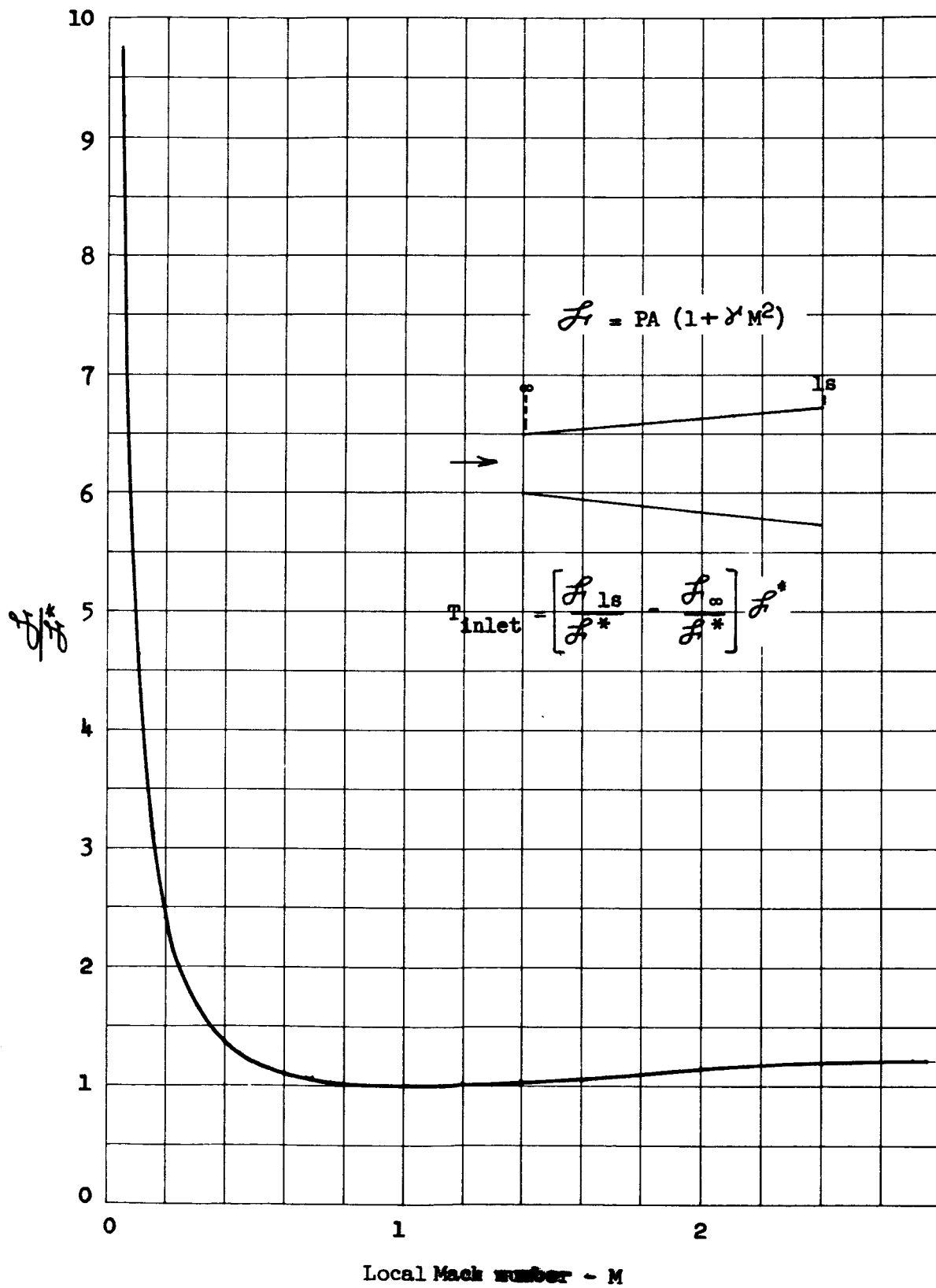


Figure 25 - Adiabatic impulse function -  $F$

The subsonic performance of the two inlets (Figure 24b) is considered to be identical. As contrasted with the supersonic case where the mass flow was assumed constant for a given set of flight conditions, the mass flow of the subsonic case varies due to frictional and non-uniformity effects.

## 2. Mixing Section

The operating characteristics of the mixing section are best described in terms of the flow conditions of the rocket exhaust and secondary air stream at the location where the streams enter the mixing section, i.e., at the exit plane of the rocket nozzle. As discussed in Sections B.2 and C.2, these conditions must be such that with a given mixing section geometry, the flow becomes choked at some axial location within the mixing section. The theoretical data for these flow conditions, with consideration given to mixing, may be obtained utilizing the mixing program described in Section B.3. However, to generate such data over a wide range of rocket flow conditions and mixing section geometries is very time consuming. The inviscid analysis, on the other hand, may be employed to generate parametric data which, although not including the effects of mixing, provides a method for establishing trends and the lower limit of combustor performance. The operating characteristics of the mixing section have therefore been separated into two sections -- inviscid and viscous operating characteristics.

### a. Inviscid Operating Characteristics

The inviscid operating conditions of the combustor are determined through use of the Inviscid Plume Program in the following steps:

1. Specify primary conditions and combustor geometry.

2. Select a secondary mass flow ( $\dot{m}_s$ ), total temperature ( $T_{1s}^\circ$ ) and total pressure ( $P_{1s}^\circ$ ).
3. Calculate flow conditions in combustor with Inviscid Program (Duct Shape Input).
4. Vary secondary total pressure ( $P_{1s}^\circ$ ) until the sonic condition is reached.
5. Select new values of  $\dot{m}_s$  and repeat Steps 3 and 4.
6. Select new values of  $T_{1s}^\circ$  and repeat Steps 3 and 4.

Figure 26 describes a variety of duct and nozzle geometries to which the inviscid analysis was applied. Figure 27 is a plot of  $\dot{m}_s$  versus  $P_{1s}^\circ$  for constant values of  $T_{1s}^\circ$  for configurations A and C. Notice that the points plot as straight lines and intersect the  $P_{1s}^\circ$  axis ( $\dot{m}_s = 0$ ) at a common point for each configuration, defined as  $P_0$ . This corresponds to the secondary total pressure at which the primary jet plume expands sufficiently to be just tangent to the duct wall and completely restricts the secondary flow. The value of  $P_0$  is a function only of primary conditions and duct geometry, and is independent of other secondary flow conditions. The data may then be shown as in Figure 28 with  $\dot{m}_s (T_{1s}^\circ)^{1/2}$  plotted versus  $P_{1s}^\circ - P_0$  for each configuration. From this curve one can determine mass flow rate for given combustor geometries and secondary total temperature as a function of secondary total pressure. For later comparison with the inlet operating characteristics, the same secondary conditions for choking are shown in Figure 29 with  $P_{1s}/P_{1s}^\circ$  plotted versus  $P_{1s}^\circ$ . These curves are independent of secondary total temperature and could be plotted as Mach number versus  $P_{1s}^\circ$ .

In discussing the performance of the combustor section, it is helpful to consider the following general statements, whose validity

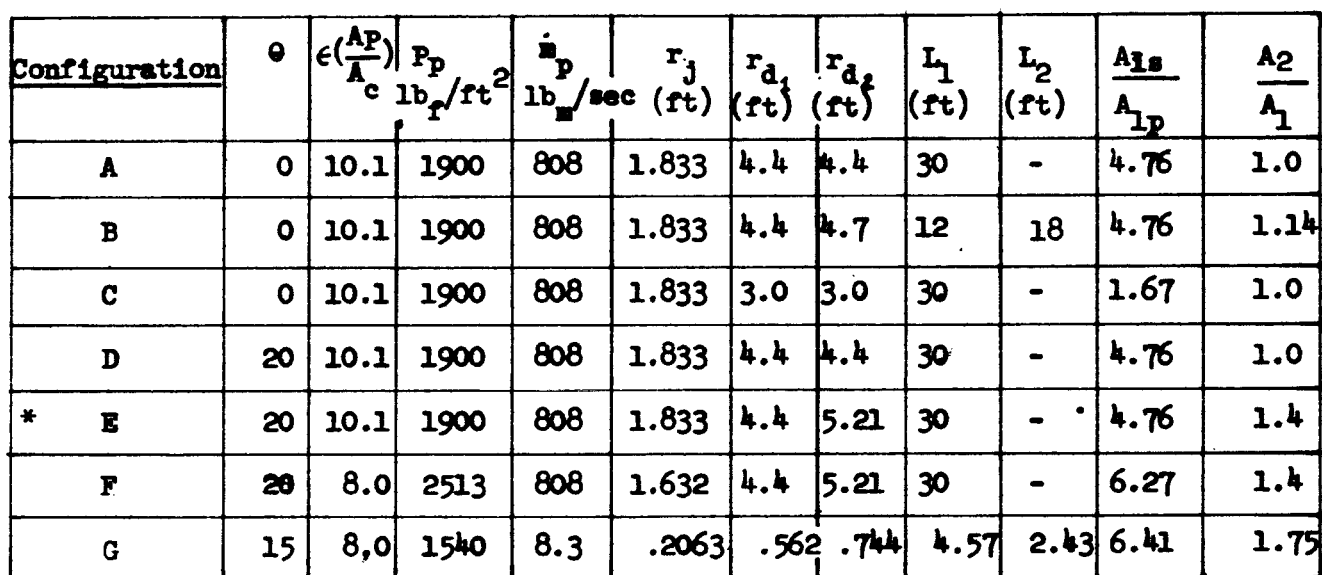


**FIGURE 26 COMBUSTOR CONFIGURATIONS**

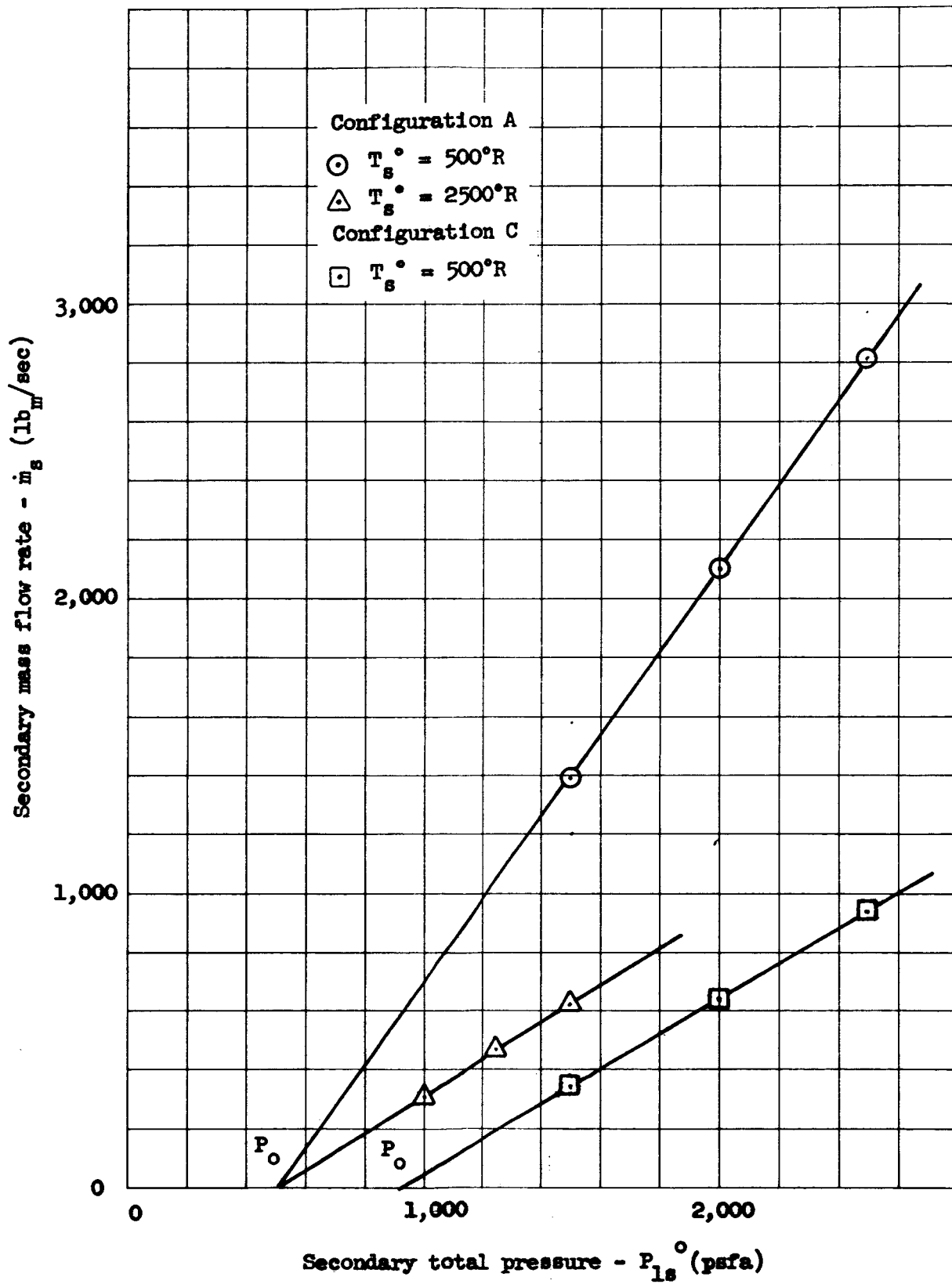


Figure 27 - Combustor inviscid operation characteristics

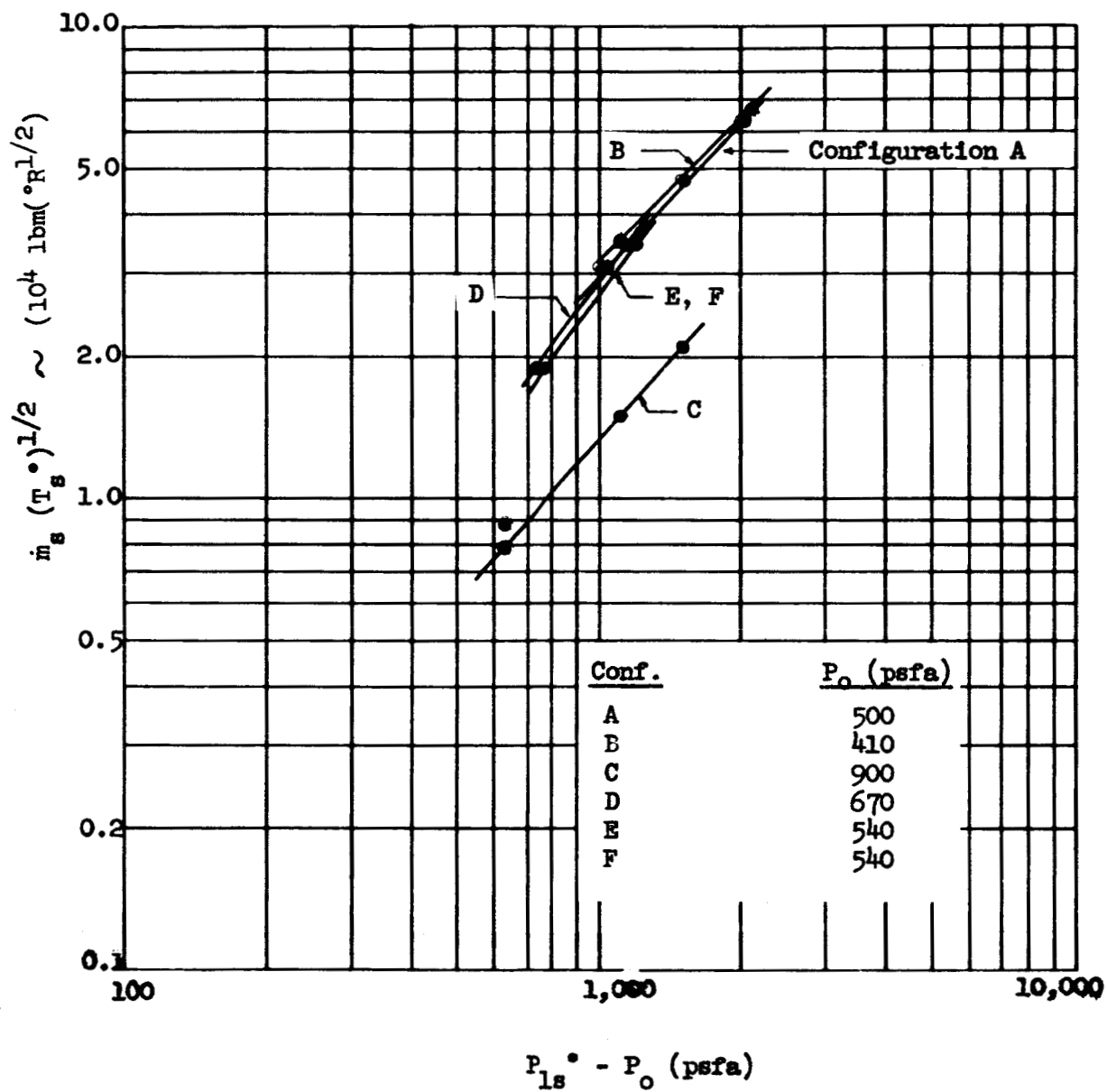


Figure 28 - Combustor inviscid operating characteristics

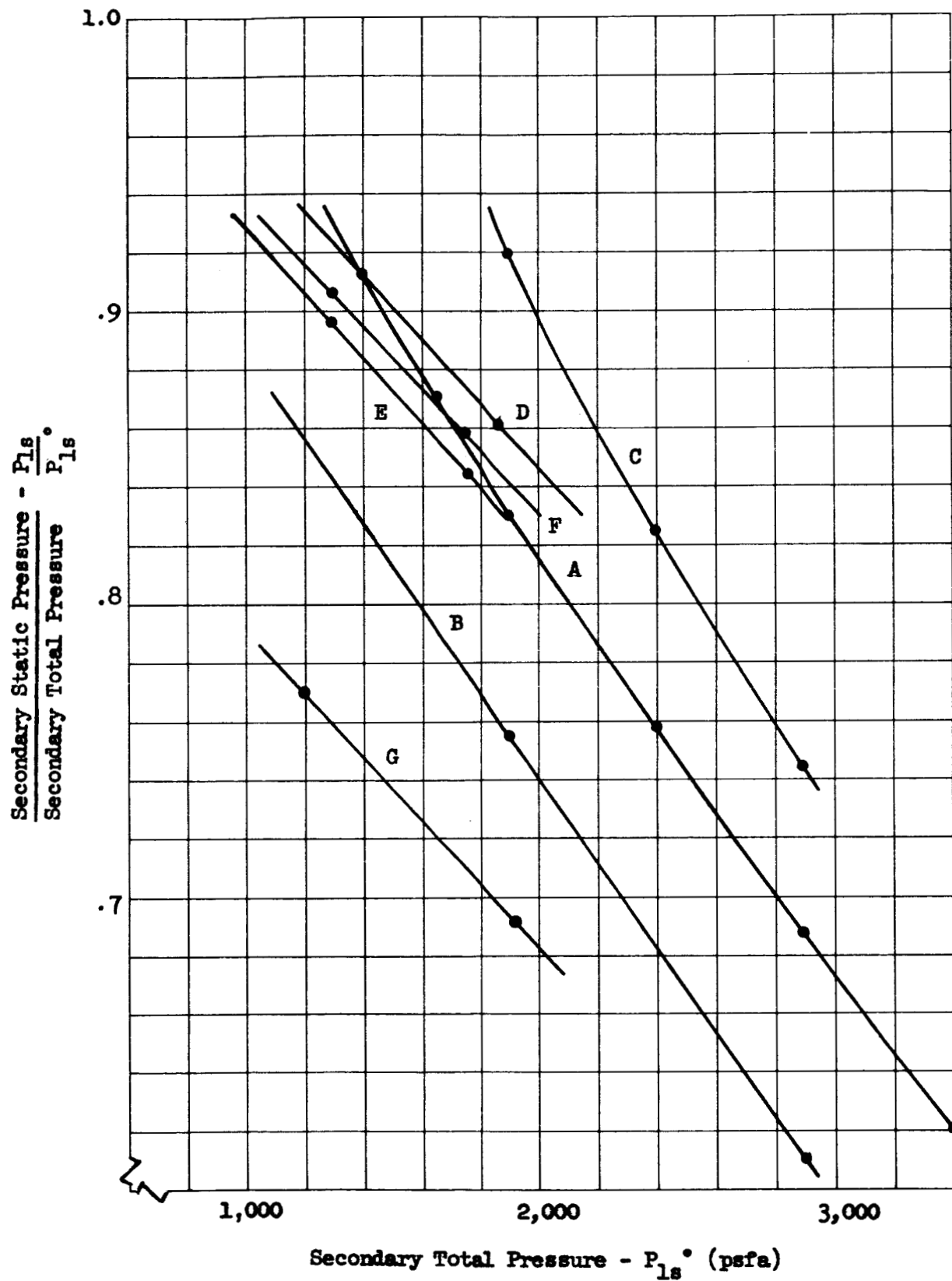


Figure 29 - Combustor Inviscid Operating Characteristics

is established elsewhere in this report.

1. Increasing secondary weight flow increases augmented specific impulse.
2. Increasing the quality (high total pressure and low Mach number) of the secondary flow increases performance. (Increased secondary stream quality is reflected in a shift of the combustor line upward and to the right in Figure 29, as from A to C.)
3. The development of thrust can occur only when there are surfaces properly oriented to receive it.

With respect to these statements and referring to configuration A as a base line in Figures 28 and 29, the following effects of geometry are apparent:

1. Increasing secondary to primary area ratio or diverging the duct ~~requires~~ higher secondary flow rate for the same quality (total pressure) secondary flow (Figure 28, Configuration C to A and B).
2. Decreasing secondary to primary area ratio requires higher quality air for the same flow rate. (The plume need not expand so far to choke the secondary, or in other terms, higher pressure is required to force the secondary past the plume, Figure 28, A to C.)
3. Increasing divergence angle of the primary nozzle is beneficial in increasing secondary flow quality. (Figure 29, A to D).
4. Decreasing primary nozzle area ratio is only slightly beneficial in increasing secondary flow quality. (Figure 29, E to F).
5. Increasing secondary to primary area ratio and divergence of the duct provides more surface area oriented to accept internal thrust.

Based upon the above observations, it can be stated that increasing secondary to primary area ratio and divergence angle of the duct are beneficial in producing internal thrust developing surfaces and in increasing flow rate capability, but detrimental in that the combustor requires a lower quality secondary flow to operate with the secondary choked.

b. Viscous Operating Characteristics

In order to determine the operating characteristics of the combustor, with mixing and combustion of the primary and secondary streams, the configuration illustrated in Figure 30 was selected. The primary rocket is assumed to have the following operating characteristics:

Propellants -  $\text{LO}_2/\text{RP-1}$

Mixture ratio = 2.3

Combustion pressure = 1,000 psia

Flow rate = 808 lb/sec

Area ratio = 10.1:1

Exit diameter = 3.666 ft

Optimum specific impulse =  $302 \frac{\text{lb}_f - \text{sec}}{\text{lb}_m}$

Exit velocity = 9734 ft/sec

Exit temperature = 3681°R

Exit pressure = 12.9 psia

The conditions of the secondary stream at the exit plane of the primary nozzle are assumed to be compatible with those provided by the two-shock inlet discussed in Section A-1.

Consider a vehicle with a flight Mach number of 2.37 at an altitude

$$\frac{A_e}{A_1} = 1.8 \quad \frac{A_2}{A_1} = 1$$

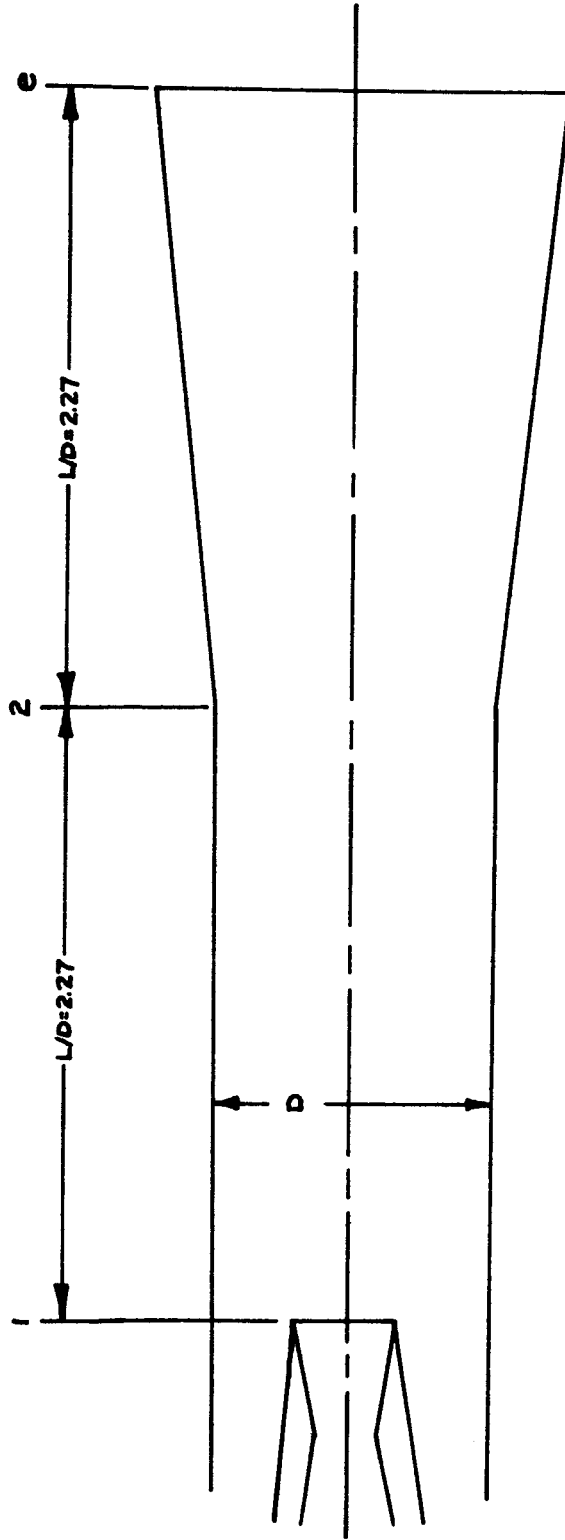


Figure 30 - Mixing Section Study Configuration

of 50,000 feet. The secondary flow conditions at the nozzle exit plane are as follows:

$$P_{1s} = 2145 \text{ psfa}$$

$$T_{1s} = 809^\circ\text{R}$$

$$M_{1s} = 0.35$$

$$\dot{m}_s = 1215 \text{ lb/sec}$$

$$u_{1s} = 489 \text{ ft/sec}$$

Employing these initial conditions and the technique for calculating the mixed flow field as discussed in Section B-3, the results presented in Figure 31 were obtained. The results are in the form of Mach number profiles, obtained from velocity and temperature profiles at various axial locations in the mixing section. It is seen that as the flow proceeds in the downstream direction the Mach number gradient approaches zero. The minimum Mach number at the duct exit ( $X/D = 4.54$ ) is greater than unity, thus indicating that the flow is choked.

Shown in Figure 32 is the pressure ratio  $(P/P^\circ)_{1s}$  as a function of  $P_{1s}^\circ$  illustrating the comparison of the mixing theory with the theoretical data obtained from the viscid theory. It is recalled that the pressure ratios obtained from the inviscid theory are those for which choked flow was obtained due only to the blockage effect provided by the rocket exhaust plume, it being assumed that no mixing occurred between the two streams. Thus, judging from the data obtained from the mixing analysis, it appears that as a result of mixing the pressure ratios which produce choked flow are greater than those predicted from the inviscid theory. Further discussion pertaining to this trend is presented in Volume II of the present

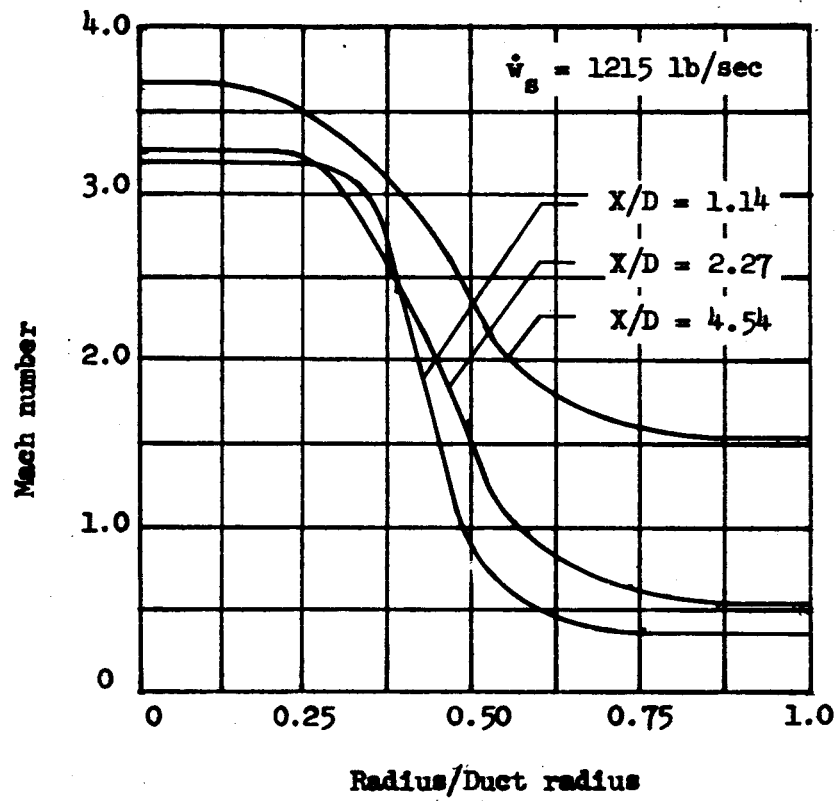


Figure 31 - Mach Number Profiles

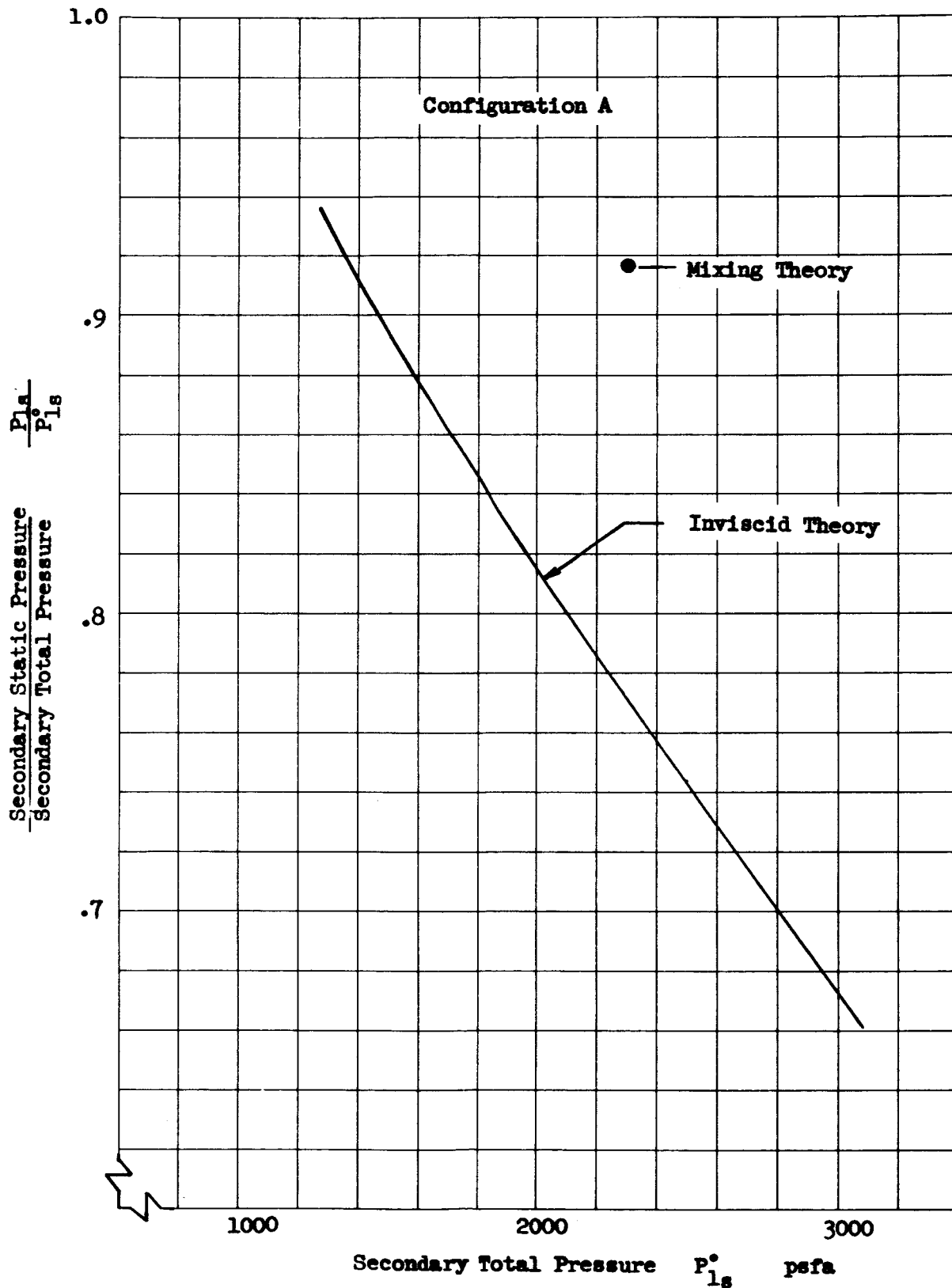


Figure 32 - Comparison of Theoretical Combustor Inviscid and Viscous Operating Characteristics

report. It may be stated here, however, that work thus far indicates that the inviscid theory may be employed to predict the lower limit of combustor performance. The upper limit of combustor performance has not been determined analytically, but appears to correspond to those conditions at which the mixed flow becomes choked at the combustor exit, i.e., the minimum Mach number in the profile at the combustor exit is equal to unity.

c. Mixing Length

The operating characteristics of the mixing section are strongly affected by its length. For given flow conditions, the basic requirement which must be fulfilled in establishing the length of the mixing section is that it be sufficient for the flow to become choked. From thrust considerations the duct should be quite long, but when consideration is given to duct weight and drag, it is obvious that an optimum length exists which gives a maximum net thrust-to-weight ratio. Thus, techniques which reduce the required duct length and improve thrust producing capability are of interest. Since the required duct length, as dictated by the choking criteria, may be reduced by choking further upstream, and the thrust increased by maintaining higher pressures throughout the mixing section, a technique which satisfies both conditions simultaneously is desired. Such conditions can be obtained by increasing the rate of mixing between the two streams. For example, due to momentum interchange which is proportional to the rate of mixing, the secondary stream is accelerated at a more rapid rate, and thus attains the choking condition more rapidly with increased rate of mixing. Also, increased rate of mixing results in more rapid heat release due to chemical

reactions, and thus, higher pressures are capable of being sustained throughout the mixing section. Hence, techniques which improve the rate of mixing between the rocket jet and the secondary air stream are of importance. One technique which has been demonstrated experimentally to be effective, is the use of turbulence and vortex generators in the secondary stream. Other techniques which improve the rate of mixing comprise the following:

1. Multiple rocket exhaust nozzles, which when distributed throughout the secondary stream effect an increase in the area of contact between the two streams.
2. Multiple secondary streams
3. Devices which alter the boundary layers immediately upstream of the point where the two streams first come into contact.

### 3. Inlet-Combustor Matching

Once the operating characteristics of both the inlet and the combustor have each been defined, the problem of selecting the match point of the two, if possible, is largely solved. In Figure 33 are plotted static to total pressure ratio vs. total pressure for the secondary stream with a primary-combustor combination of Configuration E shown in Figure 26.

Curve 1 was generated based upon inviscid choking of the secondary and represents the lower limits of combustor performance discussed in the preceding section. Also plotted are the same variables for the Mach 2.37, two-shock inlet shown previously. At a given altitude, the intersection of inlet and combustor curves defines a match point of compatible operation. These configurations match at altitudes between approximately

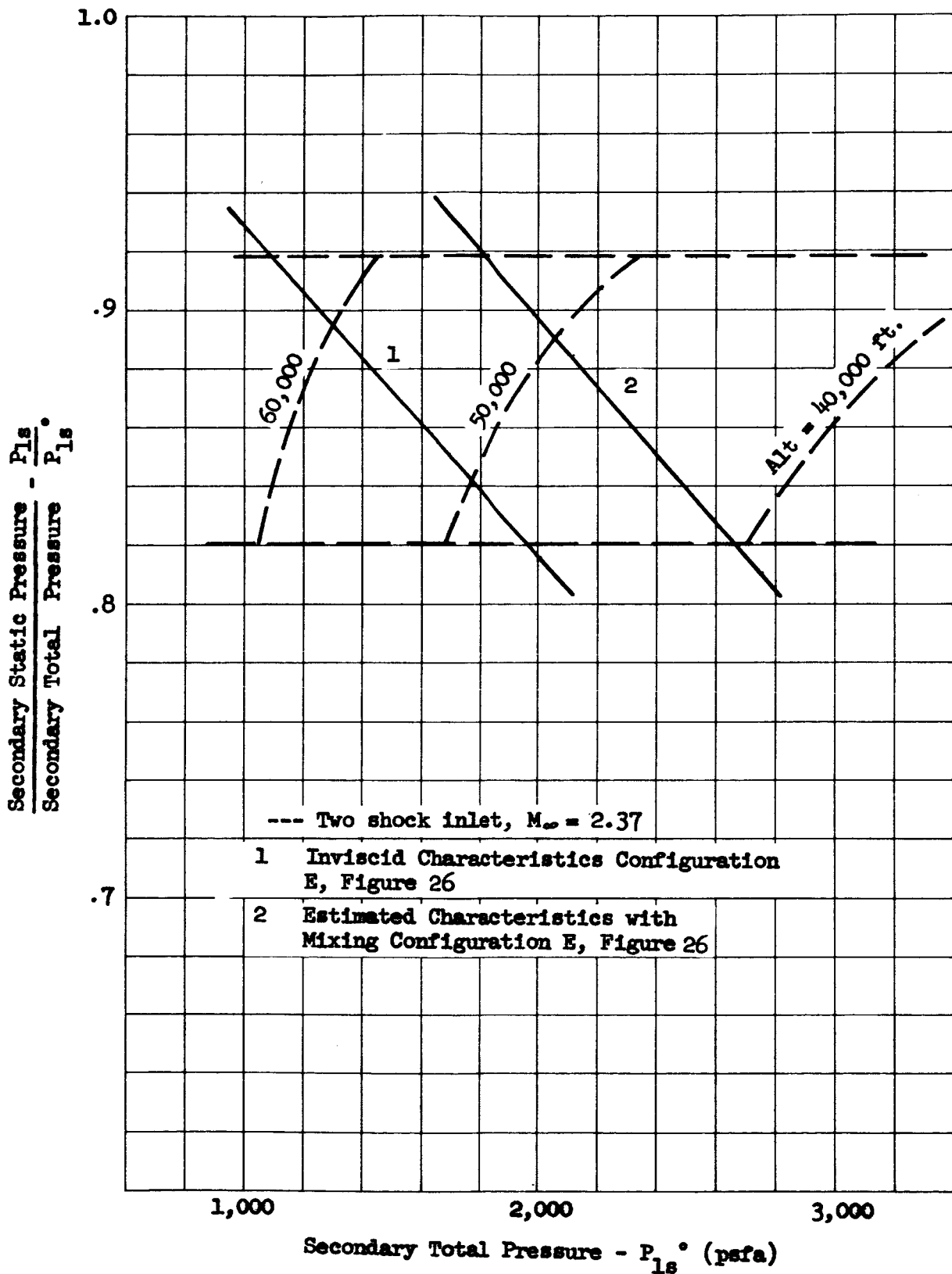


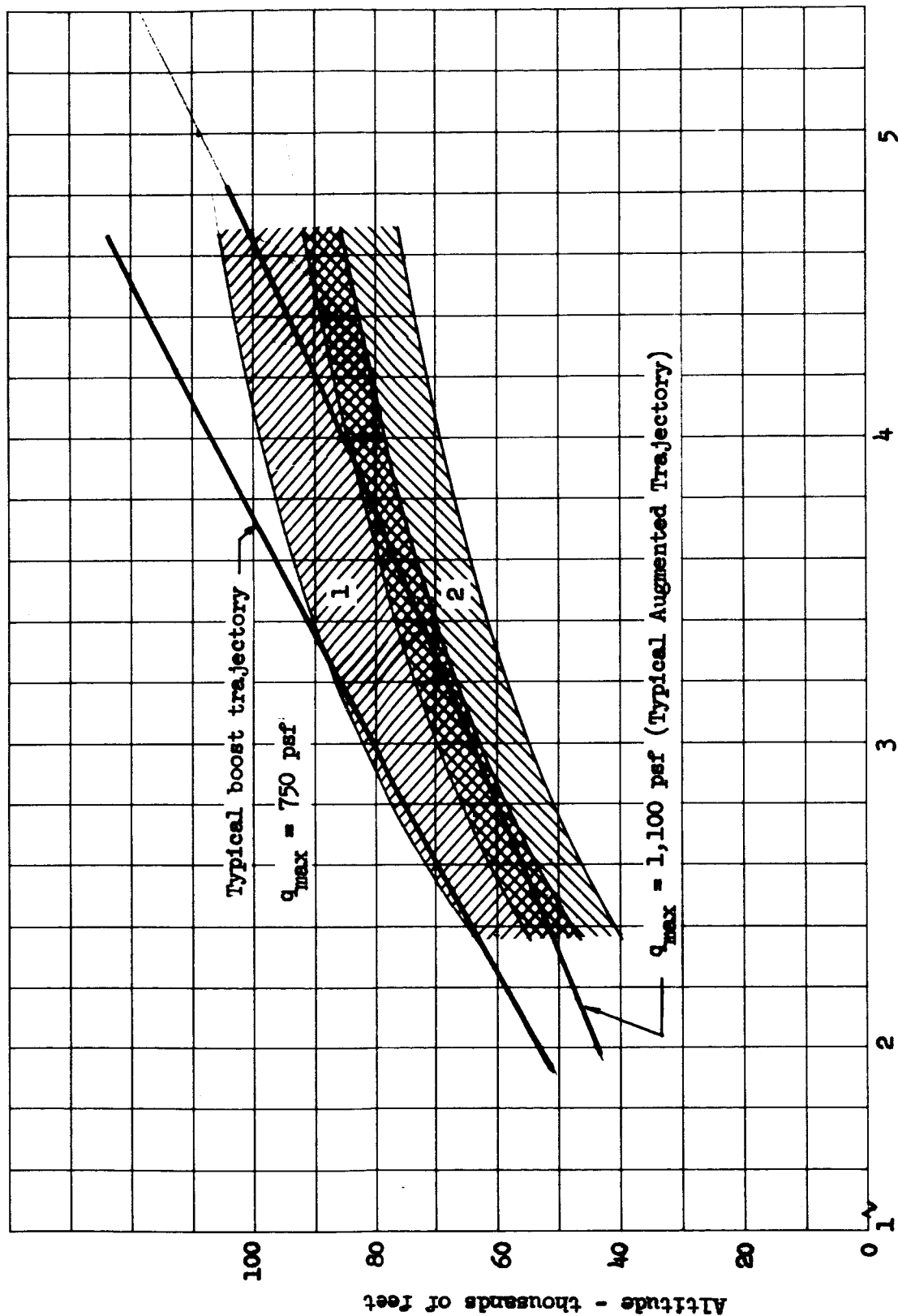
Figure 33 - Inlet-combustor match point operation

47,000 and 64,000 feet, with the normal shock at the inlet throat and exit, respectively. Above the higher altitude, the shock is disgorged so that the flow rate drops to accommodate the matching. Below 47,000 feet, the shock must pass downstream into the combustor section where it will either form obliquely off the nozzle plume or mixing zone at the proper strength to cause choking behind it, or will pass completely out of the engine. In this case the inlet will produce only drag, and while analysis of supersonic secondary flow with shocks in the combustor is not possible with the analytical methods developed during this study, it does not appear likely that this situation will produce enough thrust to overcome inlet drag at the relatively low flight Mach numbers being considered.

Curve 2 represents the operating characteristics of the same combustor with the mixing effects adding their perturbation to the inviscid operation. For this curve these effects have been estimated by comparison between the experimental data and the inviscid operating line calculated for that geometry. This corresponds to the situation discussed in the preceeding inviscid operation section, in which the combustor can handle a higher quality secondary stream. Subsequent to the estimation of the location of Curve 2, isolated points recently calculated in the mixing analysis indicate that this estimate is conservative, and that the line could be higher.

If one uses combustor operating conditions typical of Curve 2 in Figure 33, the match points move to lower altitudes and better augmentation factors, in general, but the range of operation is still limited.

Figure 34 shows the trajectory limits of the combustor operating along



Flight Mach Number -  $M_\infty$

Figure 34 - Inlet combustor matching effects on trajectory

Curves 1 and 2 with the two-shock inlet, compared with a typical C-5 vehicle trajectory. Spectacular examples of the importance of considering matching conditions are at Mach 2.37 and 3.11 at 40,000 feet, where there are no match points with either Curve 1 or 2 of Figure 33. Using maximum inlet recovery (inlet upper limit line), however, augmentation factors of 1.5 and 2.0 are predicted by the one-dimensional analysis.

The effect of mixing is to move the range of operation to the lower altitudes, where increased augmentation generally results from higher weight flows and higher total pressures. However, if one attempts to increase weight flow by increasing the size of the duct (increasing  $A_{1s}$  and  $A_{1s}/A_{1p}$ ), combustor operating conditions will be lower, the match point trajectories will be higher and the flow rate for the larger duct will decrease. There is, then, an optimum inlet-combustor combination for the selected primary rocket, disregarding structural and thermal protection weights, which provides maximum augmented engine performance, considering the trades involved with duct size, weight flow, and match point trajectories. Determination of the optimum configuration has not been made in this study. The capability has been developed, however, to perform the parametric evaluation necessary to arrive at optimum configurations as functions of trajectories based upon an analytical model which realistically describes the physical phenomena.

With a vehicle having the capability to vary its trajectory aerodynamically it should be possible to fly along a trajectory giving optimum engine performance. However, the ballistic path followed by a vehicle

such as the C-5 prevents this maneuvering ~~except~~ by thrust modulation.

The necessity for such a trajectory control and matching could be eliminated if a combustor-primary combination could be found whose operating conditions curve in Figure 26 were nearly horizontal and at a high  $P_{1s}/P_{1s}^*$  so that match points could be obtained at all altitudes and Mach numbers. It appears possible that this could be achieved by throttling the primary engines. When the chamber pressure of the primary increases, the jet exit pressure also increases and the combination of higher weight flow and higher pressure produces more constriction of the secondary flow by virtue of increased mixing and pluming of the jet. This would tend to move the normal shock forward toward the throat and increase the inlet performance. Reducing primary weight flow would produce the opposite results. It might be possible to increase the augmentation sufficiently at certain conditions to offset the weight penalties occasioned by having to carry a larger engine than is needed for portions of a flight.

#### B. Powerplant Performance

It is customary to refer to engine performance in terms of thrust, specific impulse, or thrust coefficient. Since this study is primarily a comparison of what can be achieved with and without the addition of a secondary air system, the augmented performance is described in terms of the augmentation factor,

$$F_{AUG} = \frac{I_{s_{AUG}}}{I_{s_R}(\text{THEORETICAL})}$$

The augmented specific impulse is defined as the theoretical augmented thrust produced by the engine divided by the sum of primary propellant and secondary fuel flow rates:

$$I_{s_{AUG}} = \frac{T}{\dot{m}_p + \dot{m}_s} \left( \frac{lb_f}{lb_m/sec} \right) \quad (64)$$

Referring to Figure 22, the engine system thrust is determined from the thrust produced by its components:

$$T = T_{INLET} + T_{ROCKET} + T_{DUCT} \quad (65)$$

$$T_{INLET} = \int_I P dA = \dot{m}_s V_{IS} + P_{IS} A_{IS} - \dot{m}_s V_{\infty} - P_{\infty} A_{\infty} - P_{\infty} (A_{IS} + A_{IP} - A_{\infty}) \quad (66)$$

$$T_{ROCKET} = \int_R P dA = \dot{m}_p V_{IP} + P_{IP} A_{IP} \quad (67)$$

$$T_{DUCT} = \int_I^e P dA = (\dot{m}_s + \dot{m}_p + \dot{m}_{SF}) V_e + P_e A_e - \dot{m}_p V_{IP} - P_{IP} A_{IP} - \dot{m}_s V_{IS} - P_{IS} A_{IS} - P_{\infty} (A_e - A_{IP} - A_{IS}) \quad (68)$$

$$T = (\dot{m}_s + \dot{m}_p + \dot{m}_{SF}) V_e - \dot{m}_s V_{\infty} + A_e (P_e - P_{\infty}) \quad (69)$$

This equation is **similar** to Equation (17) used in the one-dimensional cycle analysis. There are assumed to be no heat transfer or frictional effects between the engine system and its boundaries.

In order to retain a degree of realism in the generation of parametric data, most of the effort was oriented toward the S-1A and S-2A configurations with perturbations from these baselines. The theoretical rocket specific impulse for the LO<sub>2</sub>/RP-1 engines of these configurations is shown in Figure 35. The reference specific impulse ( $I_{s_R}$ ) is, in this case, the specific impulse at a nozzle area ratio of 16 at the appropriate altitude conditions.

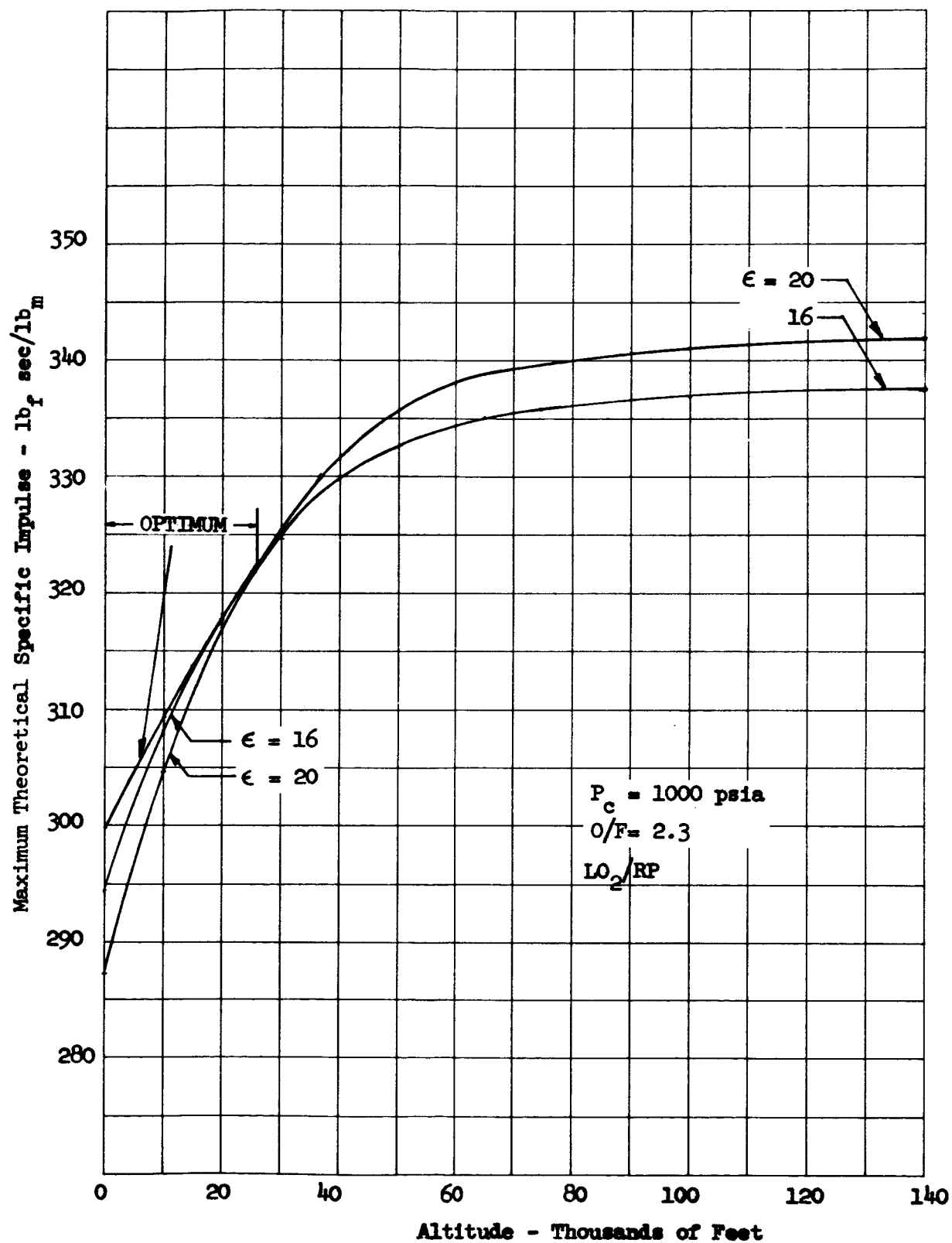


Figure 35 - Theoretical Rocket Specific Impulse

# 1. One Dimensional Cycle Analysis (Unmatched Inlet-Combustor Operation)

The engine performance data presented in this section were calculated as outlined in Section B.1., without regard to the inlet-combustor matching requirements. In all cases, the supersonic solution to the one-dimensional analysis was used. When studying these data it is of paramount importance to remember that conclusions drawn must be tempered with judgement and awareness of the matching limitation. However, the trends which are shown have been confirmed, in general, with the analyses considering matching.

## a. Base Line Performance

The calculated performance of the two base line configurations are as shown in Figures 36 and 37 and are based upon the following assumptions:

### Primary Rocket

$$\text{LO}_2/\text{RP-1}$$

$$\text{O/F} = 2.3$$

$$P_c = 1000 \text{ psia}$$

$$\epsilon = 10.1 : 1$$

$$\dot{m}_p = 28,253 \text{ lb}_m/\text{sec}$$

$$A_{1p} = 370.35 \text{ ft}^2$$

$$P_{1p} = 1899.4 \text{ lb/ft.}^2$$

### S-1A

$$A = 1247 \text{ ft}^2$$

$$A_{1s} = 1730$$

$$A_2/A_1 = 1.4$$

$$\eta_{KE} = 0.92$$

$$A_e = A_2 = 2944 \text{ ft}^2$$

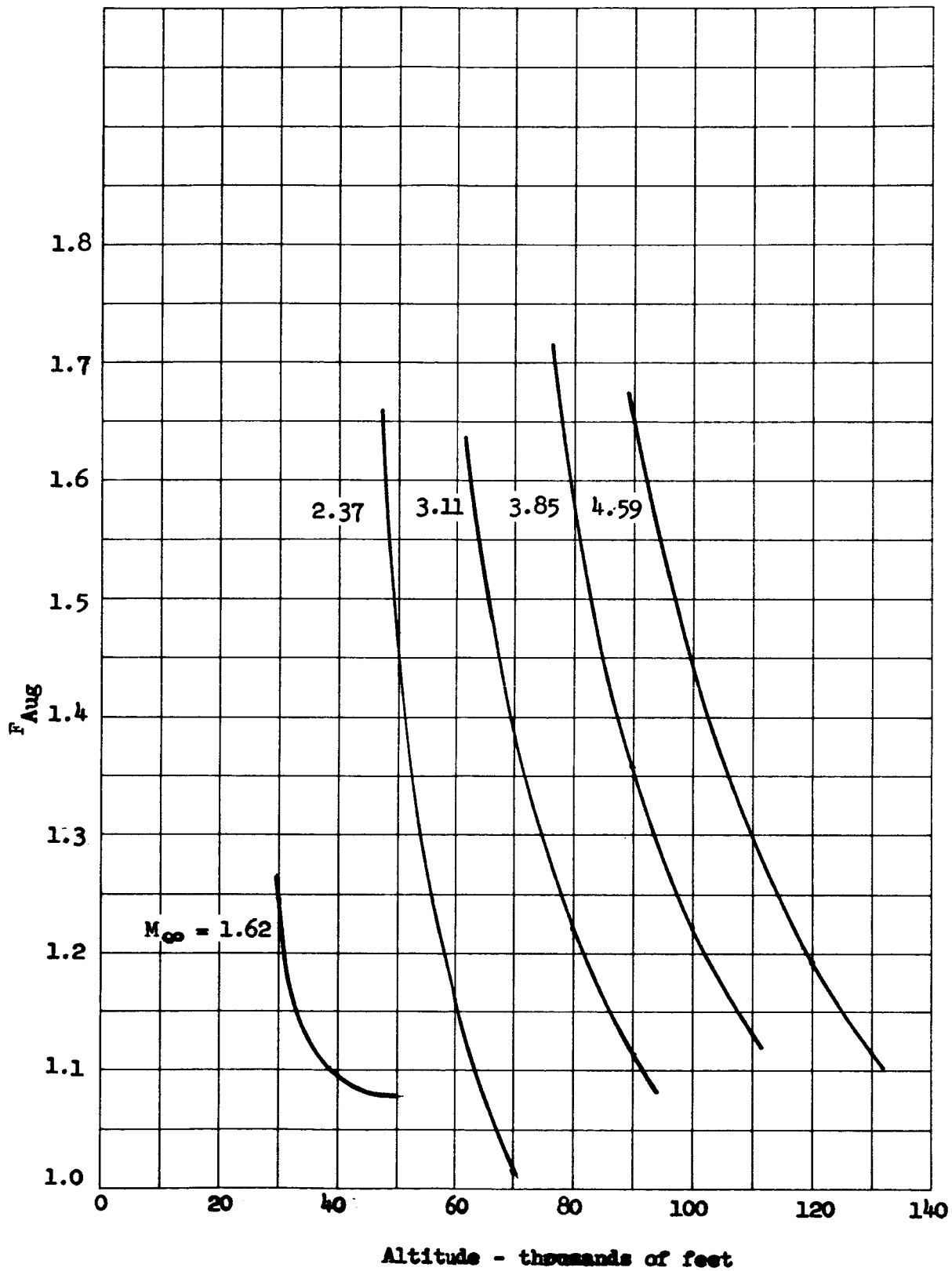


Figure 36 - S-1A Baseline Performance

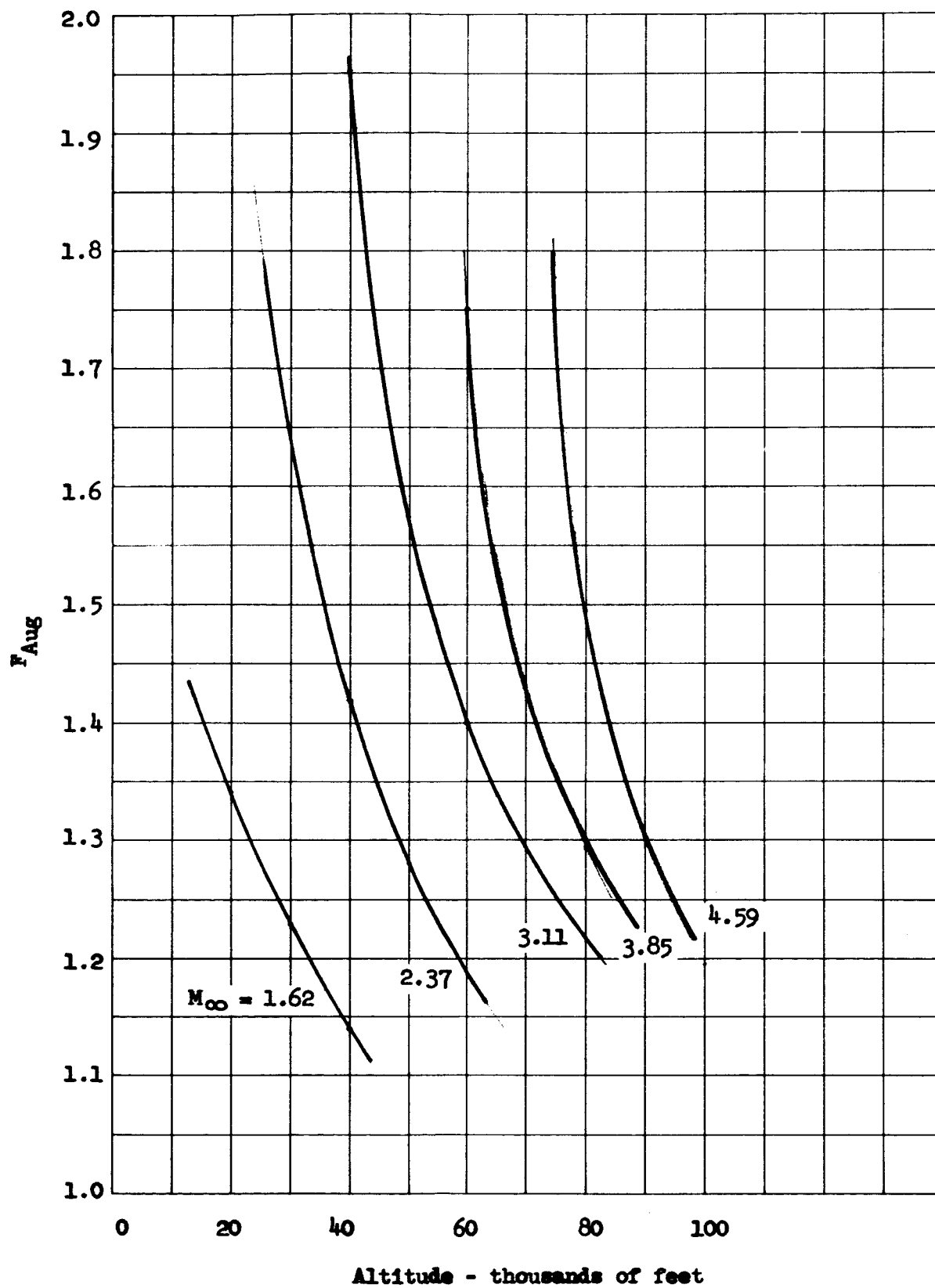


Figure 37 - 8-2A base line performance.

### S-2A

Inlet capture area and total pressure recovery are for 2-shock inlet (Mach 3 design point)

$$A_{\text{cowl}} = 1933 \text{ ft}^2$$

$$A_{1s} = 1760 \text{ ft}^2$$

$$A_2 = 1.4 A_1, A_e = 1.285 A_2 = 1.8 A_1$$

#### b. Parametric Performance

The effects on the performance of the base line designs due to variation of a number of parameters are discussed in the paragraph below.

Incomplete Afterburning: The effect on S-1A performance of no secondary combustion was determined by replacing the oxygen in the air with nitrogen for two flight conditions.

The calculated performance was as follows:

M	Alt.	$P_s$	$\dot{m}_s / \dot{m}_p$	$(F_{\text{Aug}})_{\text{Comb.}}$	$(F_{\text{Aug}})_{\text{No. Comb.}}$
3.11	80,000	1544	0.368	1.216	1.213
2.37	50,000	3398	1.19	1.465	1.457

Apparently the effects of non-afterburning are not significant at the lower weight flow ratios and the major results of secondary air addition accrue from momentum interchange only and these results are sufficient to produce respectable augmentation.

Primary Area Ratio: The primary rocket area ratio was varied from 8 to 16 in the S-1A configuration, with the results on augmentation factor as shown in Figure 38 for a typical trajectory. For this

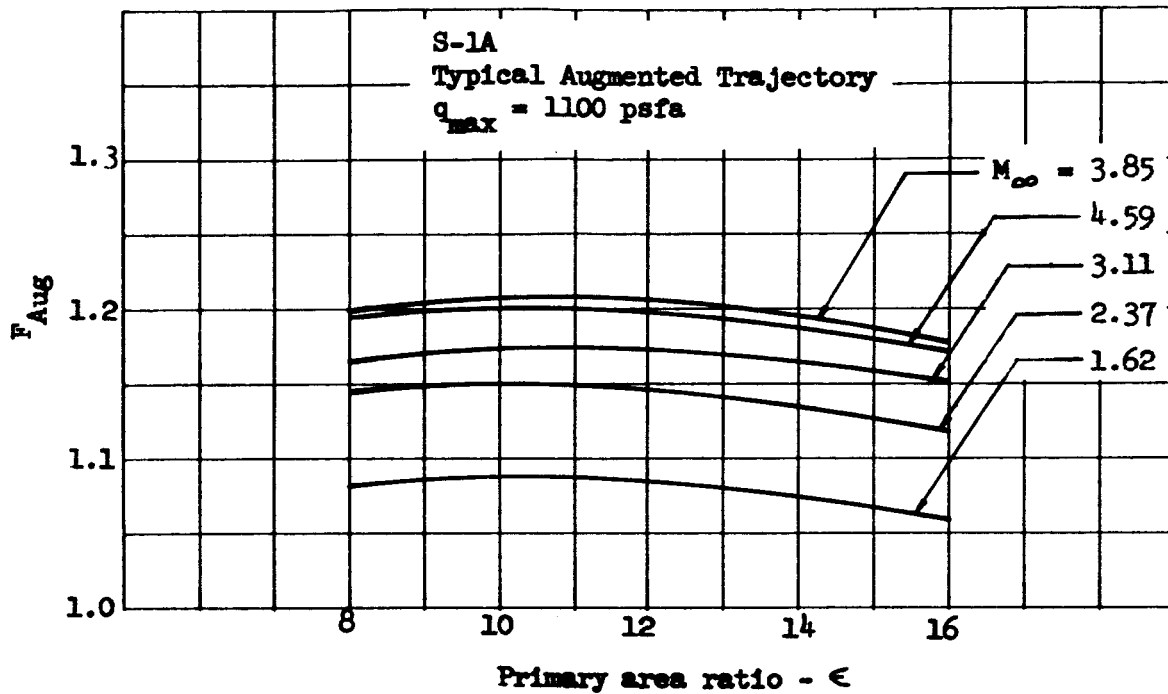


Figure 38 - Effects of Primary Area Ratio on Augmentation

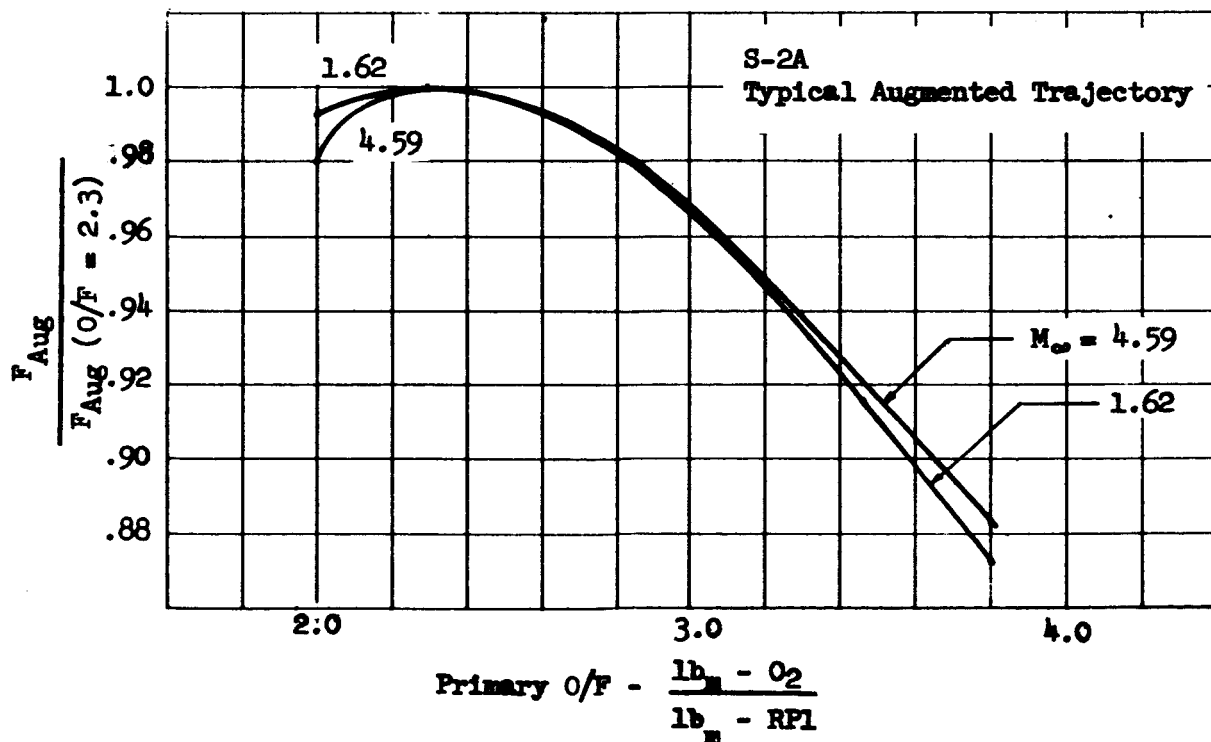


Figure 39 - Effects of Primary O/F on Augmentation

configuration, an area ratio of about 10 to 12 is optimum, regardless of the point on the trajectory. This indicates that the optimum area ratio is more a function of combustor geometry than of secondary conditions.

Primary Oxidizer-Fuel Ratio: The effect of varying primary O/F on the augmented engine differs little from the effect on the rocket alone, further indicating the relative insensitivity of augmented performance to heat release in the combustor. Figure 39 illustrates these effects. The optimum mixture ratio for the augmented engine is only slightly richer than that for the pure rocket with the same chamber pressure and area ratio. This does not preclude the possibility that at very high secondary to primary mass flow ratios the beneficial effect of a more fuel rich primary might be substantial.

Inlet Total Pressure Recovery: As has been stated in the section on inlet and combustor operation, high inlet total pressure recovery contributes to high augmentation factors. This is demonstrated by the data shown in Figures 40 and 41. The data in Figure 40 were generated for the S-1A configuration along a typical trajectory by replacing the  $\eta_{KE} = 92\%$  inlet with a normal shock inlet having the same capture area. At low supersonic Mach numbers the normal shock inlet performs virtually as well as the better inlet. At higher Mach numbers, however, the detrimental effects of the normal shock recovery are more serious. The slight tail-up of the curve beginning at Mach 4 is due to the fact that the augmented performance even with the better inlet has begun to fall off very sharply. In Figure 41, augmentation factor is plotted versus secondary total

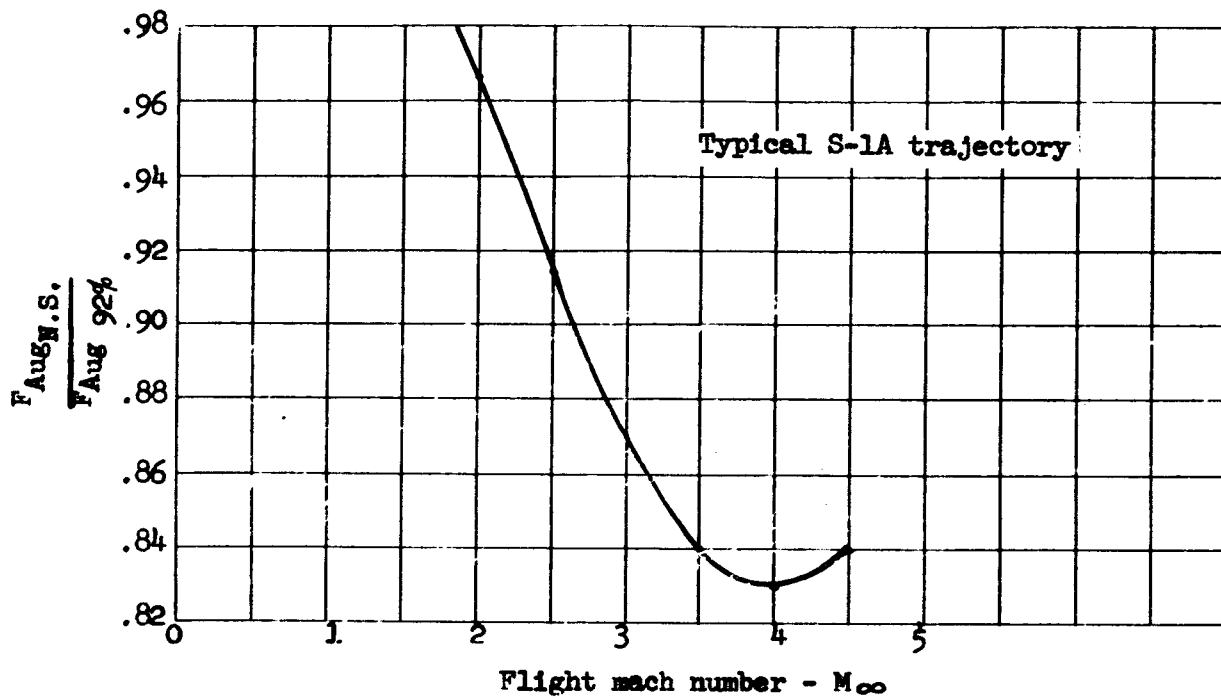


Figure 40 - Effects of Normal Shock Recovery on S-1A Performance

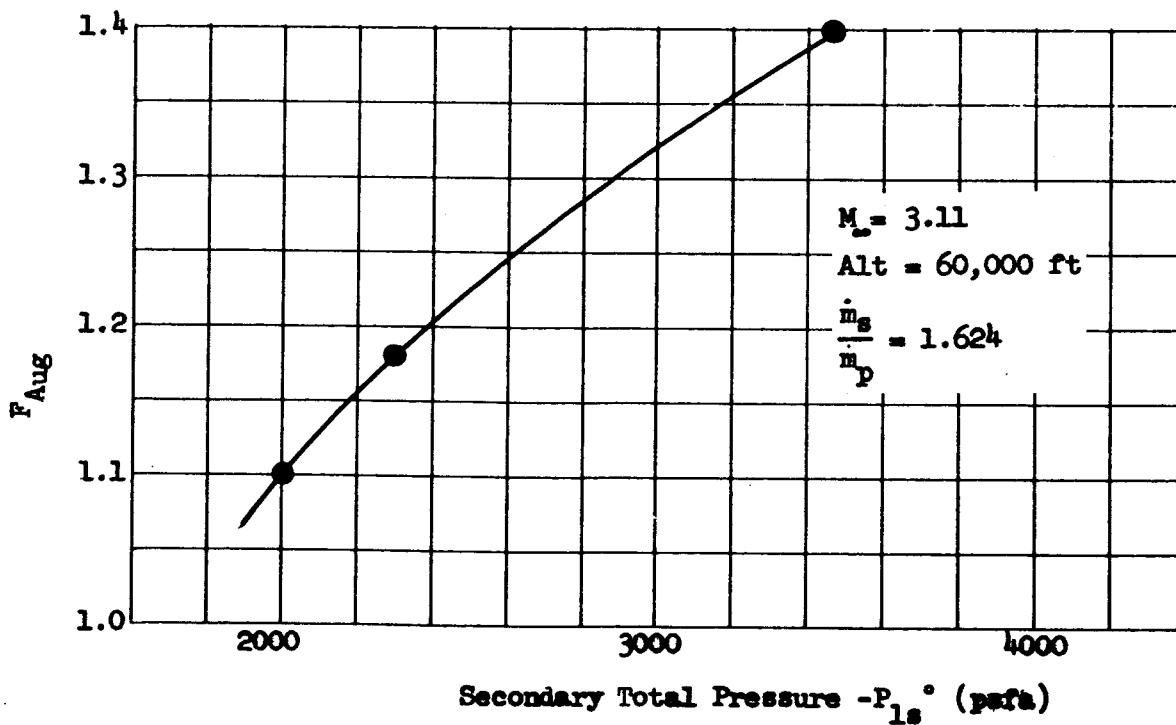


Figure 41 - Effect of Variable Inlet Recovery on S-2A Performance

pressure (or recovery) for the S-2A configuration at a single Mach number and altitude of 3.11 and 60,000 feet respectively. It is seen that augmentation factor increases as secondary total pressure increases, for a constant secondary flow rate.

Secondary Flow Rate and Mach Number: The data in Figures 42 and 43 were generated for a flight Mach number of 3.11 and altitude of 60,000 feet without specific configuration orientation, with augmentation shown as a function of secondary to primary mass flow ratio. In Figure 42 the inlet geometry was assumed to be such that the secondary Mach number at station 1 was equal to one. In Figure 43 the inlet diffusion process was greater, producing a secondary Mach number of 0.27 with its associated higher static pressure. Both configurations were completely expanded so that the duct exit pressure was equal to ambient pressure. The difference in combustor area ratio between the two resulted from lack of solutions to the one-dimensional equations at some points, but does not substantially affect the results.

Two things may be mentioned here: first, increasing flow rate has a beneficial effect on augmentation in both cases, and second, the better augmentation is produced by the engine system in which the inlet ~~diffuses~~ the secondary air to a lower Mach number at the entrance to the combustor. However, it should be emphasized that the performance data for the low secondary Mach number situation were not based upon a matched situation between inlet and combustor and also that the deleterious effects of this requirement become more pronounced at the higher secondary to primary area ratios associated with the higher mass flow ratios. The result of the

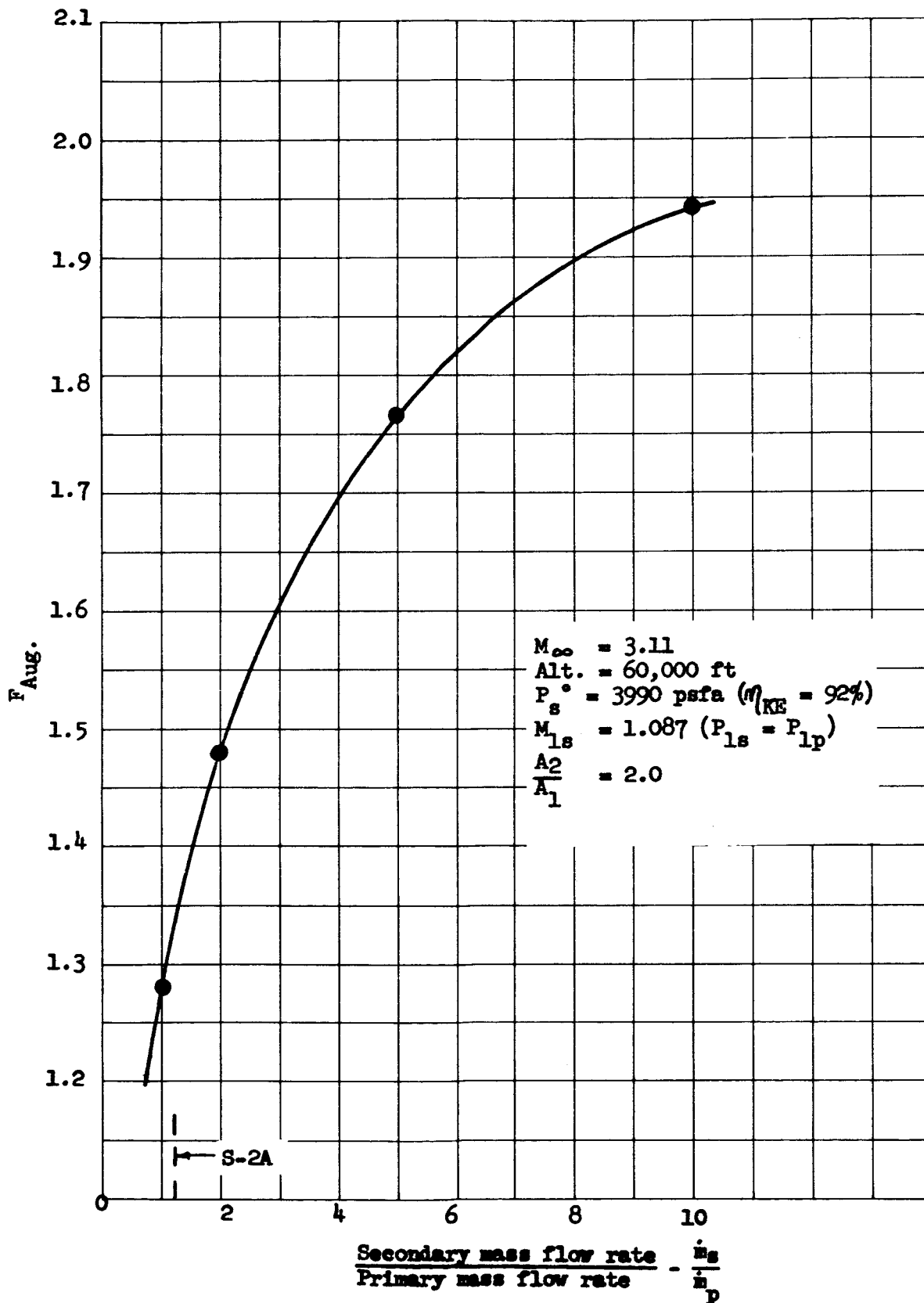


Figure 42 - Effects of Secondary Flow Rate on Augmentation

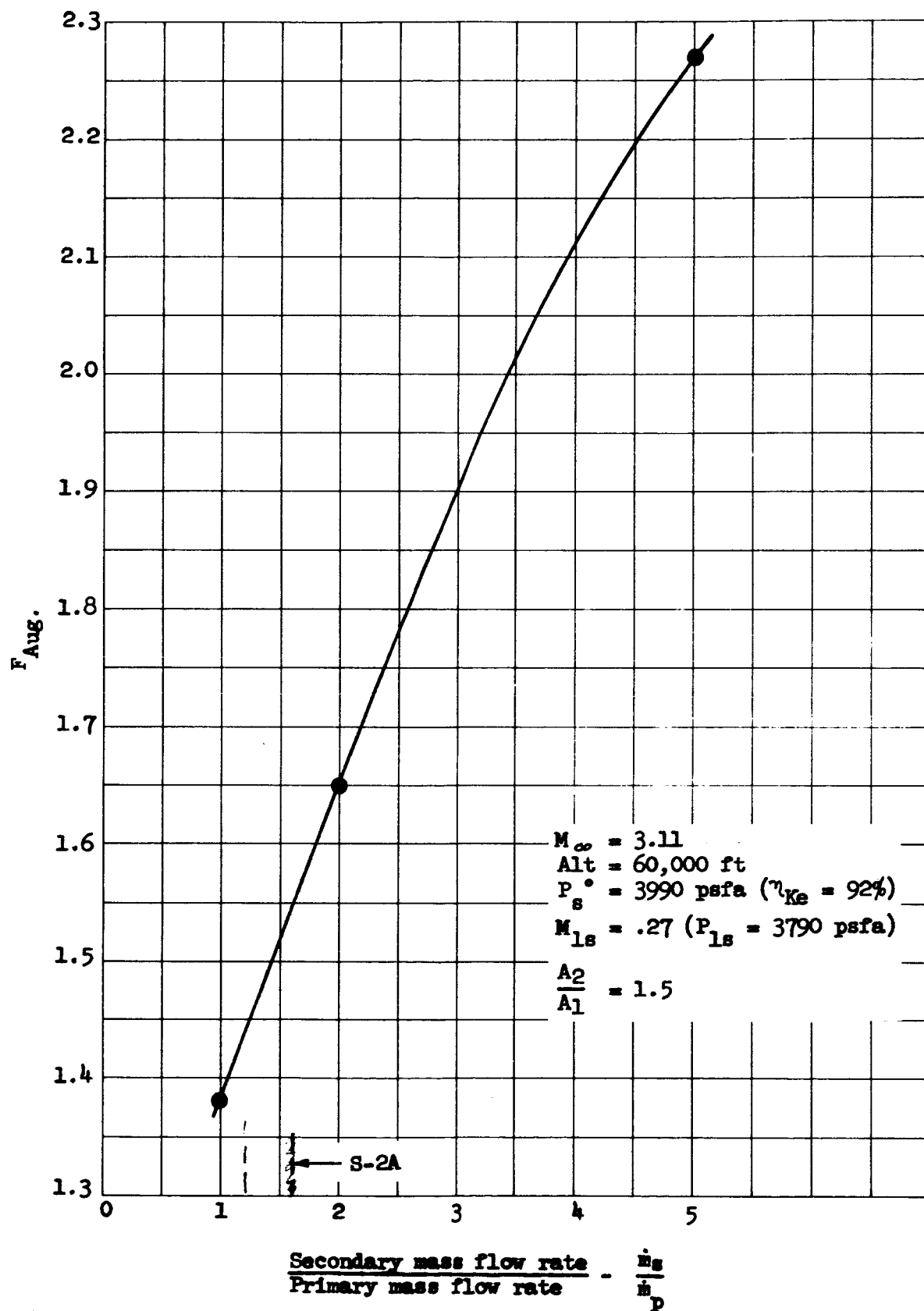


Figure 43 - Effects of Secondary Flow Rate on Augmentation

sonic secondary flow at station 1 is to decouple the inlet from the effects of the combustor operating characteristics.

The effects of such a technique on S-2A augmentation factor is shown in Figure 44 where augmentation factor is plotted versus the dynamic pressure  $q$ , for two flight Mach numbers - 2.37 and 4.59. The performance of the standard S-2A, with the two-shock inlet operating at its point of maximum total pressure recovery, is compared to the same configuration, with the inlet modified so that the secondary flow is just sonic at station 1. Also shown is the performance of a sonic inlet with a kinetic energy efficiency of 92%. At both Mach numbers, the performance for all configurations increases with  $q$ , and the subsonic injection inlet shows superior performance over the sonic injection inlet with the same recovery, especially at the higher flight Mach number.

The reasons for this better performance are shown in Figure 45, where the thrust contributions of the three engine components, primary, inlet and combustor, are shown for both two-shock inlets. The sonic injection inlet produces only drag on the system, and the thrust contributed by the combustor is insufficient to make up this decrement. However, at extremely high  $q$  trajectories, the sonic injection may still provide better augmentation than the other system, suffering the penalties accruing from the matching requirements.

Mixing Section Divergence: The effect of duct divergence on the S-2A performance at the higher Mach number and altitudes is shown in Figure 46. In all cases the exit area is fixed at 1.8 times the initial duct area at station 1. The nozzle expansion ratio is either

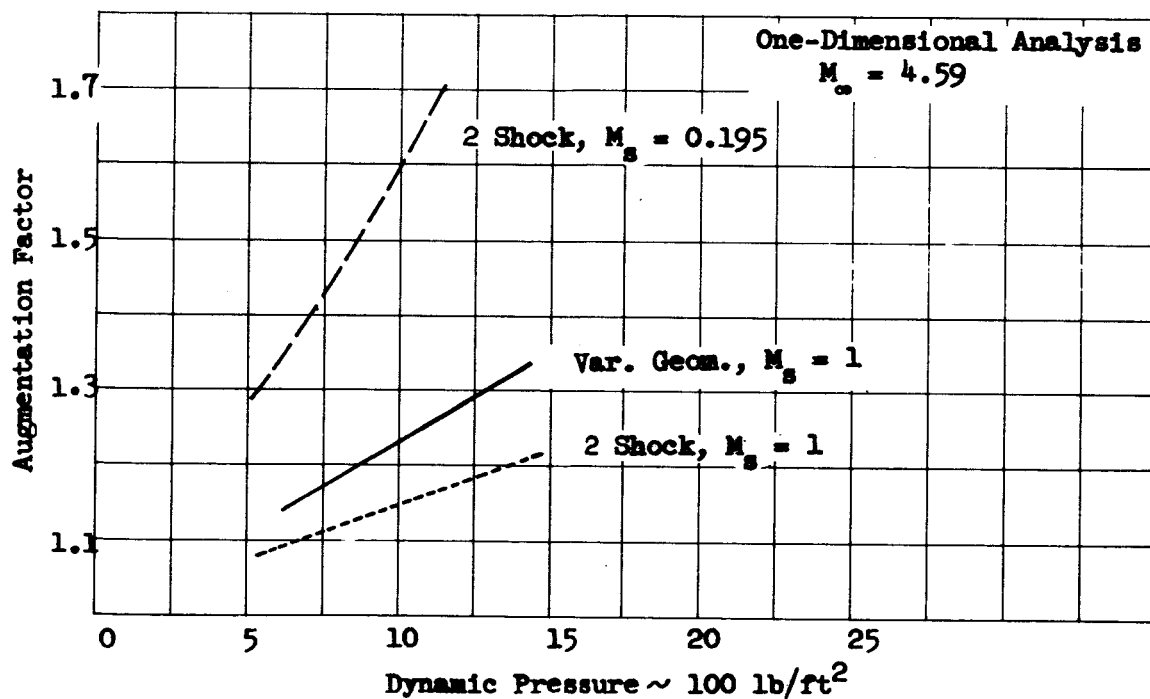
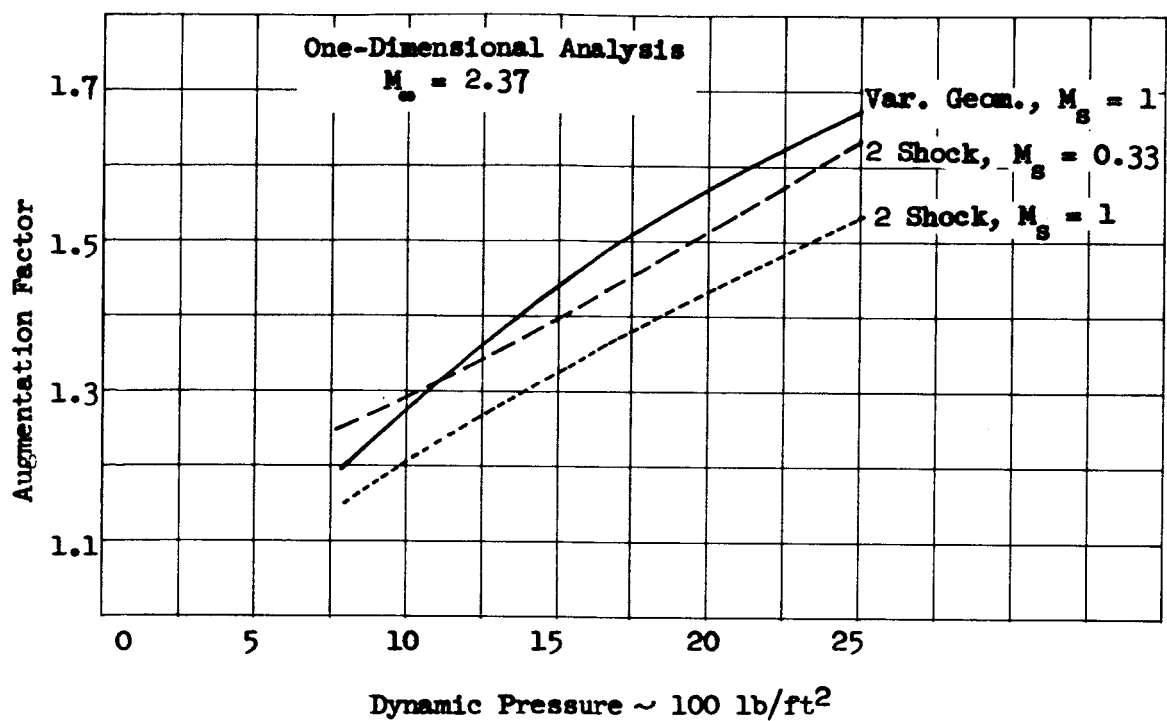


Figure 44 - Effect of Secondary Mach Number on Augmentation Ratio

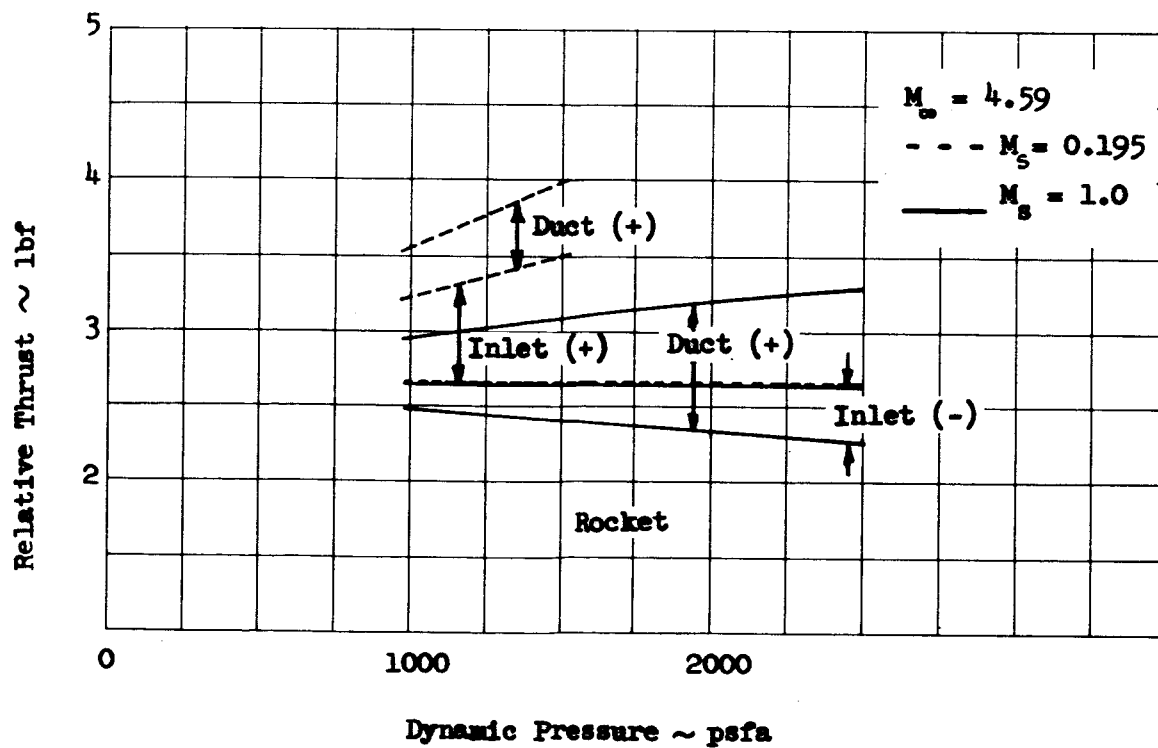
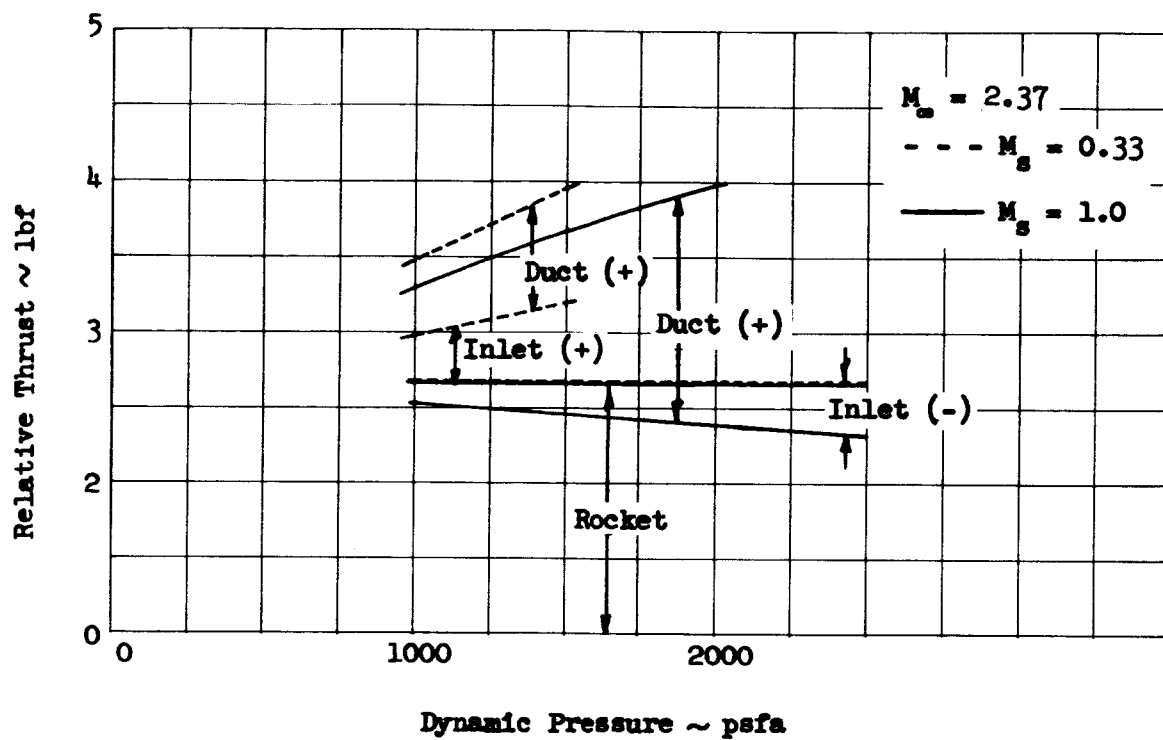


Figure 45 - Component Thrust Contribution

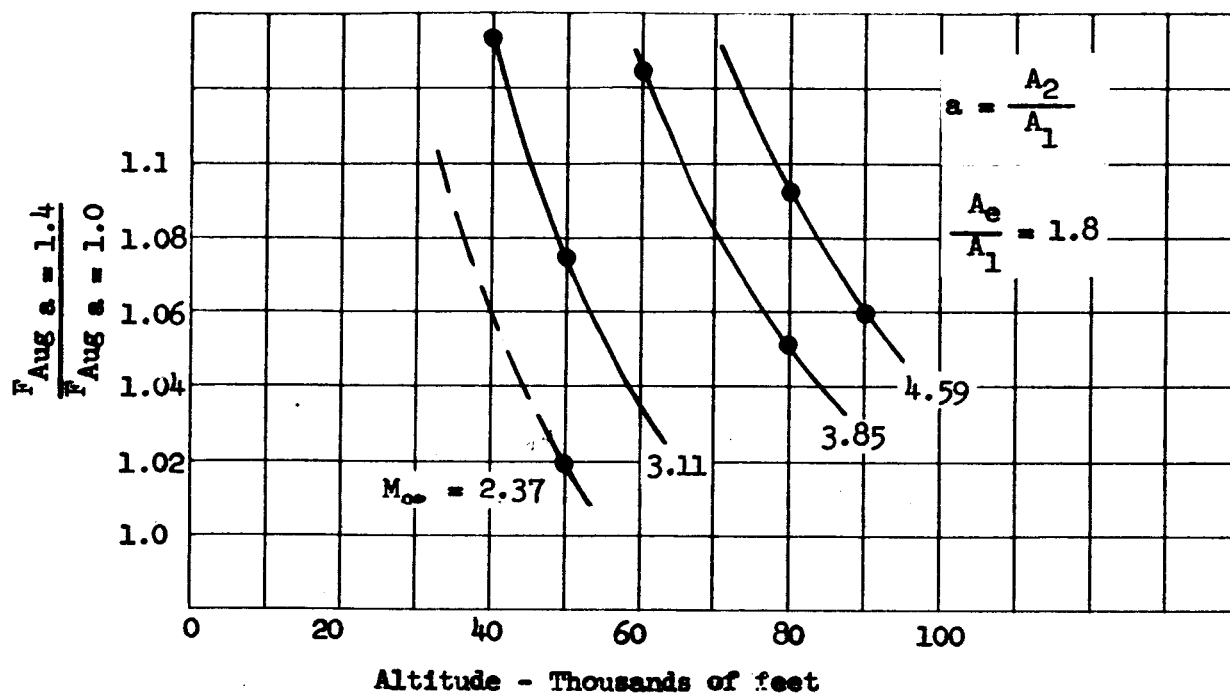


Figure 46 - Effect of Combustor Area Ratio on S-2A Augmentation

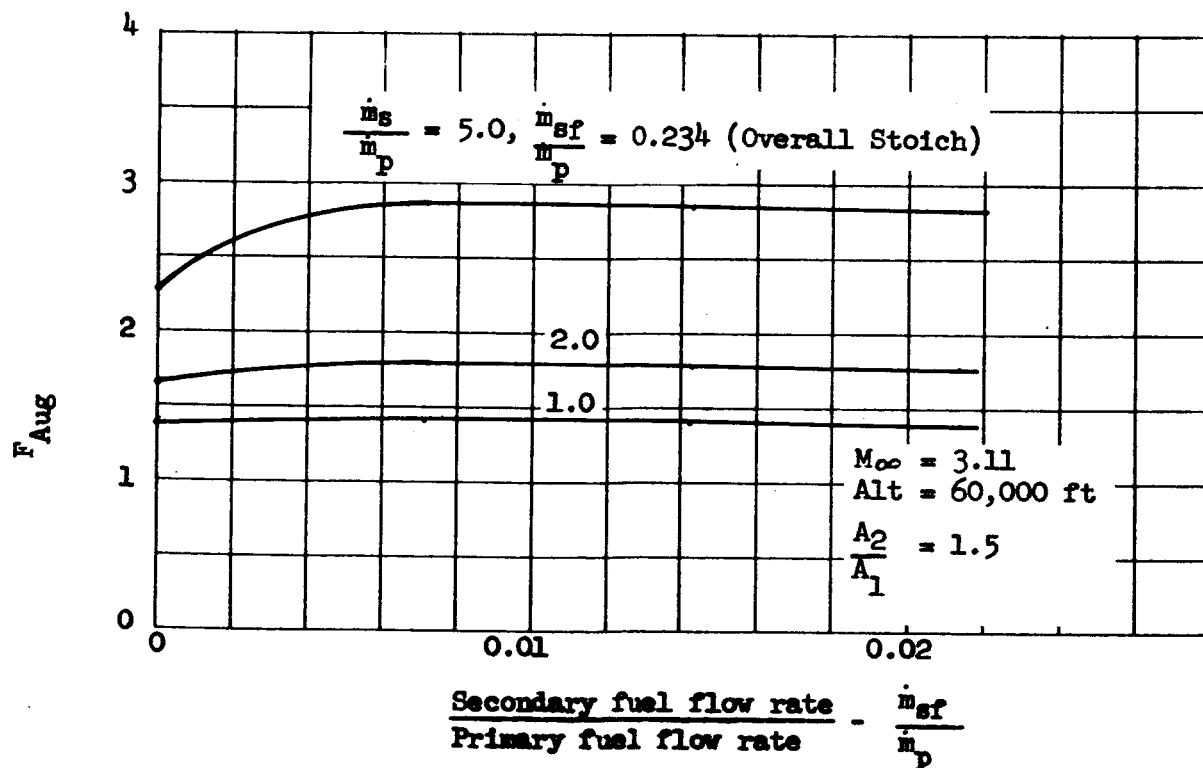


Figure 47 - Effects of Secondary Fuel Injection on Augmentation

1.8 or 1.285 to correspond with the duct area ratios of 1.0 and 1.4, respectively. The higher divergence duct provides slightly better augmentation factors at all conditions studied.

Secondary Fuel Injection: The secondary to primary mass flow ratio for an overall stoichiometric oxidizer to fuel ratio is 1.55.

Figure 47 presents augmentation factor versus secondary fuel to primary propellant flow rate, where the secondary fuel is injected with zero velocity at station 1. At the high secondary to primary weight flow ratio of 5, the secondary fuel addition produces a slight increase initially but then begins to fall off. The fact that the augmentation ratio is thereafter only slightly affected by increasing secondary fuel addition is further illustration of the relative insensitivity of performance to combustor heat release.

## 2. Engine Performance With Inlet-Combustor Matching

The calculations for engine performance based upon matched operation of the inlet and combustor have been performed in two ways: first, the secondary conditions established for compatible operation in Figure 33 were input into the One-Dimensional Cycle Analysis, which calculated performance for those operating conditions based upon the complete mixing and chemical equilibrium assumptions. Secondly, from Figure 24, selected conditions which the inlet is able to provide and which lie above the inviscid operating line, were used as inputs to the Two-Dimensional Mixing Analysis. This program provided the duct thrust which was added, by hand calculations to the thrusts produced by the primary rocket and the inlet, according to equations (65) through (69) at the beginning of this section. In the following paragraphs it will

be shown that there is acceptable correlation between the two methods.

a. S-2A Engine Performance With Matching

These calculations were performed by the first method, above, based upon the operating characteristics of the two-shock inlet, and combustor Configuration E in Figures 26 and 33. This configuration has the same geometric features as the S-2A engine configuration, except that the S-2A has a multiple nozzle arrangement. The area ratios,  $A_{1s}/A_{1p}$ , and  $A_2/A_1$ , and the primary rocket conditions, are the same for both configurations. The approximation of the multiple arrangement by use of the single jet and duct was discussed in Section C.2.

Figure 48a shows S-2A augmentation factors plotted versus altitude as a function of flight Mach number for the operating match points of Curve 2 in Figure 33. A comparison of these data with the S-2A baseline augmentation factors in Figure 37, calculated without regard to matching, reveals the critical effects of the matching requirement. Not only is augmentation reduced drastically, but the range of operation is now confined between narrow limits.

Figure 48b shows the same performance data based upon the operating match points of Curve 1, which operates with lower quality air. This condition results in lower augmentation factors at the same altitude, and also shifts the operating range to higher altitudes and resultant lower flight dynamic pressures.

These data demonstrate the desirability, from an engine performance standpoint, of improving combustor characteristics and the quality

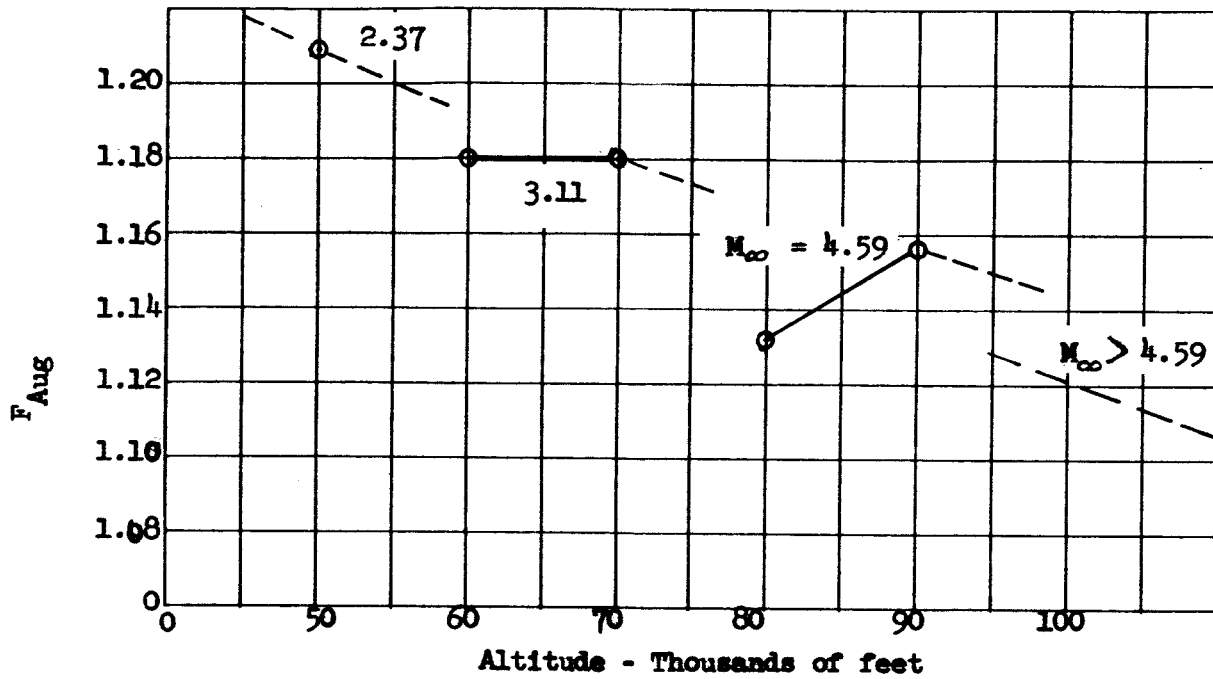


Figure 48 a - Mixing Match Point Operation

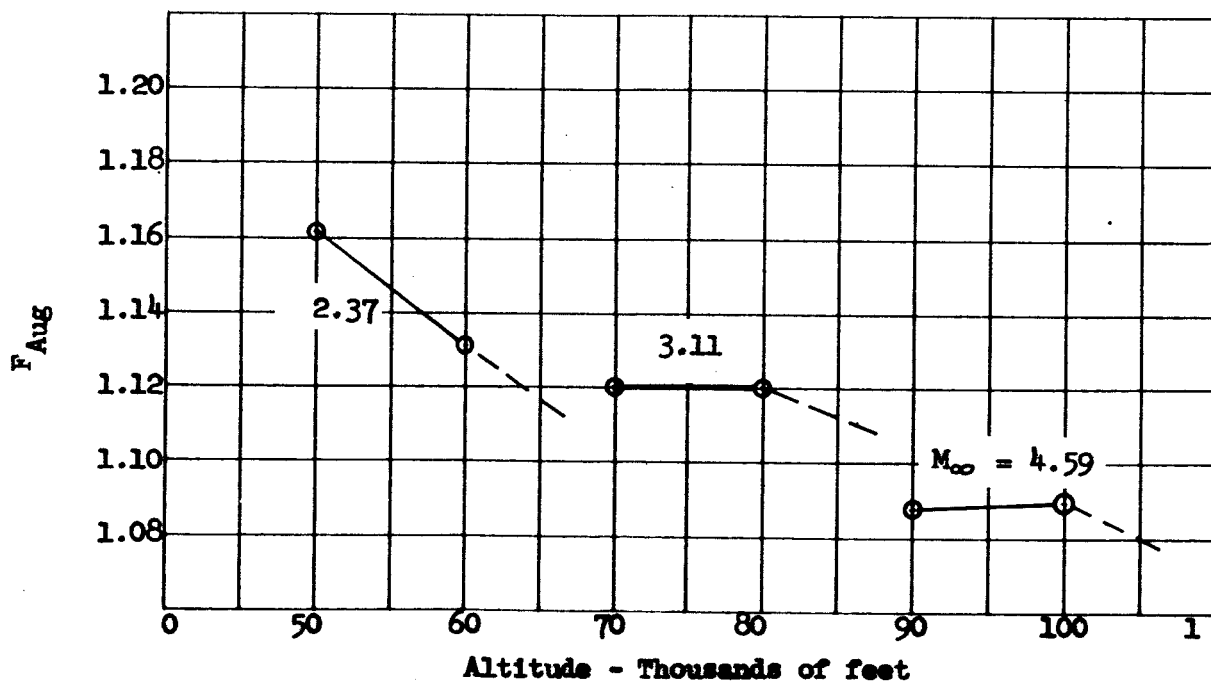


Figure 48 b - Inviscid Match Point Operation

Figure 48 - S-2A Performance with Matching

of the secondary air it can utilize through use of proper geometry and improved mixing techniques.

b. Engine Performance From Two-Dimensional Mixing Analysis

In order to determine the effects of secondary flow rate, altitude, rocket mixture ratio, and Reichardt's coefficient (a parameter which is a measure of turbulence in the mixing region), the duct geometries shown in Figure 49 were selected. The selection of these configurations was predicated upon the results obtained with other configurations; for example, constant area and divergent ducts. The constant area duct generally does not give large augmentation ratios since there is no net unbalanced area in the plane normal to the axis of symmetry, except the inlet, upon which pressure forces may act. The diverging duct provides additional unbalanced area but the requirement of choked flow generally necessitates the pressure  $P_{1s}$  to be lower than that required for the constant area duct. Obviously, the higher the pressures throughout the duct, the higher will be the net engine thrust for the same net unbalanced area. Undoubtedly, there is a configuration which gives an optimum net thrust for every given flight condition. However, it was beyond the scope of this study to determine the optimum configurations. Configuration I is constant area for  $L/D = 1.52$  and then diverges to an area ratio of  $A_e/A_1 = 1.8$  at  $L/D = 3.04$ . Configuration II, the smaller duct, is constant area for  $L/D = 2.27$  and then diverges to an area ratio of  $A_e/A_1 = 1.8$  at  $L/D = 4.54$ .

Case 1

It is instructive to first consider the larger duct since it brings

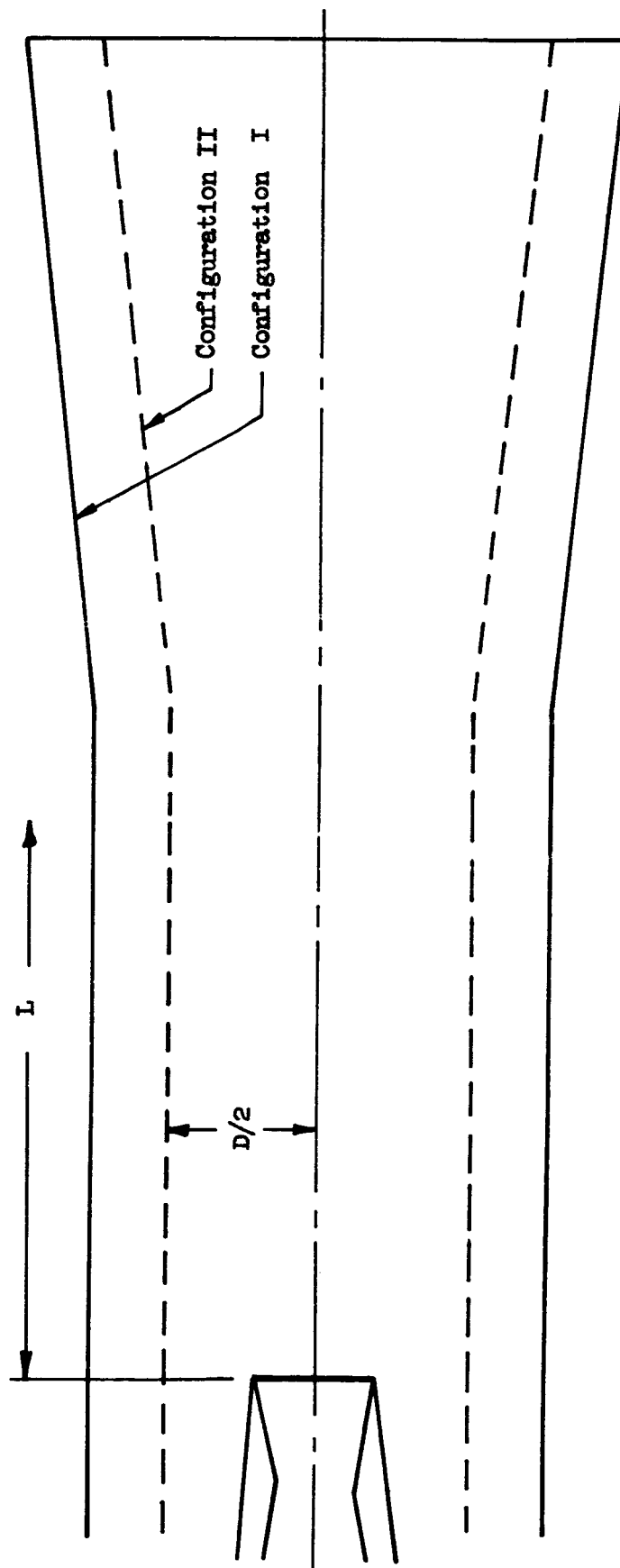


Figure 49 - Configuration Employed in Engine Performance Studies

to attention a fundamental problem that may be encountered using one-dimensional solutions. The ratio of the duct area to the rocket exit area,  $A_1/A_{1p}$  is 12.96. The primary rocket is assumed to have the following operating conditions:

Propellants -  $LO_2/RP-1$

Mixture ratio = 2.3

Combustion pressure = 1,000 psia

Flow rate = 808 lb/sec

Area ratio = 10.1

Exit diameter = 3.666 ft

Optimum specific impulse =  $302 \frac{lb_f - sec}{lb_m}$

Exit velocity = 9734 ft/sec

Exit temperature = 3681 °R

Exit pressure = 12.9 psia

The secondary air stream conditions at the exit plane of the nozzle are assumed to correspond to those provided by a two-shock inlet operating at  $M_\infty = 2.37$  and an altitude of 50,000 feet with the normal shock located at the inlet throat. The inlet design and performance characteristics are presented in Section C-1. The air stream conditions at the exit plane of the rocket nozzle are:

Static temperature = 809 R

Static pressure = 2145 psfa

Mach number = 0.35

Flow rate = 3040 lb/sec

Velocity = 489 ft/sec

Employing these initial conditions and the technique for calculating the mixed flow field as discussed in Section B-3, the results

presented in Figure 50 were obtained. The results are presented in the form of Mach number profiles, obtained from velocity and temperature profiles, at various axial locations in the mixing section. It is noted that a considerable portion of the mixed flow remains subsonic throughout the entire duct, a condition which can be physically possible only if the exit static pressure is equal to the ambient pressure. The pressure distribution for the above flow through the duct is presented in Figure 51 and, as can be seen, the exit pressure is 2250.0 psfa. The ambient pressure at the assumed altitude of 50,000 feet is 244.0 psfa, which is considerably less than the mixing section exit pressure. Consequently, such an analytical situation cannot physically exist since the ambient pressure would propagate upstream through the subsonic flow, changing the secondary flow conditions at the exit plane of the rocket nozzle. It is interesting to note that if one did not consider this phenomena, but assumed that the secondary conditions were not affected, the augmentation ratio as calculated from the above flow conditions is 1.84. The corresponding value obtained from the one-dimensional solution is approximately 1.70. It should be noted, however, that the secondary flow conditions which give this augmentation ratio are physically impossible if consideration is given to the choking condition as predicted by the theoretical Mach number profiles.

#### Case 1A

In order to determine the secondary flow conditions that are compatible with the physical situation, the secondary conditions for the above case must be altered until the results indicate that the flow

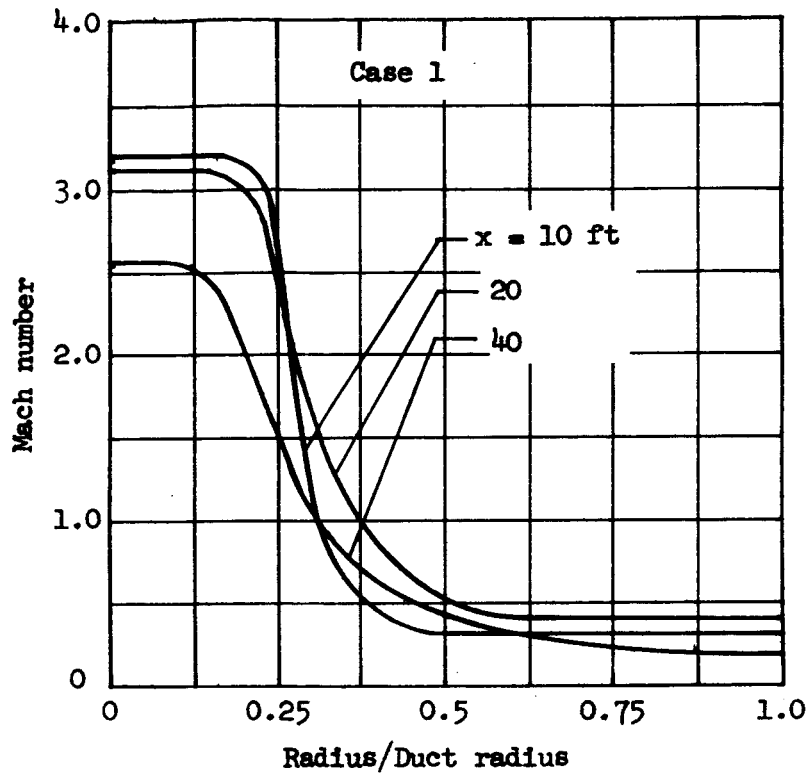


Figure 50 - Mach number profiles

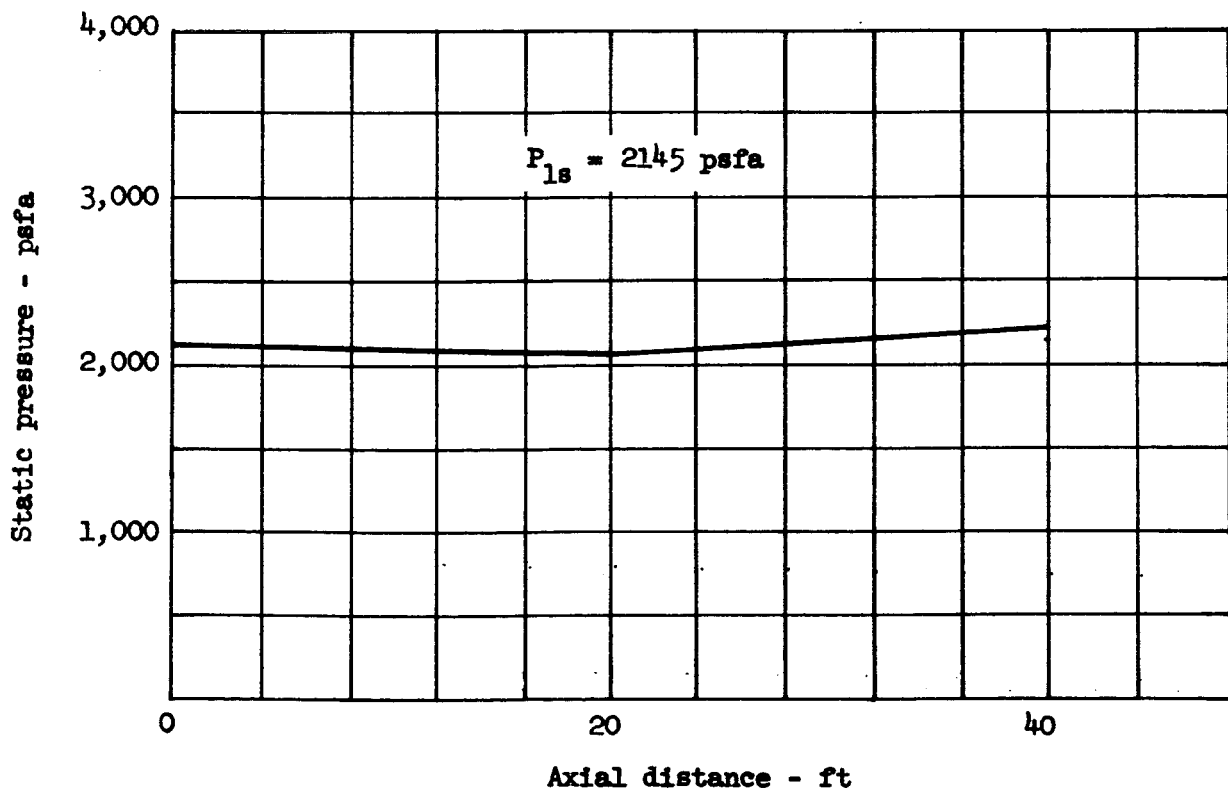


Figure 51 - Case 1 Mixing Section Pressure Distribution

through the duct is choked. In an attempt to obtain choked flow the secondary flow conditions at the nozzle exit plane were altered by permitting the inlet normal shock to move downstream of the inlet **throat**. Those conditions are as follows:

Static pressure = 1920 psfa

Static temperature = 544 R

Mach number = 0.40

Flow rate = 3040 lb/sec

Velocity = 544 ft/sec

The resulting Mach number profiles are shown in Figure 52. Comparing the minimum Mach numbers in the exit profiles for the two sets of secondary flow conditions, it is seen that the minimum exit Mach number for the later case has increased from that of the former case but is still subsonic. Consequently, further changes in the secondary flow conditions must be made until the choking condition occurs. As a point of interest, the augmentation ratio obtained for the second case of secondary flow conditions is 1.51, thus indicating that the trend is toward lower augmentation ratios as the choking condition is approached.

#### Case 2

Consider now Configuration II with identical secondary pressure, temperature, and velocity as in Case 1. Thus, since Configuration II has a smaller flow area than that of Configuration I, the decrease in flow area effects a proportional decrease in secondary flow rate. The Mach number profiles were presented previously in Section A-3, Figure 31. As can be seen, the minimum Mach number at the duct exit is supersonic indicating that the entire flow is choked. The

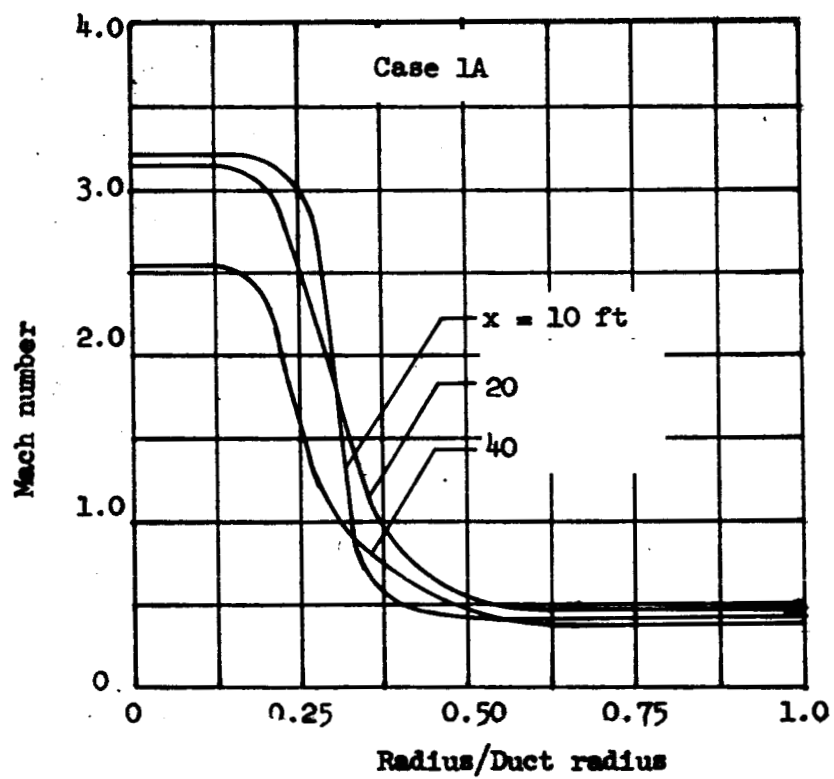


Figure 52 - Mach Number Profile

augmentation ratio for this flight condition ( $M_\infty = 2.37$  at 50,000 feet) is 1.14. Thus, decreasing the secondary flow rate by decreasing the flow area results in the choking condition occurring with a relatively high pressure  $P_{1s}$ . However, since the net unbalanced area decreases, the augmentation ratio is also lower than that given for the larger diameter duct. From the results of the above two cases, it appears that there is an optimum duct flow area which would provide a maximum augmentation ratio for given secondary pressure, temperature, and velocity.

### Case 3

Another method of effecting a change in secondary weight flow, other than changing the flow area, is to operate at a different altitude with the same flight Mach number. In order to determine this effect an altitude of 40,000 feet was selected. With the inlet operating with the normal shock at the throat, the secondary flow conditions are:

Static pressure = 3445 psfa

Static temperature = 809°R

Mach number = 0.35

Flow rate = 1960 lb/sec

Velocity = 489.0

The Mach number profiles for this flight condition are presented in Figure 53, which illustrated that the flow was choked. The augmentation ratio for this flight condition is 1.33. Thus, the augmentation ratio was increased 16 percent above that obtained at an altitude of 50,000 feet. However, it should be noted that the dynamic pressure increased by approximately 60 percent at the

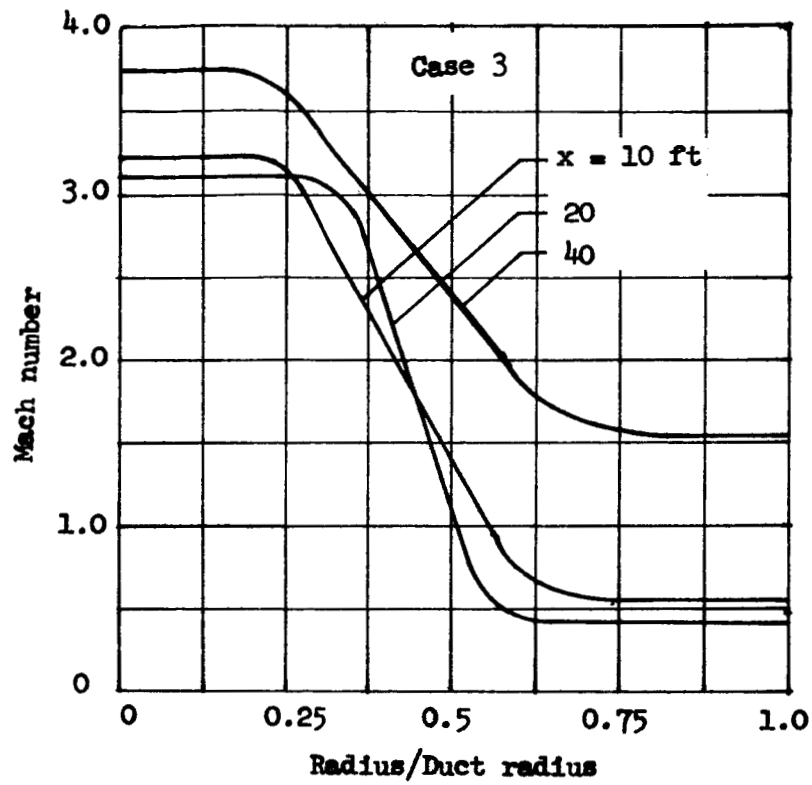


Figure 53 -Mach number profiles

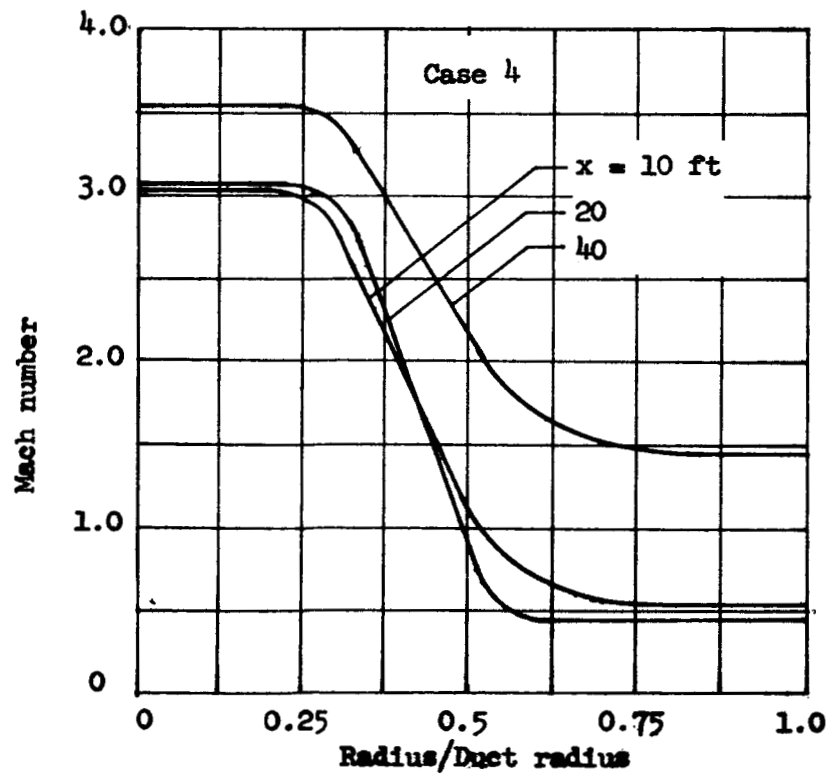


Figure 54 - Mach number profiles

lower altitude ( $q = 1540$  psf at 40,000 feet and  $q = 960$  psf at 50,000 feet).

#### Case 4

In the previous cases the rocket exhaust conditions were constant and only changes of the secondary stream were studied. Since the engine thrust is dependent to some extent upon the amount of energy released within the mixing section it is of interest to determine the effect of decreasing the rocket mixture ratio, thus providing additional fuel for combustion with the air stream.

The results presented in Figure 54 were obtained for secondary flow conditions corresponding to those of Case 2 and a rocket mixture ratio of 2.0. Upon comparing the Mach number profiles with those of Case 2 it is seen that the exit Mach numbers in the outer portion of the flow field have increased only slightly. Comparison of the temperature profiles at the duct exit for the two cases, as shown in Figure 55, also show only slight increases in temperature due to the increased combustion. The augmentation ratio for this case is 1.19, an increase of approximately 4.5 percent over that obtained for Case 2. Thus, it appears that within the range 2.0 to 2.3 there is relatively small effect of mixture ratio on the augmentation ratio.

#### Case 5

Considerable interest has been devoted to methods of increasing the rate of mixing between two streams by the utilization of turbulence or vortex generators. The effect of such devices may be assessed analytically by assuming that the increased rate of mixing is described by an increase in Reichardt's coefficient. Shown in

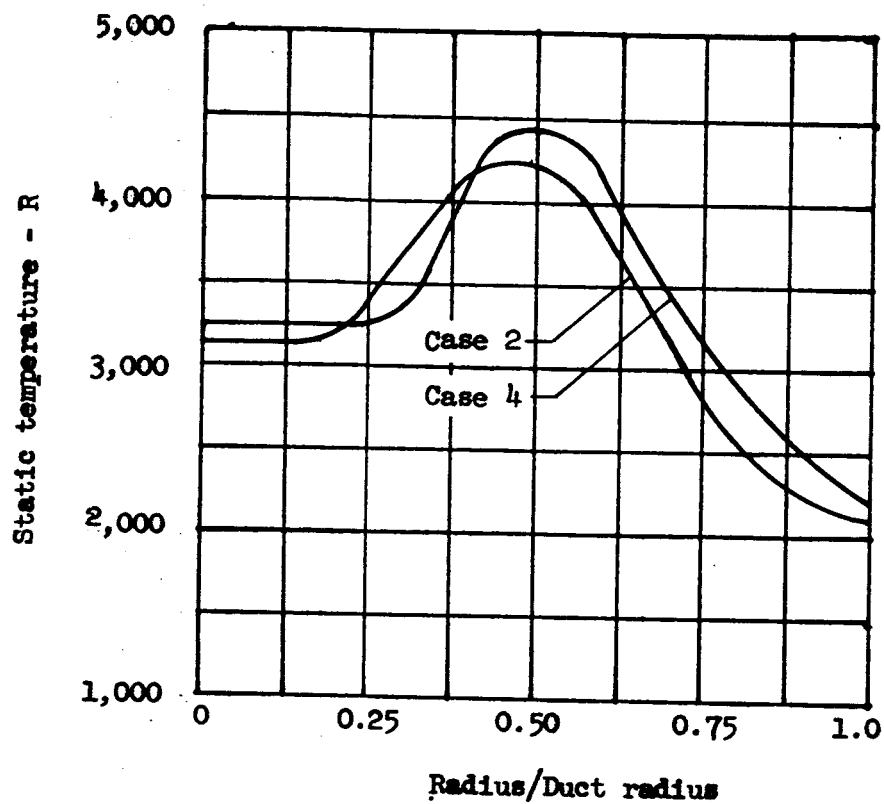


Figure 55 - Static Temperature Profiles

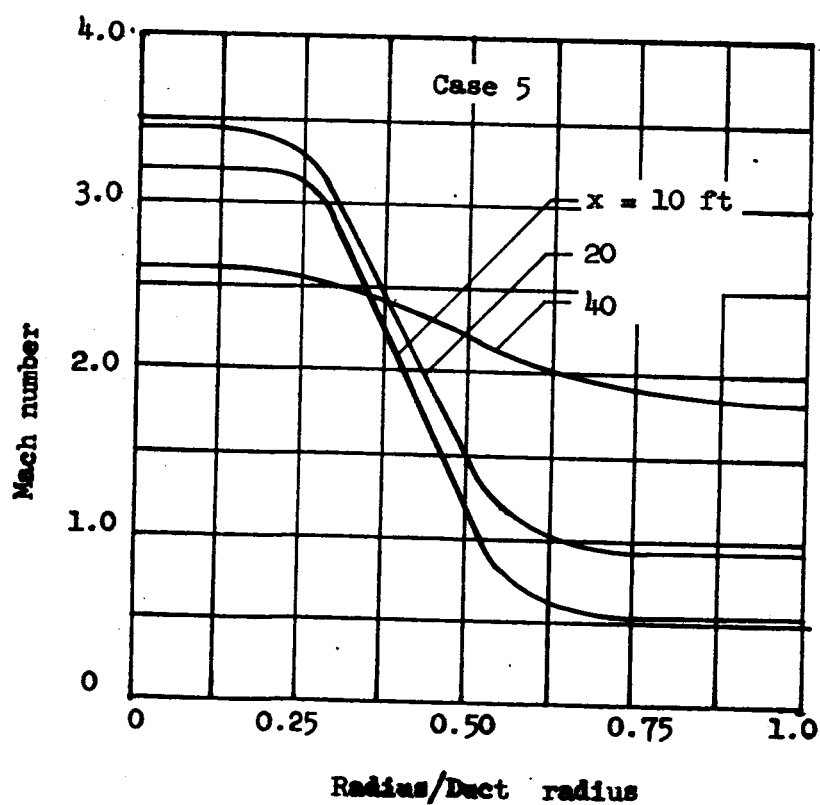


Figure 56 - Mach Number Profile

Figure 56 are the Mach number profiles for secondary flow conditions corresponding to those of Case 2, with Reichardt's coefficient increased by a factor of approximately five. As can be seen, the entire flow is choked, with the exit Mach numbers in the outer portions of the flow greater than those of Case 2. Shown in Figure 57 are the inner and outer boundaries of the mixing region as determined from concentration profiles for the two values of Reichardt's coefficient. As can be seen, the mixing region occupies the entire duct at axial locations of approximately 5 and 10 feet for the high and low Reichardt's coefficients, respectively. The augmentation ratio for this case is 1.20, an increase of approximately 5.3 percent over that obtained for Case 2.

In Figure 58 is presented the augmentation ratio as a function of dynamic pressure based upon results obtained from the mixing analysis for Configuration II. The augmentation ratio is seen to increase with increasing dynamic pressure - the maximum calculated value being 1.4 at a dynamic pressure of approximately 2500 psf.

Shown in Figure 59 is the augmentation ratio as a function of area ratio  $A_{1s}/A_{1p}$ , for a free stream Mach number of 2.37 and an altitude of 50,000 feet. The augmentation ratio increases slightly with increasing area ratio. As noted previously the larger combustor provides greater area upon which pressure forces may act, but the requirement of choked flow generally necessitates the pressure  $P_{1s}$  to be lower than that required for the small combustor. Consequently, the integrated pressure over the forward-facing area is only slightly larger than that of the smaller duct and hence, the aug-

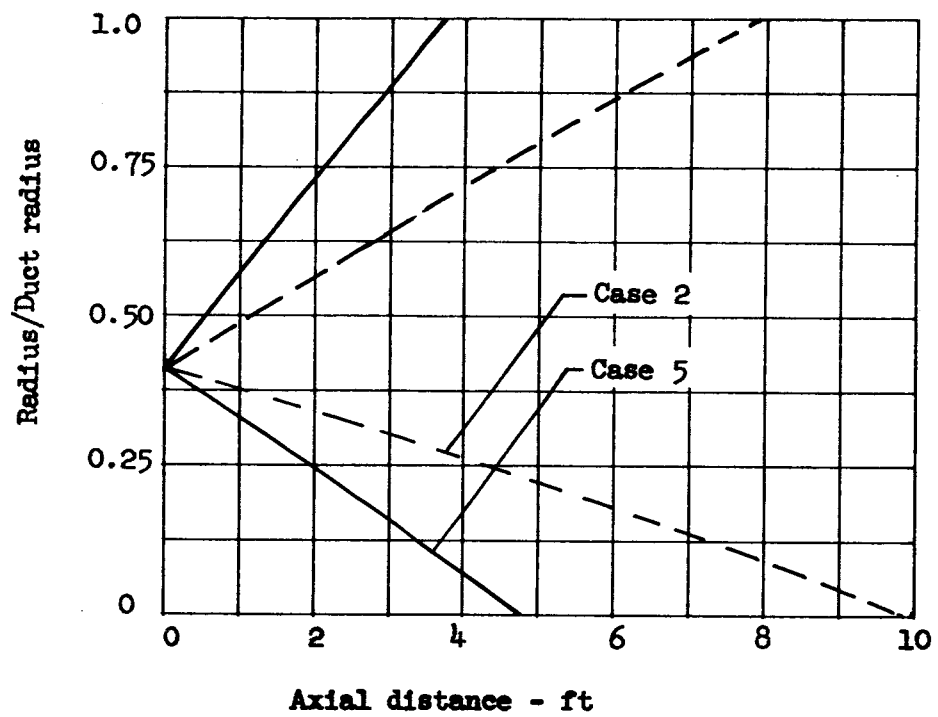
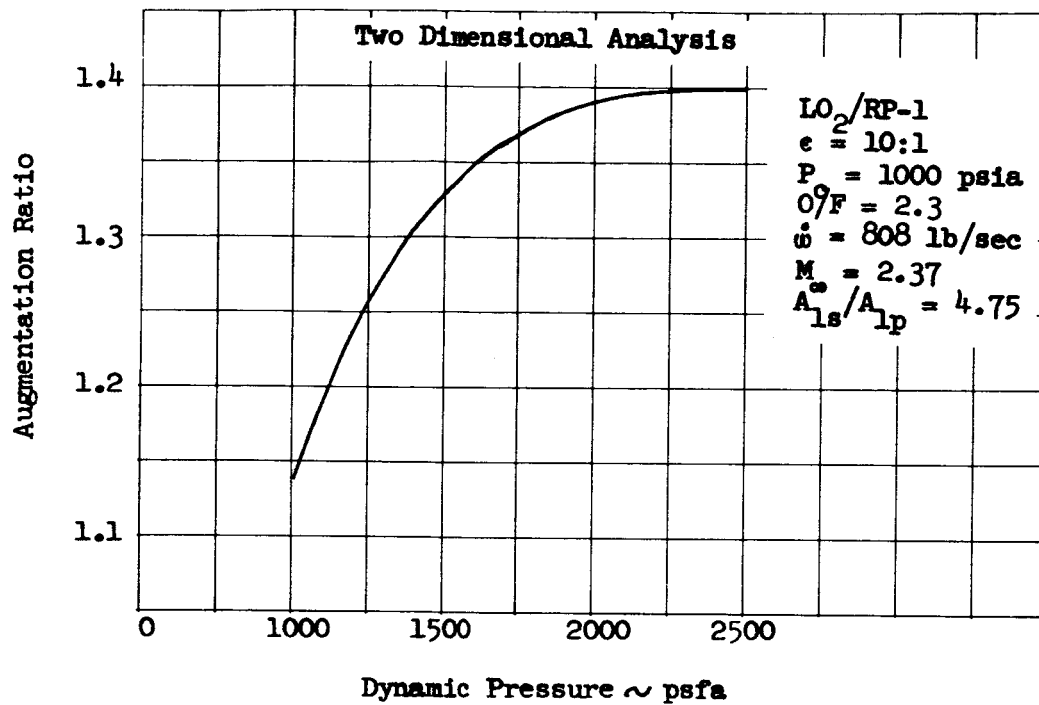


Figure 57 - Mixing Region Boundaries



10

Figure 58 - Theoretical Augmentation Rate  
With Change in Dynamic Pressure

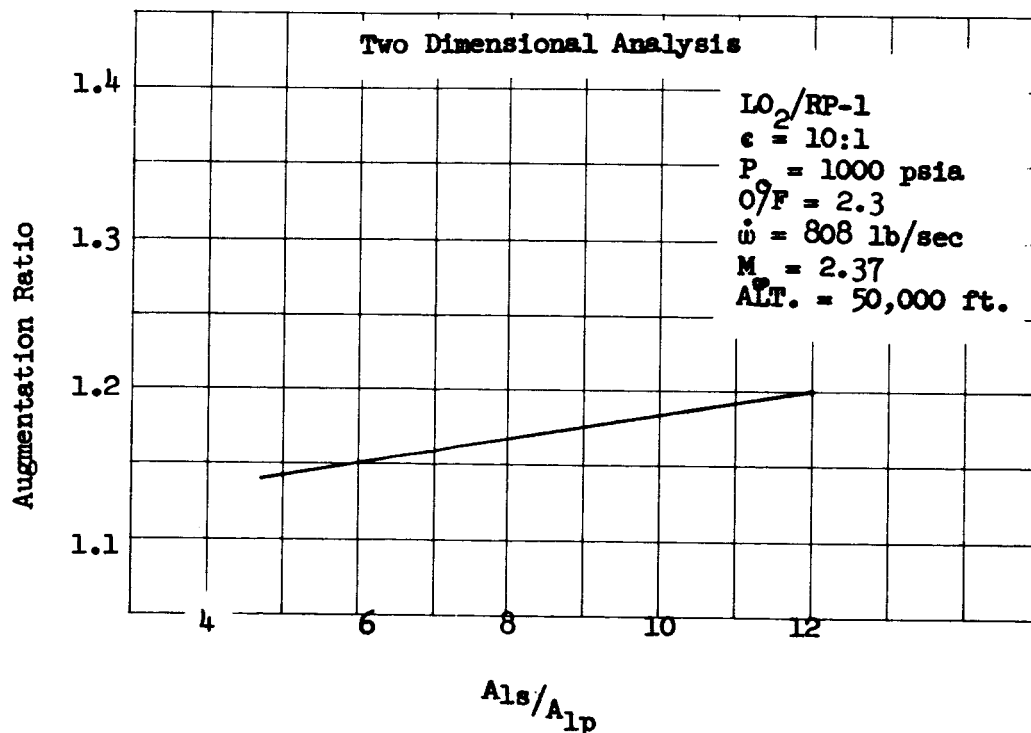


Figure 59 - Theoretical Augmentation Ratio  
With Change in Area Ratio

mentation ratio increases only slightly.

The augmentation ratios for the various cases discussed above are presented in Table 2 along with the corresponding flow conditions. It should be noted that, in order to accurately establish the relative effects of the parameters, the choking location in the mixing section should be identical for all cases - preferably at the mixing section exit.

TABLE 2

## AUGMENTATION RATIOS FOR VARIOUS FLOW CONDITIONS

Case No.	Altitude ft.	$M_\infty$	q psf	P <sub>1s</sub> psfa	T <sub>1s</sub> R	u <sub>1s</sub> ft/sec	M <sub>1s</sub>	$\frac{A_{1s}}{A_{1p}}$	$\frac{\dot{V}_s}{\dot{V}_p}$	$\frac{\dot{Q}}{\dot{Q}_p}$ ft <sup>2</sup> /sec	O/F	Augmentation Ratio
1	50,000	2.37	958	2145	809	489	0.35	12.0	3.76	3.62	2.3	1.82*
1a	50,000	2.37	958	1920	544	544	0.4	12.0	3.76	3.58	2.3	1.51*
2	50,000	2.37	958	2145	809	489	0.35	4.75	1.51	3.62	2.3	1.14
3	40,000	2.37	1540	3455	809	489	0.35	4.75	2.44	3.62	2.3	1.33
4	50,000	2.37	958	2145	809	489	0.35	4.75	1.51	3.62	2.0	1.19
5	50,000	2.37	958	2145	809	489	0.35	4.75	1.51	15.0	2.3	1.20
--	30,000	2.37	2480	3910	825	780	0.533	4.75	3.8		2.3	1.40

\*Exit flow not choked

## CONCLUSIONS AND RECOMMENDATIONS

### Conclusions:

1. The analytical models have been developed for gaseous flow that are capable of predicting system performance to an accuracy commensurate with good engineering practice.
2. Utility of the models is reduced by the external iteration technique required to obtain satisfactory solutions from the mixing program.
3. It is imperative to consider the coupling between the air inlet and the mixing section and the resultant matching operation in arriving at realistic augmented engine performance.
4. The critical effect of the inlet-combustor matching has not been fully explored, but the judicious use of throttleable high pressure primary rockets and/or secondary fuel may offer a promising approach to this problem.
5. The results indicate that high dynamic pressures improve engine performance.

### Recommendations

1. Modify the mixing program to incorporate internal iteration techniques to arrive at desired duct configurations.
2. Generate broader parametric maps of performance in the regimes where augmentation appears favorable, based upon the inlet-combustor matching requirement.
3. Investigate the advantages of using a high chamber pressure throttleable primary rocket and/or secondary fuel injection in order to operate stably at high dynamic pressures.

4. Modify existing programs as necessary and explore novel air augmented design concepts, which provide altitude compensating effects, increased mixing of the streams, variable inlets and exits, and dual mode operation.
5. Develop an analytical model for the analysis of solid primary rocket air augmentation systems.
6. Perform studies to permit selection of the most promising engine concepts for various applications.
7. Conduct an experimental program to further verify the analyses, obtain additional basic mixing data, evaluate mixing section performance with impingement of the mixing zones of multiple jets, and investigate the interaction of the inlet and combustor.

## REFERENCES

1. Rasof, B.; Theoretical Performance of a Ducted Rocket; Jet Propulsion Laboratory, CIT, Report No. 3-3, August 14, 1945.
2. Lorell, J.; Static Performance of the Ducted Rocket; Jet Propulsion Laboratory, CIT, Report No. 3-8, August 5, 1946.
3. Riley, C. F.; The Ejector Ramjet as a Means for Obtaining Static Thrust; University of Michigan, Report No. EM-6-4, February 10, 1948.
4. Sutherland, G. S.; Performance Analysis of Ram Rockets and Thrust Augmentors; Boeing Airplane Company Document No. D-17950, July 1956.
5. Glassman, I. and Charyk, J. V.; The Ramrocket; Jet Propulsion Engines, Princeton series, Vol. XII, 1959, p. 625-661.
6. Perini, L. L., Walker, R. E., and Dugger, G. L.; Preliminary Study of Thrust Augmentation of a Rocket; Applied Physics Laboratory, JHU, Report TG-545, January 1964.
7. Knox, F. M.; Air-Augmented Rocket (One-Dimensional); The Boeing Company Report No. AS1961, April 16, 1964.
8. Huff, V. N.; Gordon, S.; and Morrell, V. E.; General Method and Thermodynamic Tables for Computation of Equilibrium Composition and Temperature of Chemical Reactions; NACA Report No. 1037, 1951.
9. Savage, L. E.; Air-Augmented Power Plant Design Program (Plumed Mix-Master); The Boeing Company Report AS1927, June 5, 1964.
10. Addy, L. A.; On the Steady State and Transient Operating Characteristics of Long Cylindrical Shroud Supersonic Ejectors (With Emphasis on the Viscous Interaction Between the Primary and Secondary Streams); Ph. D. Thesis, University of Illinois, 1963.

11. Libby, P. A.; A Theoretical Analysis of the Turbulent Mixing of Reactive Gases with Application to the Supersonic Combustion of Hydrogen; General Applied Science Laboratories Technical Report No. 242, June 1961.
12. Vasiliu, J.; Turbulent Mixing of a Rocket Exhaust Jet with a Supersonic Stream Including Chemical Reactions; Journal of the Aerospace Sciences, January 1962.
13. Mikhail, S.; Mixing of Coaxial Streams Inside a Closed Conduit; Journal of Mechanical Engineering Science, Volume 2, No. 1, 1960.
14. Wu, J. C.; On the Finite-Difference Solution of Laminar Boundary Layer Problems; Proceedings of the 1961 Heat Transfer and Fluid Mechanics Institute.
15. Schlichting, H.; Boundary Layer Theory, 4th Edition; McGraw-Hill Book Company, Inc., 1960.
16. Pai, S. I.; Fluid Dynamics of Jets; D. Von Nostrand Company, Inc., 1954.
17. Maydew, R. C., and Reed, J. F.; Turbulent Mixing of Axisymmetric Compressible Jets (in the Half-Jet Region) with Quiescent Air; Sandia Corporation, SC-4764 (RR), March 1963.
18. Korst, H. H., Chow, W. L., and Zumwatt, G. W.; Research on Transonic and Supersonic Flow of a Real Fluid at Abrupt Increases in Cross Section-Final Report; Engineering Experimental Station, University of Illinois, M.E. Tech. Report 392-5, December 1959.
19. Miles, J. B.; Stanton Number for Separated Turbulent Flow Past Relatively Deep Cavities; Ph. D. Thesis, University of Illinois, 1963.
20. Penner, S. S.; Chemistry Problems in Jet Propulsion; Pergamon Press, 1957.
21. Emmons, D. L.; A One-Dimensional Analysis of a Flow System in Chemical Non-Equilibrium with Application to Combustor and Exhaust Nozzle Flow Problems; The Boeing Company Document D2-35256, January 25, 1964.

# APPENDIX

## DISTRIBUTION LIST

<u>COPIES</u>	<u>RECIPIENT</u>	<u>DESIGNEE</u>
	NASA Marshall Space Flight Center Huntsville, Alabama 35812	
1		Office of Technical Information, M-MS-IPC
1		Purchasing Officer, Code PR-CH
1		Patent Office, M-PAT
	NASA Headquarters Washington, D. C. 20546	
4		Mr. Henry Burlage, Jr., Chief Liquid Propulsion Technology, RPL
1		Mr. Vernon E. Jaramillo Advanced Manned Mission, MTC
25	Scientific and Technical Information Facility P. O. Box 5700 Bethesda, Maryland 20014	NASA Representative, Code CRT
	NASA Marshall Space Flight Center Huntsville, Alabama 35812	
1		Mr. Donald Thompson, Technical Mgr. Code R-P&VE
2	Ames Research Center Moffett Field, California 94035	Harold Hornby Mission Analysis Division
2	Goddard Space Flight Center Greenbelt, Maryland 20771	Merland L. Moseson Code 623
2	Jet Propulsion Laboratory California Institute of Technology 4800 Oak Grove Drive Pasadena, California 91103	Robert F. Rose Propulsion Div. 38

<u>COPIES</u>	<u>RECIPIENT</u>	<u>DESIGNEE</u>
2	Langley Research Center Langley Station Hampton, Virginia 23365	Floyd L. Thompson Director
2	Lewis Research Center 21000 Brookpark Road Cleveland, Ohio 44135	Dr. Abe Silverstein Director
2	Marshall Space Flight Center Huntsville, Alabama 35812	Hermann K. Weidner Code R-P&VED
2	Manned Spacecraft Center Houston, Texas 77001	Robert R. Gilruth Director
2	Western Operations Office 150 Pico Boulevard Santa Monica, California 90406	Robert W. Kamm Director
1	Advanced Research Projects Agency Washington 25, D. C.	D. E. Mock
1	Aeronautical Systems Division Air Force Systems Command Wright-Patterson Air Force Base Dayton, Ohio 45433	D. L. Schmidt Code ASRCNC-2
1	Air Force Missile Development Center Holloman Air Force Base, New Mexico	Maj. R. E. Bracken Code MDGRT
1	Air Force Missile Test Center Patrick Air Force Base, Florida	L. J. Ullian
1	Air Force Systems Command, Dyna-Soar Air Force Unit Post Office Los Angeles 45, California	Col. Clark Technical Data Center
1	Arnold Engineering Development Center Arnold Air Force Station Tullahoma, Tennessee	Dr. H. K. Doetsch
1	Bureau of Naval Weapons Department of the Navy Washington 25, D. C.	J. Kay, Code RTMS-41

<u>COPIES</u>	<u>RECIPIENT</u>	<u>DESIGNEE</u>
1	Defense Documentation Center Headquarters Cameron Station, Building 5 5010 Duke Street Alexandria, Virginia 22314 Attn: TISIA	
1	Headquarters, U. S. Air Force Washington 25, D. C.	Col. C. K. Stambaugh Code AFRST
1	Picatinny Arsenal Dover, New Jersey 07801	I. Forsten, Chief, Liquid Propulsion Laboratory
1	Rocket Research Laboratories Edwards Air Force Base Edwards, California 93523	Colonel Silk
1	U. S. Atomic Energy Commission Technical Information Services Box 62 Oak Ridge, Tennessee	
1	U. S. Army Missile Command Redstone Arsenal, Alabama 35809	Dr. Walter Wharton
1	U. S. Naval Ordnance Test Station China Lake, California 93557	Code 451 Chief, Missile Propulsion Division
1	Chemical Propulsion Information Agency Johns Hopkins University Applied Physics Laboratory 8621 Georgia Avenue Silver Spring, Maryland	Neil Safeer
1	Aerojet-General Corporation P. O. Box 296 Azusa, California	L. F. Kohrs
1	Aerojet-General Corporation P. O. Box 1947 Technical Library, Bldg. 2015, Dept. 2410 Sacramento 9, California 95809	R. Stiff

<u>COPIES</u>	<u>RECIPIENT</u>	<u>DESIGNEE</u>
1	Aeronutronic A Division of Ford Motor Company Ford Road Newport Beach, California	D. A. Carrison
1	Aerospace Corporation 2400 East El Segundo Boulevard P. O. Box 95085 Los Angeles, California 90045	John G. Wilder MS-2293 Propulsion Dept.
1	Arthur D. Little, Inc. Acorn Park Cambridge 40, Massachusetts	A. C. Tobey
1	Astropower, Inc., Subsidiary of Douglas Aircraft Company 2968 Randolph Avenue Costa Mesa, California	Dr. George Moc Director, Research
1	Astrosystems, Inc. 1275 Bloomfield Avenue Caldwell Township, New Jersey	A. Mendenhall
1	Atlantic Research Corporation Edsall Road and Shirley Highway Alexandria, Virginia	A. Scurlock
1	Beech Aircraft Corporation Boulder Facility Box 631 Boulder, Colorado	J. H. Rodgers
1	Bell Aerosystems Company P. O. Box 1 Buffalo 5, New York	W. M. Smith
1	Bendix Systems Division Bendix Corporation Ann Arbor, Michigan	John M. Brueger
1	Boeing Company P. O. Box 3707 Seattle 24, Washington	J. D. Alexander
1	Chrysler Corporation Missile Division Warren, Michigan	John Gates
1	Curtiss-Wright Corporation Wright Aeronautical Division Wood-ridge, New Jersey	G. Kelley

<u>COPIES</u>	<u>RECIPIENT</u>	<u>DESIGNEE</u>
1	Douglas Aircraft Company, Inc. Missile and Space Systems Division 3000 Ocean Park Boulevard Santa Monica, California 90406	R. W. Hallet, Chief Engineer Advanced Space Tech.
1	Fairchild Stratos Corporation Aircraft Missiles Division Hagerstown, Maryland	J. S. Kerr
1	General Dynamics/Astronautics Library & Information Services (128-00) P. O. Box 1128 San Diego, California 92112	Frank Dore
1	General Electric Company Re-Entry Systems Department Box 8555 Philadelphia, Pennsylvania 19101	F. E. Schultz
1	General Electric Company Flight Propulsion Lab Department Cincinnati 15, Ohio	D. Suichu
1	Grumman Aircraft Engineering Corp. Bethpage Long Island, New York	Joseph Gavin
1	Kidde Aero-Space Division Walter Kidde and Company, Inc. 675 Main Street Belleville 9, New Jersey	R. J. Hanville Director of Research Engineering
1	Lockheed California Company 10445 Glen Oaks Boulevard Pacoima, California	G. D. Brewer
1	Lockheed Missiles and Space Company Attn: Technical Information Center P. O. Box 504 Sunnyvale, California	Y. C. Lee Power Systems R&D
1	Lockheed Propulsion Company P. O. Box 111 Redlands, California	H. L. Thackwell
1	The Marquardt Corporation 16555 Saticoy Street Box 2013 - South Annex Van Nuys, California 91409	Warren P. Boardman, Jr.

<u>COPIES</u>	<u>RECIPIENT</u>	<u>DESIGNEE</u>
1	Martin Division Martin Marietta Corporation Baltimore 3, Maryland	John Calathes (3214)
1	Martin Denver Division Martin Marietta Corporation Denver, Colorado 80201	J. D. Goodlette Mail A-241
1	McDonnell Aircraft Corporation P. O. Box 6101 Lambert Field, Missouri	R. A. Herzmark
1	North American Aviation, Inc. Space & Information Systems Division Downey, California	H. Storms
1	Northrop Corporation 1001 East Broadway Hawthorne, California	W. E. Gasich
1	Pratt & Whitney Aircraft Corp. Florida Research and Development Center P. O. Box 2691 West Palm Beach, Florida 33402	R. J. Coar
1	Radio Corporation of America Astro-Electronics Division Defense Electronic Products Princeton, New Jersey	S. Fairweather
1	Reaction Motors Division Thiokol Chemical Corporation Denville, New Jersey 07832	Arthur Sherman
1	Republic Aviation Corporation Farmingdale, Long Island, New York	Dr. William O'Donnell
1	Rocketdyne (Library Dept. 586-306) Division of North American Aviation 6633 Canoga Avenue Canoga Park, California 91304	E. B. Monteath
1	Space General Corporation 9200 Flair Avenue El Monte, California	C. E. Roth
1	Space Technology Laboratories Subsidiary of Thompson-Ramo-Wooldridge P. O. Box 95001 Los Angeles 45, California	G. W. Elverum

<u>COPIES</u>	<u>RECIPIENT</u>	<u>DESIGNEE</u>
1	Stanford Research Institute 333 Ravenswood Avenue Menlo Park, California 94025	Thor Smith
1	TAPCO Division Thompson-Ramo-Wooldridge, Inc. 23555 Euclid Avenue Cleveland 17, Ohio	P. T. Angell
1	Thiokol Chemical Corporation Redstone Division Huntsville, Alabama	John Goodloe
1	United Aircraft Corporation Research Laboratories 400 Main Street East Hartford 8, Connecticut 06108	Erle Martin
1	United Technology Center 587 Methilda Avenue P. O. Box 358 Sunnyvale, California	B. Abelman
1	Vought Astronautics Box 5907 Dallas 22, Texas	Warren C. Trent
1	National Engineering Science Company 711 South Fair Oaks Avenue Pasadena, California	G.V.R. Rao
1	Texaco Experiment Inc. Richmond 2, Virginia	Mr. Rodney McGann
1	Dynamic Science Corporation 1445 Huntington Drive South Pasadena, California	Melvin Gerstein
1	Los Angeles Division North American Aviation, Inc. International Airport Los Angeles 9, California	Maury Sulkin
1	Illinois University S. Wright Street Urbana, Illinois	H. H. Korst
1	General Applied Science Labs, Inc. Merrick & Stewart Avenue Westbury, New York	Antonio Ferri